

**FINITE ELEMENT SIMULATIONS AND OPTIMIZATION OF
BERDUT LINEAR MOTOR FOR A NOVEL ELEVATOR SYSTEM**

By

Ezequiel Fernando Medici

A Thesis Submitted in Partial Fulfillment
of the Requirements for the Degree of

**MASTER OF SCIENCE
in
MECHANICAL ENGINEERING**

**UNIVERSITY OF PUERTO RICO
MAYAGÜEZ CAMPUS**

Approved by:

David Serrano, Sc.D.
President, Graduate Committee

Date

Frederick A. Just-Agosto, Ph.D.
Member, Graduate Committee

Date

Gustavo Gutierrez, Ph.D.
Member, Graduate Committee

Date

Paul Sundaram, Ph.D.
Chairperson of the Department

Date

Luis Godoy, Ph.D.
Representative of Graduate Studies

Date

Abstract

The present project has the objective to model and simulate a special linear motor known as a Berdut linear motor. The motor's governing equations are derived from Maxwell's equation and Newton's law of motion. These equations are coupled through the Lorenz force. Appropriate boundary conditions and initial conditions are also determined. This system does not have an exact solution. The set of equations are solved by a numerical technique. The finite element method was chosen because it is extensively used, and there are commercial software packages that solve coupled multiphysics. Maxwell® is used for the work described in the thesis. Numerical results are compared with experimental results obtained from measurements taken from a small linear motor prototype based on the Berdut Technology. Once the model is calibrated, the work proceeds to evaluate and estimate the theoretical efficiency of the motor under other conditions and other geometrical configurations. With this information, it is possible to optimize the different parameters of the motor for different applications. A novel elevator design configuration was selected as the case study in the thesis. The linear motor will be optimized for thus relatively low speed application. The objective function is formulated in terms of design variables subject to different constraints such as comfort, packaging, speed and travel distance. The tradeoff of using a linear motor over the traditional elevator is also explored.

Resumen

El presente proyecto tiene como objetivo simular y modelar un motor eléctrico lineal especial conocido como Berdut Linear Motor. Las ecuaciones de movimiento que describen el comportamiento del motor son una suma de las ecuaciones de Maxwell y la ecuación de Newton de la mecánica. Estas ecuaciones están acopladas a través de la fuerza de Lorenz. El modelo matemático consta además de apropiadas condiciones de frontera y condiciones iniciales. Este sistema no tiene una solución exacta. Para resolverlo, es necesario para utilizar alguna técnica numérica. El software comercial de elementos finitos, Maxwell[®], fue seleccionado para resolver el sistema de ecuaciones del modelo resultante descrito en esta tesis. Los resultados numéricos se comparan con resultados experimentales obtenidos de la medida de un prototipo experimental pequeño del motor lineal. Una vez que el modelo es calibrado, se procede a evaluar y estimar la eficiencia teórica del motor bajo otras condiciones y configuraciones geométricas. Con esta información, es posible optimizar los diferentes parámetros del motor para diferentes aplicaciones. En esta tesis en particular se estudiara la optimización del motor para una aplicación a baja velocidad de operación para poder utilizarlo como mecanismo para un ascensor. Las restricciones usadas fueron tomadas acorde a las características de confort de edificios convencionales. Además se discuten las ventajas de usar motores eléctricos lineales como mecanismo para ascensores.

Dedication

To my parents, Alberto Médici and María Laura Lazcano, for their priceless support and interminable source of love.

Acknowledgements

I would like to thank my advisor Dr. David Serrano for his honest and sincere counseling and support during my Master's thesis.

I wish to thank the members of my committee Dr. Frederick Just and Dr. Gustavo Gutierrez.

I also wish to express my sense of gratitude and thank to Dr. Sergio Preidikman for his recommendation and invaluable suggestions.

Finally, I would like to thank the Department of Mechanical Engineering at University of Puerto Rico-Mayagüez.

Table of Contents

ABSTRACT	II
RESUMEN	III
DEDICATION.....	IV
ACKNOWLEDGEMENTS	V
TABLE OF CONTENTS.....	VI
LIST OF FIGURES.....	IX
LIST OF TABLES.....	XIV
NOMENCLATURE	XV
CHAPTER I: INTRODUCTION	1
1.1. RESEARCH MOTIVATION	1
1.2. OBJECTIVES	4
1.3. PROCEDURE	5
CHAPTER II: LITERATURE REVIEW	7
2.1. PREVIOUS STUDIES OF BERDUT PATENTS	7
2.2. HIGH POWER LINEAR MOTOR	10
2.3 MEDIUM AND LOW POWER LINEAR MOTORS	18
2.4 SPECIAL APPLICATION OF LINEAR MOTOR	22
CHAPTER III: MATHEMATICAL FORMULATION	29
3.1. GOVERNING EQUATIONS	30

3.2. BOUNDARY AND INITIAL CONDITIONS.....	34
3.2.1 Neumann Or Natural Boundary Conditions.....	35
3.2.2 Dirichlet Or Value Boundary Conditions.....	36
3.2.3 Balloon Boundaries	37
3.2.4 Initial Conditions	37
3.3. SOURCE TERMS	37
3.4. NUMERICAL ANALYSIS.....	39
3.5 POWER LOSS.....	43
CHAPTER IV: NUMERICAL RESULTS	48
4.1. GENERAL ANALYSIS.....	48
4.2. EFFICIENCY ANALYSIS AND THRUST FORCE	53
4.3.1. EFFECT OF POWER	54
4.3.3. <i>Effect of Materials</i>	59
4.3.4. <i>Effect of Coil Connections</i>	62
CHAPTER V: EXPERIMENTAL VALIDATION.....	67
5.1. 16 COIL LINEAR MOTOR EXPERIMENT	67
5.1.1. <i>Experimental Setup</i>	68
5.1.2. TEST RESULTS	70
5.2. EXPERIMENT 4 COILS	73
5.2.1. <i>Experimental Setup</i>	73
5.2.2. <i>Results</i>	76
5.3. EXPERIMENT ORBITAL MOTOR	87
5.3.1. <i>Experimental Setup</i>	88
5.3.2. <i>Results</i>	89
CHAPTER VI: CASE STUDY: DESIGN OPTIMIZATION.....	92

6.1. DESIGN VARIABLE DEFINITIONS	92
6.2. OPTIMUM BERDUT LINEAR MOTOR FOR ELEVATOR DESIGN.....	97
CHAPTER VII: CONCLUSIONS AND FUTURE WORK.....	108
7.1. CONCLUSIONS	108
7.2. FUTURE WORK	109
APPENDIX A: OPTIMIZATION POINTS	111
REFERENCES	117

List of Figures

Figure 1: Berdut Patents; A) Linear Motor, B) Orbital motor, C) Magnetic suspension	1
Figure 2: 2D Model of Berdut Linear Motor with four coils.....	3
Figure 3: Different potentials applications of Berdut Technology	4
Figure 4: (A) skate model (passive technology levitation), (B) linear motor model (active technology propulsion)	8
Figure 5: Berdut Levitation Model	9
Figure 6: German Model of Levitation Train.	10
Figure 7: Schematic drawing of Japanese model: A) Position of rail coils, B) Position of car coils.	11
Figure 8: (A) Thrust Forces, (B) Levitations Force	12
Figure 9: Indutrac model.....	13
Figure 10: (A) Magnet pod detail; (B) A vehicle's magnet pod and suspension rail.	14
Figure 11: Cross-section of guideway beam and vehicle suspension.....	15
Figure 12: MagneMotion Maglev M ³ Model.....	15
Figure 13: Artistic Diagram of a Berdut Maglev Train	16
Figure 14: Prototype of Berdut Array	17
Figure 15: Yaskawa Electric America (YEA) Linear motor models.....	18
Figure 16: Nikon Tech. Linear motor with one side magnetic interaction.	20
Figure 17: : Detail of the coils	20
Figure 18: Nikon Tech. Linear motor with two sides magnetic interaction.	21

Figure 19: Tubular linear motor.....	21
Figure 20: Example of location of the elevators (floor plans).	23
Figure 21: Comparison between: (A) Traditional and (B) Twin elevator System.	24
Figure 22: ThyssenKrupp Elevator Company designs: (A) Twin (B) Evolution.	25
Figure 23: Elevator advantage (A) Traffic optimization (B) easy change of direction.	26
Figure 24: Storage possibilites.	27
Figure 25: Artistic view of the robotic parking	28
Figure 26: Diagram.	29
Figure 27: Equivalent magnet field of current density.	38
Figure 28: Steps in solving the model.	40
Figure 29: Maxwell mesh.	42
Figure 30: Logic diagram of iteration in each time step.	42
Figure 31: Hysteresis loop	45
Figure 32: Normal B-H Curve	46
Figure 33: B-H curve for Ceramic 5	47
Figure 34: Motor dimensions and material properties.....	49
Figure 35: Force Diagram and Motor dimensions.....	50
Figure 36: Rectangular wave (A) without dead time (B) with dead time.....	51
Figure 37: Force decrement as a function of current profile	52
Figure 38: Model used for relative rail displacement	52
Figure 39: Relative guide displacement effect.....	53
Figure 40: Efficiency curves for different input power levels.....	55

Figure 41: Thrust force for different input power levels	55
Figure 42: “T” pole parameters.....	56
Figure 43: Efficiency curves for different “T” arrays.....	58
Figure 44: Thrust force curves for different “T” arrays.....	59
Figure 45: Efficiency curves for different permanent magnet material.....	61
Figure 46: Thrust force curves for different permanent magnet material.....	61
Figure 47: Current vs. Time.....	62
Figure 48: Efficiency curves for different numbers of coils for simultaneous coil connection.	64
Figure 49: Efficiency curves for different numbers of coils. Shift connection.	65
Figure 50 Thrust force for different numbers of coils	65
Figure 51: Motor dimensions and material properties.....	68
Figure 52: A) Complete view of the rail; B) Detail of the magnets and “T” arrays...	69
Figure 53: Details of the moving part.....	69
Figure 54: Speed vs. Time for 24 volts.....	70
Figure 55: Speed vs. time for 36 volts	71
Figure 56: Speed vs. time for 48 volts	71
Figure 57: Average Thrust Force over the car	72
Figure 58: Average Thrust Force over each coil	73
Figure 59: (A) Car with the details of the brushes, (B) Lateral view of the car	74
Figure 60: View of the alternating power strip used to power the coils	74
Figure 61: (A) Rail, (B) Final assembly of rail and car	75
Figure 62: A) Data acquisition system B) accelerometer C) Calibrated resistant	76

Figure 63: Electric circuit of the experimental motor.....	77
Figure 64: Thrust force for 12 volts.....	77
Figure 65: Current for 12 volts	78
Figure 66: Thrust force for 24 volts.....	78
Figure 67: Current for 24 volts	79
Figure 68: Thrust force for 36 volts.....	79
Figure 69: Current for 36 volts	80
Figure 70: Schematic model used in Maxwell.....	80
Figure 71: Comparison of thrust force between experimental data and FE simulation for 12v	81
Figure 72: Comparison of current between experimental data and FE simulation for 12v.....	82
Figure 73: Comparison of thrust force between experimental data and FE simulation for 24v	82
Figure 74: Comparison of current between experimental data and FE simulation for 24v.....	83
Figure 75: Comparison of thrust force between experimental data and FE simulation for 36v	83
Figure 76: Comparison of current between experimental data and FE simulation for 36v.....	84
Figure 77: Comparison of the average thrust force between experiment and FE simulation for 12v	86

Figure 78: Comparison of the average thrust force between experiment and FE simulation for 24v	86
Figure 79: Comparison of the average thrust force between experiment and FE simulation for 36v	87
Figure 80: Orbital motor	88
Figure 81: Motor performance at 24 volts	89
Figure 82: Motor performance at 36 volts	90
Figure 83: Elevator performance	93
Figure 84: (A) Rail, (B) Coil.....	95
Figure 85: Example of quadratic objective function.....	98
Figure 86: Optimization convergence.....	105
Figure 87: Final values for design variables	106
Figure 88: Efficiency as a function of permanent magnet length.....	112
Figure 89: Efficiency as a function of permanent magnet width.....	113
Figure 90: Efficiency as a function of “T” pole length.....	113
Figure 91: Efficiency as a function of “T” pole width.....	114
Figure 92: Efficiency as a function of number of turns.	114
Figure 93: Efficiency as a function of coil length.....	115
Figure 94: Efficiency as a function of coil width.	115
Figure 95: Efficiency as a function of the current	116
Figure 96: Efficiency as a function of model depth.....	116

List of Tables

Table 1: Concentrator Models	57
Table 2: Magnetic properties of Ceramic5 and NeFe35	60
Table 3: Coil topology analyzed	63
Table 4: Values for the Design Variables	100
Table 5: Useful parameter values for the iterations	101
Table 6: Results obtained for each variable design	102
Table 7: Optimum point.....	106
Table 8:Results obtained for the design variables	111

Nomenclature

B = Magnetic induction	F = Vector Body Force
E = Electric field	F_L = Lorenz's Force
D = Electric displacement	\hat{n} = Vector normal to the surface
H = Magnetic intensity	Ω = Volume
P = Polarization	S = Area
M = Magnetization	t = Time
A = Magnetic vector potential	$\nabla \cdot$ = Divergence
v = Electric scalar potential	B_{in} = Normal magnetic induction
J = Current density	H_{it} = Magnetic intensity
J_s = Current source	$J_{s\perp}$ = Perpendicular current density
J_m = Equivalent magnetic current	ψ_i = Polynomial weight function
K_m = Equivalent surface magnetic current	Ae = Element area
ρ = Charge density	x_{ijk} = x coordinates of the triangle
ε = Dielectric constant	y_{ijk} = y coordinates of the triangle
μ = Magnetic Permeability	P_e = Eddy current loss
ν = Reluctivity	P_h = Hysteresis loss
c = Light velocity	σ_{eff} = Effective electric conductivity
σ = Electric conductivity	N = Number of laminations
x = Vector Displacement	ω = Frequency of electric field
\dot{x} = Vector velocity	SF = Staking factor
\ddot{x} = Vector Acceleration	η = Efficiency
$\nabla \times$ = Curl	\tilde{S} = Design variable vector
m = Mass	\tilde{g} = Constraints vector
C = Damping	$f_{(\tilde{s})}$ = Objective function
K = Stiffness	

CHAPTER I: Introduction

Berdut Technology consists of a collection of patents [1,2,3,4], which deal with electromechanical systems able to transform electrical energy into mechanical energy, Figure 1. These inventions can be divided into two groups: an active group and a passive group. The active group contains designs that use or produce energy such as motors and generators. In addition, the active group can be subdivided into two other groups according to geometric considerations. These are linear and radial depending on whether the output is a displacement or a rotation. The passive type refers to designs that do not require external energy to operate. In the passive type all of the magnetic field is generated by permanent magnets and there is no electromagnet. In this case the system does not consume electrical energy.

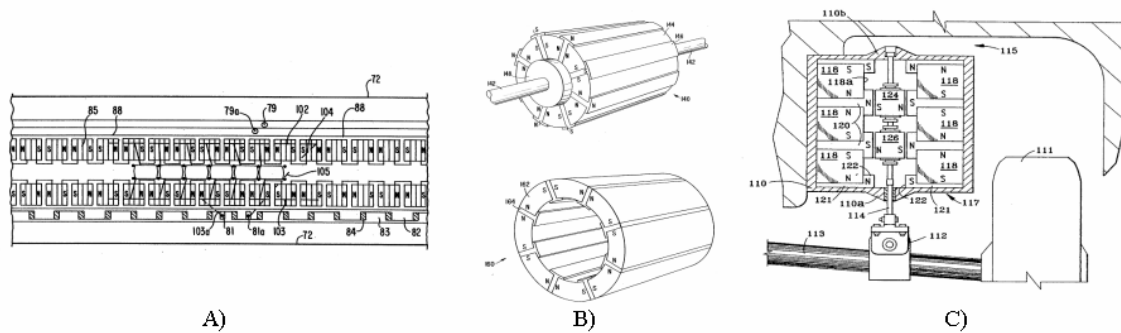


Figure 1: Berdud Patents; A) Linear Motor, B) Orbital motor, C) Magnetic suspension

1.1. Research Motivation

The first and most important application of the Berdud Technology used both type of arrays (active and passive) for a magnetic levitated train (MAGLEV). An electric

linear motor based on the active technology was designed to provide the linear thrust propulsion for the Maglev. The passive technology was the basis of the levitation mechanism for the Maglev. At this point is important to note that a magnetic levitated train differs from conventional trains in the way that it is supported from the rail. In magnetic levitation, the train is supported by magnetic arrays that sustain it without rail contact. This lack of contact allows for faster trains since no friction force is generated [5].

There are many types of arrays used in levitation systems. The principal inconvenient of Maglev trains is their elevated cost. Electromagnets in the rail and in the train are needed, and a complex control system is required. For this reason, Maglev configurations are not very popular, compared to conventional trains. A key issue in the Berdud Technology is its low cost potential. Its passive array provides a steady levitation without the need of external electrical energy and complex control systems.

Linear motors with permanent magnets require less complex control systems, lower energy consumption, simpler manufacturing process. Once again these are areas where Berdud Technology has a direct impact and potential for lower initial costs and lower operating costs. The Maglev train was an example of an application using high power levels. Applications of the linear motor that require lower power can be found, for example, in servomotors. In this research, the Berdud linear motor is studied in detail in order to characterize it and identify its advantages and limitations. In the Berdud linear motor the magnets located in the rail are permanent magnets, Figure 2. The control system and the geometrical configuration is very simple. Another important characteristic is the use of a special element in the array of permanent magnets used in the stator. The

permanent magnets are separated by a magnetic concentrator (see Figure 2), providing better performance compared to existing technologies. The technical details of The Berdud Technology and its specific differences, advantages and limitations with respect to others technologies in passive and active applications are presented in the next chapter.

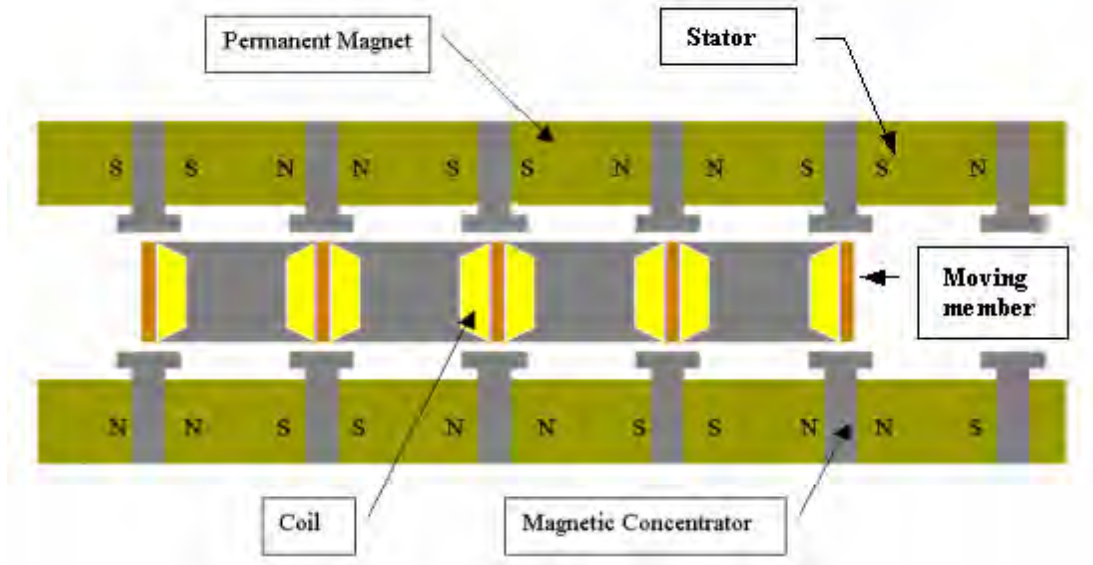


Figure 2: 2D Model of Berdud Linear Motor with four coils

In addition to Maglev propulsion, linear motors can be used to move elevators, aircraft carrier catapults, rocket launchers, etc. The orbital motor configuration could be used in manufacturing machines, power tools, home appliances, etc., replacing existing electric motor technology. Figure 3 shows these potentials applications. It is important to know how the physical parameters (dimensions of permanent magnet and coils, distance between rail and moving parts, voltage and current in the coil, material for the magnets, among others) influence the thrust force, velocity, acceleration, jerk performance, efficiency, levitation capacity and stability of machines based on Berdud Technology.

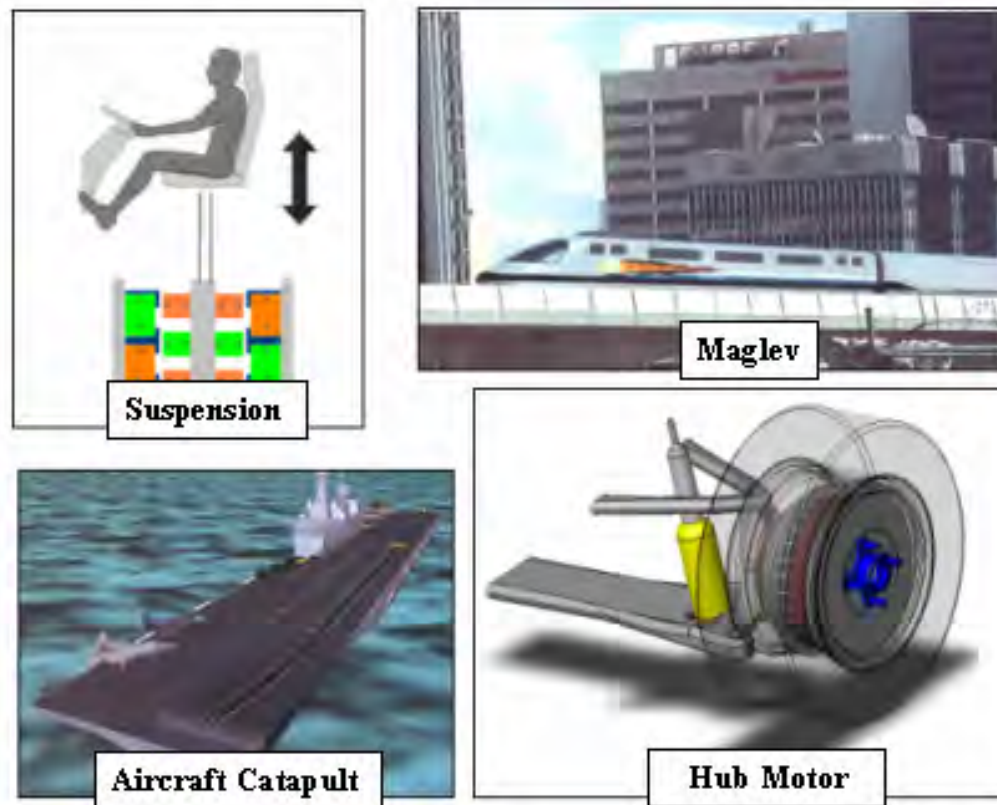


Figure 3: Different potentials applications of Berdud Technology

The potential for significantly improving this technology is the primary motivation of the proposed work. First, the linear motor will be modeled, parameters characterized and validated then the linear motor will be optimized for an innovative elevator system in order to go beyond the current elevator design limitations. The actual limitations of a commercial elevator for high buildings are the weight of its cable and the traffic optimization. The ability to transport more people in less space and time will certainly impact future elevator design and building architecture.

1.2. Objectives

The herein proposed work will meet the following objectives:

1. Characterize the Berndt linear motor and estimate the effect of changes in different parameters in the performance of the motor.
2. Validate experimentally the theoretical model and use this result to predict the behavior under other operation conditions.
3. Study of the motor efficiency.
4. Perform an optimization analysis of the Berndt linear motor subject to the constraints imposed by a novel elevator design, used as a case of study to evaluate the model and the proposed technology.

1.3. Procedure

The proposed research work is divided into the following stages:

1. Literature review.
2. Analysis of other linear motor models currently used to find limitations and advantages for each.
3. Mathematical formulation of the corresponding electromechanical problem:
 - a. Development of a representative mathematical model for this technology and identify with the necessary simplifications and assumptions.
 - b. Determine the appropriate numerical tools required to solve the mathematical model developed in step (a). Numerical methods to be considered include finite element, finite difference, finite volume, etc.
 - c. Develop a simple model for the linear motor with one coil to understand the working principle and how it is affected by the different basic

parameters such as: current intensity, windings, geometric characteristics (dimensions), and material properties.

- d. Develop a model of the linear motor with multiple coils to study the effect of distance between each coil and to estimate the effect in the net thrust force and in the efficiency.
- e. Study potential control strategies by using the power input curves.

4. Experimental setup:

- a. Compare the results obtained in step 3) with existing data to validate the model.
- b. Make an experimental setup using an existing prototype of the Berdut linear motor to obtain actual data for the behavior of the motor for different mass and voltage settings. Also, for each case, measure the consumption of energy and thrust force to obtain estimates of the efficiency experimentally.

5. After validation of the model is completed, perform an optimization analysis for the linear motor when used for an elevator system. The elevator application was selected as a case study to test the model in the novel area beyond the original scope of the technology patents. In this step the objective function and the constraints to formulate the optimization problem are determined. The numerical optimization algorithm will be selected and implemented. The optimum values obtained will be a good estimate of the most convenient dimensions, in the selected case study, for different parameters, such as geometrical dimensions, number of turns in the coil, power supplied, control strategy, etc.

CHAPTER II: Literature Review

The first previous works to be mentioned are the original Berdud patents [1,2,3,4]. The patents contain a collection of applications that use the same array in different geometric forms. Prior research [6,7,8] studied this technology and estimated the effect of some of its parameters in its performance. The study was divided into two parts: The first part described a levitation skate (passive application of Berdud Technology), and the second described a linear motor (active application of Berdud Technology). The first part was analyzed in a previous research [9,10,11] where the stiffness and damping characteristic for the Berdud array used as a levitation mechanism were modeled. Optimal values for Maglev levitation applications were presented. The second part is the main goal of this thesis.

A novel elevator design is proposed as a case study of the Berdud Technology. The traditional elevator with its advantages and limitations in addition to another novel elevator design that can be found commercially market are discussed.

2.1. Previous Studies of Berdud Patents

As previously mentioned, the study was divided into two parts. The basic difference between each part is that in the first the moving component is a permanent magnet, Figure 4 (a). In the second, the moving component is an electro magnet; see Figure 4 (b). The main difference between each model is that in the first case it does not require external electrical energy. Also the passive design (skate in levitation design) is

intended as a suspension mechanism. The details of its operation are available in the literature [9,10,11] but its operation may be summarized as follows (see Figure 5):

1. The permanent magnets arranged on the skate are positioned in the neutral position such that they are in attraction with an adjacent pole located on the stator. The pole is directly aligned with the permanent magnet.
2. At the same time the magnet on the skate is in repulsion with the poles that are directly above and below the pole it face on the stator.
3. Any displacement in the vertical direction away from the equilibrium position is opposed by the stator magnets.
4. The array has a number of similar arrangements in the vertical position which all work in parallel therefore the levitation force is directly proportional to the number of units in the array.
5. The force-displacement characteristics in the vertical direction define the skate's stiffness and damping characteristics.

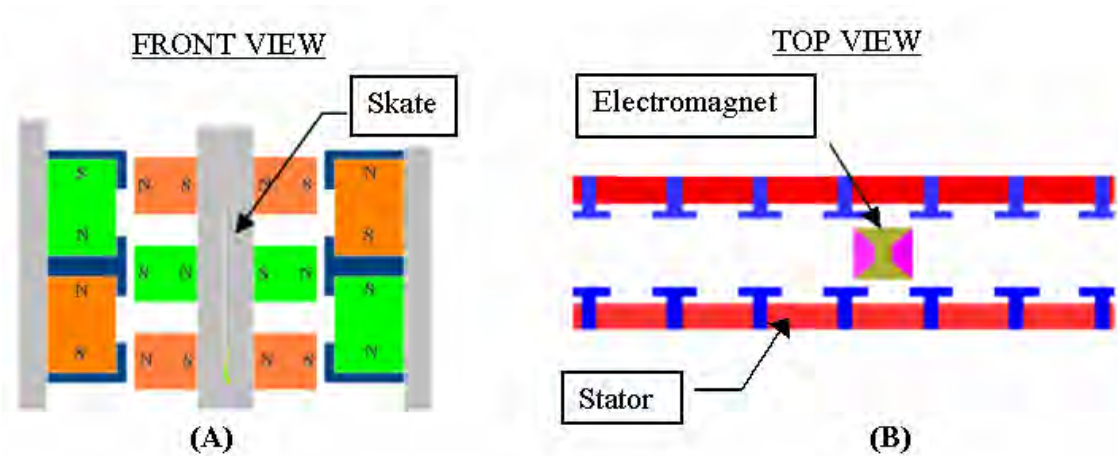


Figure 4: (A) skate model (passive technology levitation), (B) linear motor model (active technology propulsion)

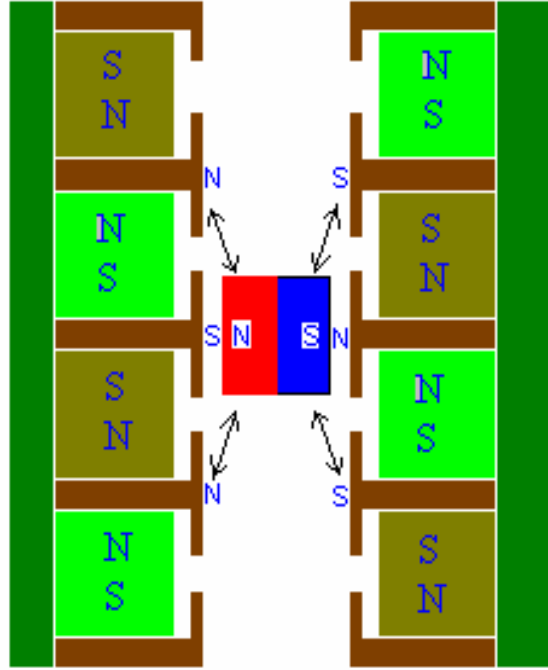


Figure 5: Berndt Levitation Model

L. Morales and D. Serrano [6,10] studied the characterization of the skate model as an equivalent spring constant for a levitated train system using Berndt poles. The skate was modeled with finite elements and validated with experiments. J. Robles [7], J. Robles and D. Serrano [11] analyzed the dynamic response and damping characteristics of a Berndt skate for a magnetically levitated train. Again finite element modeling was performed with experimental validation. In addition, J. Robles compared this design with magnetic levitation designs currently available. A preliminary study on the use of Berndt Technology in propulsion was performed by O. Flores [8]. He identified the most relevant parameters that affect the behavior of the motor but the work did not include experimental validation or design optimization. E. Medici and D. Serrano [12,13] validate a numerical model using motor prototype and they also analyzed numerically the effect of the current profile in thrust force of the motor.

2.2. High Power Linear Motor

Magnetic train levitation technology had its beginnings in Germany in the 1970. This technology, known as Transrapid [14], consists of a double system of electromagnets: one set in the rail and the other in the vehicle or mobile section. The electromagnets that are located in the mobile section are continuously active; the electromagnets that are located in the rail are only energized when the train passes over them. The polarities of the electromagnets are synchronized and originate a resultant thrust force. Figure 6 is a schematic diagram of the system. In this model, the levitation forces are by attraction.

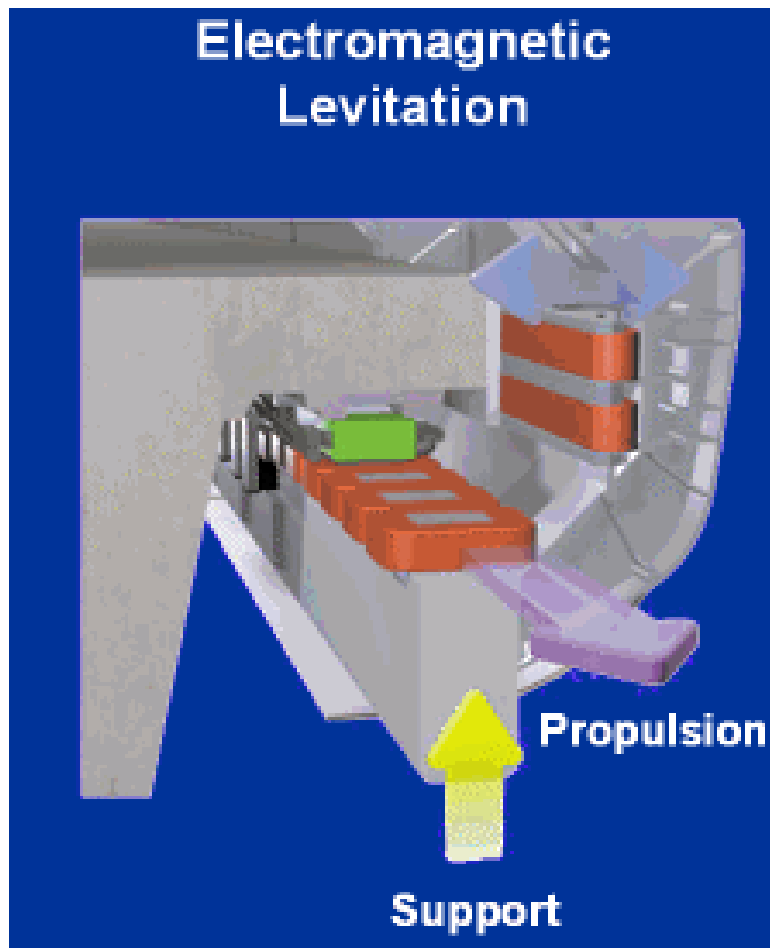


Figure 6: German Model of Levitation Train.

The lower magnets have different polarity than the upper magnets and therefore attract, but before they contact, a control system switches off the energy in the coils and they separate by the force of gravity. This cycle repeats 1000 times a second. The other levitation system design is the Super Conducting Magnet (SCM) [15] [16]. The SCM was developed in Japan in the 1970's. This system has a SCM in the train, Figure 7 (b), and two sets of coils in the rail, Figure 7 (a). One, for levitation and guidance, and the others for propulsion.

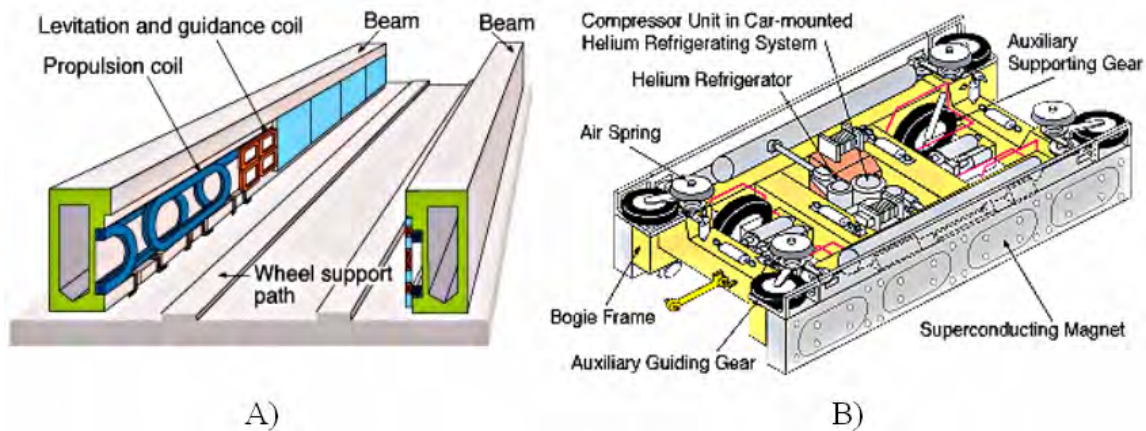


Figure 7: Schematic drawing of Japanese model: A) Position of rail coils, B) Position of car coils.

The vehicle with the SCM passes at high speed in front of the levitation coil (that has a form of an “8”, Figure 8 (B)) and some centimeters below the center of the “8” structure. In this configuration, when there is a relative movement between the SCM and the coil, in the lower coil, a magnetic field is induced that has the same polarity as the SCM and the opposite polarity of that in the upper coil. Therefore, the set of repulsion and attraction forces produce a vertical levitation force. On the other hand, the propulsion coils are energized inducing alternating magnetic poles opposite to that of the

magnetic fields on the train. These magnetic fields generate a set of attractive and repulsive forces, Figure 8 (A), over the SCM and propel the train.

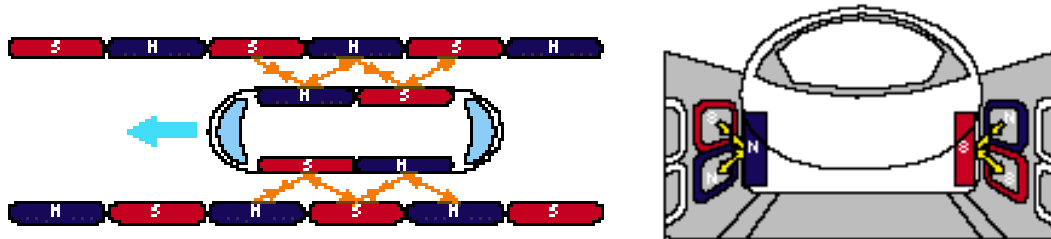


Figure 8: (A) Thrust Forces, (B) Levitations Force

A third levitation technology is the Indutrac [17] model. The Indutrack model has permanent magnets in the mobile section. The field of permanent magnets is orientated at 90° from each other. Figure 9 shows this array, also is known as the Halbach array in honor of its designer [18] In this array the magnetic field is concentrated on one side and almost eliminated on the other side. In the rail there are arrays of individuals coils that operate each as a closed circuit. When the vehicle passes over the coil, the permanent magnets generate current in the coil. These currents generate an electromagnetic field that opposes the permanent magnet field and produces the levitation force. The design has the advantage that it does not need external energy for levitation but this array increases the net drag when it is in motion because the induced field dissipates power through heat transfer in the coils. When a permanent magnet has relative displacement with respect to an electric conductor, a proportional current to the rate of change in the distance (speed) is generated in the conductor. When a current circulates in an electric conductor, an electromagnetic field is generated in the surrounding. The current circulates in the

conductor with a direction such that the generated magnetic field has opposite flux lines to that of moving magnet. This effect is known as Lens's Law. As a consequence of the opposite magnetic fields repulsive forces are generated between the magnet and the conductor. This repulsive force originates the levitation. A main disadvantage of this technology is that the generated current in the conductor is dissipated as heat and is reflected as an extra drag force on the permanent magnets, thus reducing the overall efficiency of the system. This model also requires an additional set of coils for generating the propulsion force.

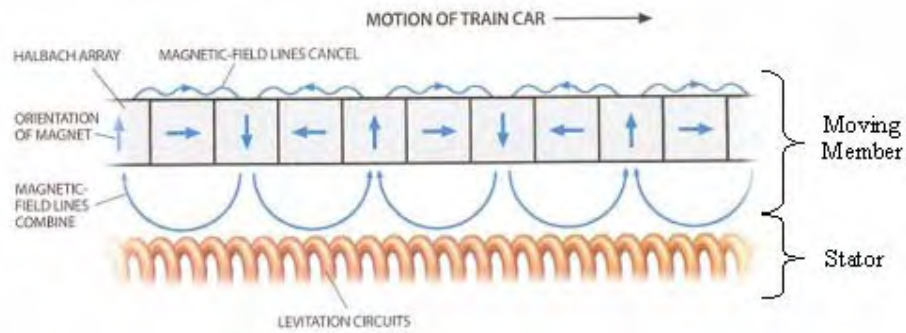


Figure 9: Indutrac model.

As a consequence of previous discussion, it can be inferred that these technologies have high cost and low efficiency and the search of an alternative technology was motivated. In recent years new developments include Magnemotion Maglev System M3 [19,20] technology and Berdut Technology. The Magnemotion Maglev System M³ technology has a linear synchronous motor (LSM) for the suspension, guidance and propulsion. The LSM is an electrical motor that has electromagnets in the car and rail and permanent magnets in the car. When the electromagnets in the car and in the rail are energized an attraction force is originated between them. This attraction force

is the levitation force. When the electromagnets are not perfectly aligned (as a consequence of some lateral perturbation) the action force has a component in the direction of the shift. In this design, this component of the force produces the guidance and propulsion force. Figure 10 (A) shows the location of the electromagnets in the pod in the car and Figure 10 (B) and Figure 11 shows the cross sectional lateral view of the rail and the pod and the location of the electromagnets. Figure 12 shows a small model of this technology.

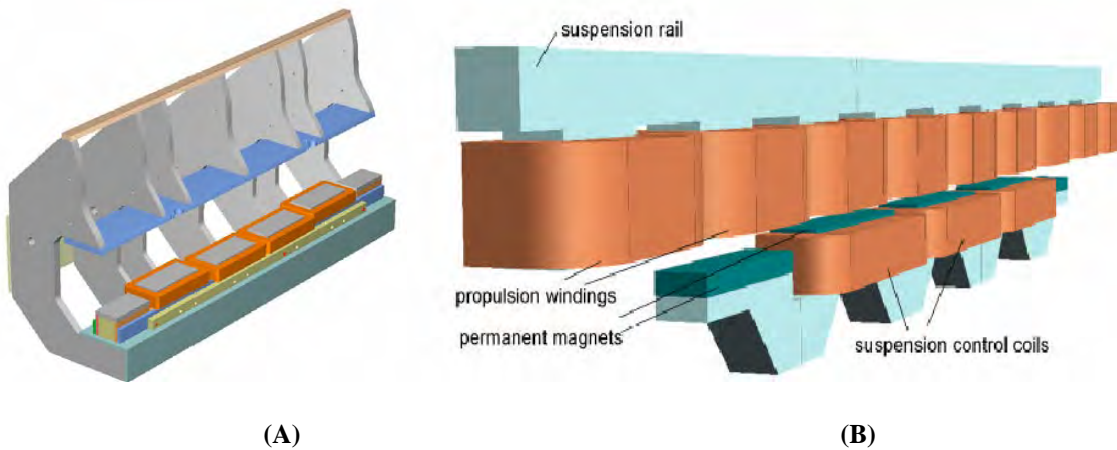


Figure 10: (A) Magnet pod detail; (B) A vehicle's magnet pod and suspension rail.

The Magnemotion Maglev System M³ technology similar to the German approach except for the addition to permanent magnet located in the pod. In the German system the levitation and thrust forces are generated from electromagnets only. Also, the lateral loads are restrained easily. When the lateral force originates a relative displacement between the car and the rail, the same force that generates the levitation (vertical force) now has a horizontal component. The horizontal component appears on both rails and with the same direction producing a constraining of lateral force. The Magnemotion Maglev System M³ technology was also proposed for use in other applications, which

require less power such as those described in the next section. The working principle is the same and therefore is not repeated.

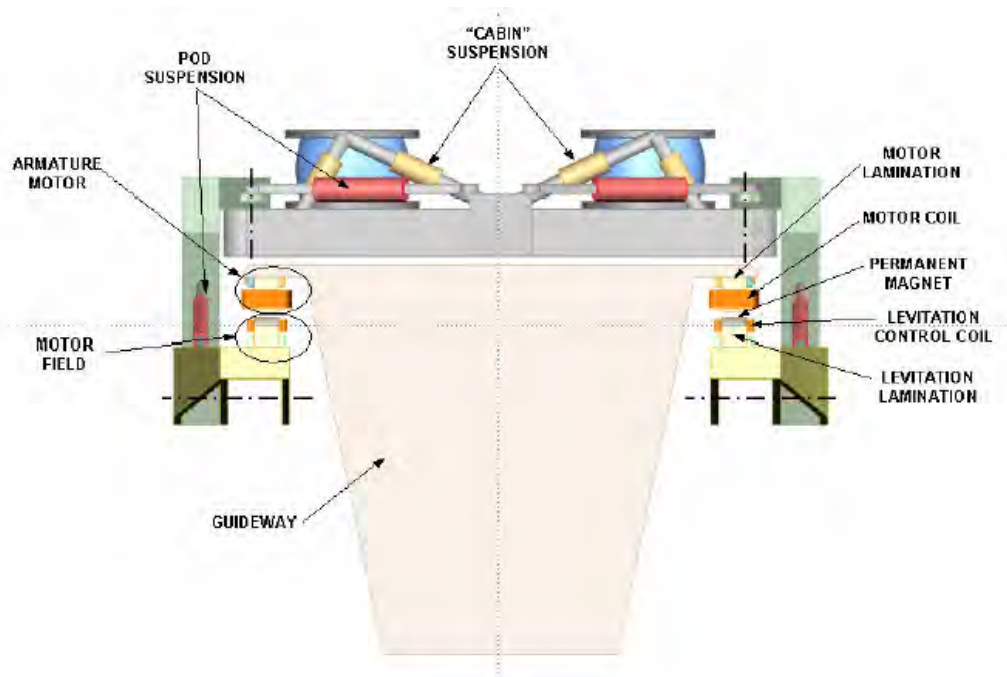


Figure 11: Cross-section of guideway beam and vehicle suspension.

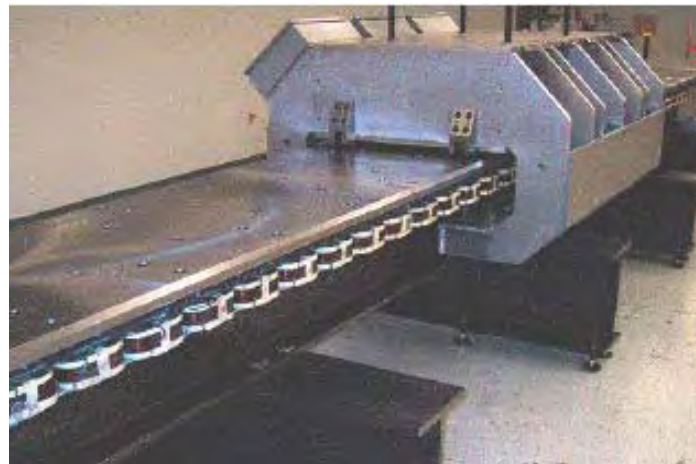


Figure 12: MagneMotion Maglev M³ Model.

A new technology, Berdud Technology consists of a simple array of the electromagnets and magnets. The Berdud Technology combines the two designs to obtain

the levitation force and the thrust force. On both sides of the car there are sets of skates and in the middle of the car there is a linear motor. Figure 13 and Figure 14 show this array. Figure 13 is an artistic cross section view of the train and illustrates the position of the levitation skates and the position of the linear motor. Figure 14 shows a photograph of a scale model of the train with the levitation skates and the linear motor.

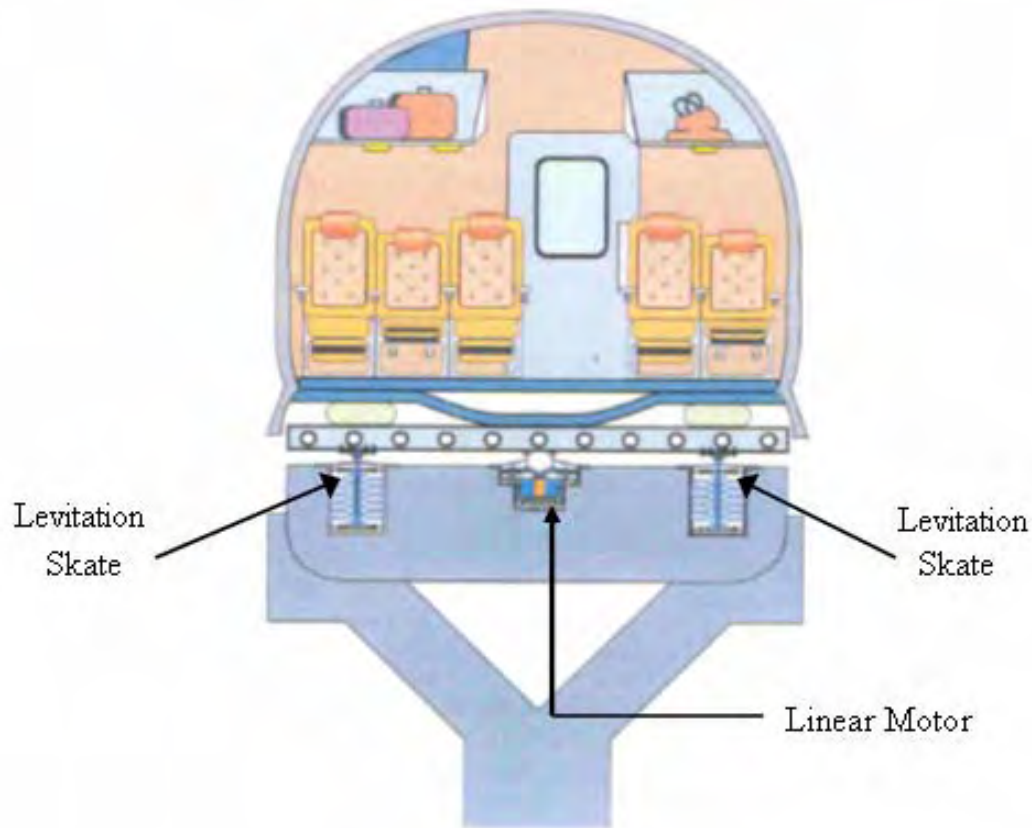


Figure 13: Artistic Diagram of a Berdud Maglev Train

The skate is a vertical array of permanent magnets shown in Figure 4 (A). When the car is loaded a reaction force appears in the opposite directions. As previously mentioned, when one magnet is located between other two, if the polarization is correct, the central magnet will be located in a stable equilibrium point Figure 5. Any force,

which displaces the central magnets from its vertical equilibrium position, will be rejected by an opposing force. Figure 5 shows a schematic model of the system with one central magnet, where the arrows indicate the direction of the vertical force. Figure 4 shows a levitation skate with several permanent magnet units.

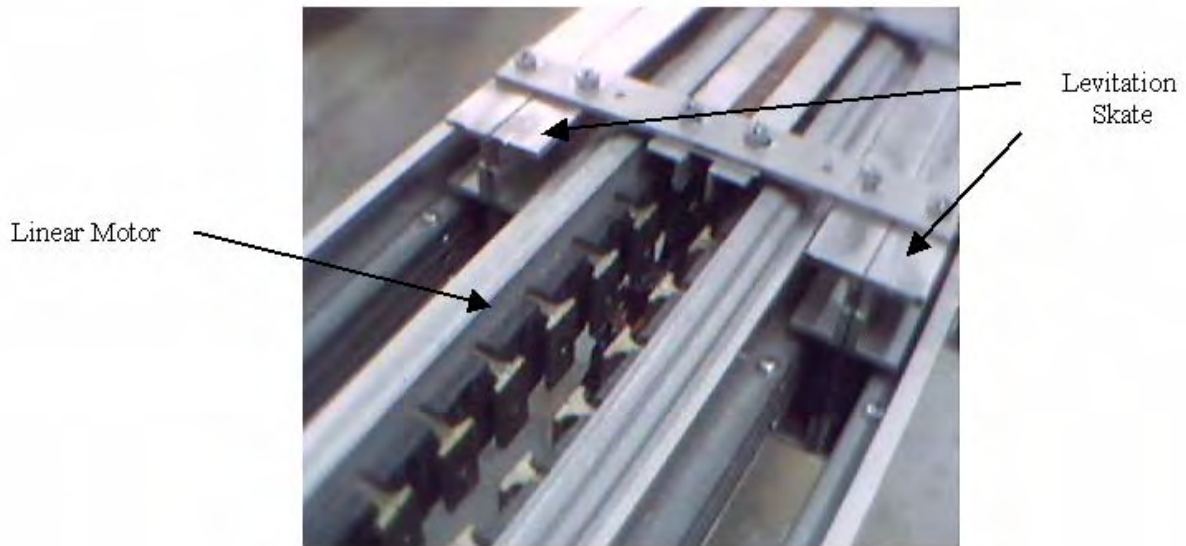


Figure 14: Prototype of Berdut Array

The total force acting in the central magnet originates the levitation force. The number of units used in the levitation skate will depend on the nominal load to be carried by the system. The force displacement characteristics are a function of the geometry and materials used. Also, for stability reasons two skates one on each side train is used.

The motor is a horizontal array of permanent magnets laid along a central rail and electromagnets attached to the train's cars. In the rail, there are permanent magnets separated by magnetic concentrators. The coils are mounted on the car. When the coils are energized, they interact with the permanent magnets on the rail and generate the thrust force. This technology has the advantage of passive levitation (using the skate)

because it does not require a control system. The levitation is totally independent of the motor.

2.3 Medium and Low Power Linear Motors

Servomotors are applications that require low power linear motors. There are many types of linear motors that use permanent magnets. For example, in Figure 15, a line of servomotors of the Yaskawa Electric America [21] is shown. In the Figure, three different models of linear motors are shown.

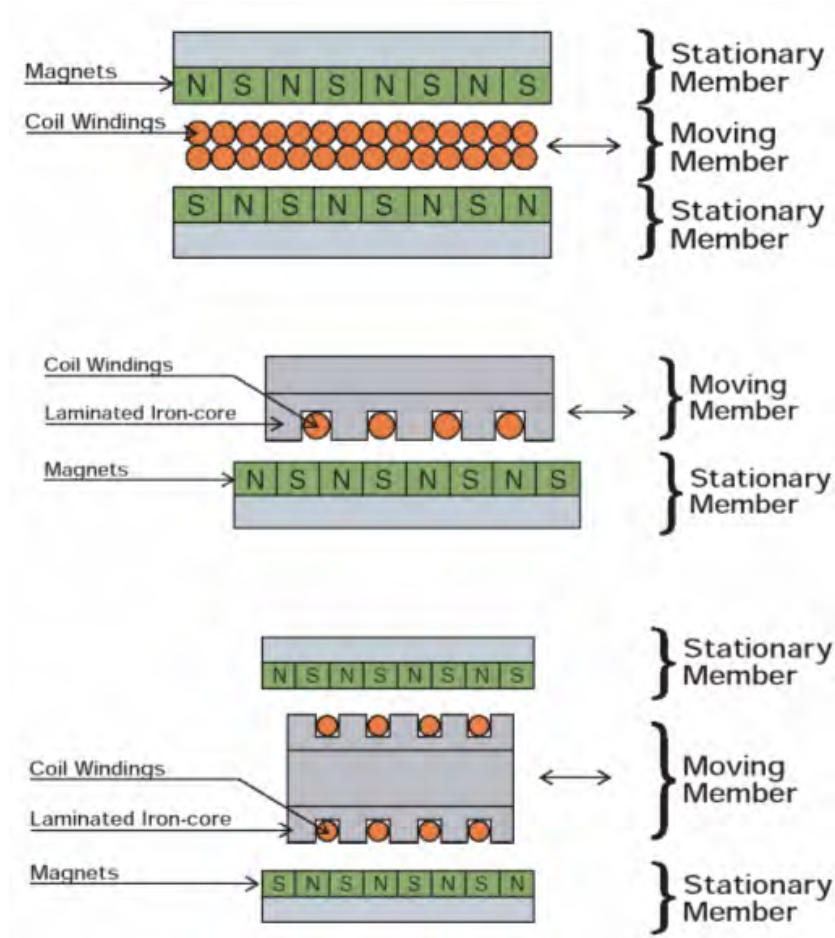


Figure 15: Yaskawa Electric America (YEA) Linear motor models.

In the first model the moving part uses only a winding as its core. It has the advantage that the time response is faster, because the mass of the moving part is very low but as a consequence of not having a magnetic core it cannot obtain a high thrust force. The second design has a magnetic core but the magnetic interactions are located only on one side. It has the advantage of having a free surface to connect to other mechanisms. The third design is a typical linear motor with two sides of permanent magnetic interactions and one electromagnetic core. It has the advantage of high thrust force and efficiency but the time response is lower than that of the first design and the only way to connect to other mechanism is through its core, using a throttle.

In the same line another new linear motor was patented by Nikon Tech.[22], Figure 16. The Nikon design differs from the YEA designs in that it has the permanent magnets located on the moving member and the position of the coils is such that they produce a magnetic field parallel to the magnetic field of the electromagnets. Also, the electromagnets are located in layers as shown in details in Figure 17. This special array of electromagnets can be activated individually depending on the polarization of the magnet passing in front of it. Notice the magnets are arranged in the same pattern as the Hallback array. The reason of that is to maximize the polarization in a specific zone in order to increase the force on the moving member.

Nikon Tech [23] recently patented another linear motor with coils on the two sides of the moving member as shown in Figure 18. This design differs from the previous Nikon linear motor in that the electromagnets are located in the moving member and the permanent magnets are located in the stator. In addition, another difference between them

20

position resolution and compact design. This is the case shown in the Figure 19

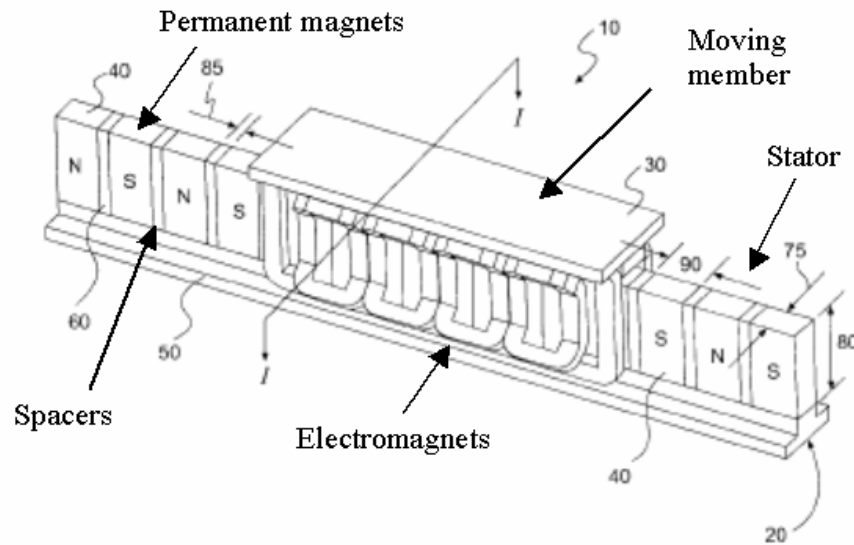


Figure 18: Nikon Tech. Linear motor with two sides magnetic interaction.

This tubular design [24] differs from all of previous designs in that the coils totally enclose the permanent magnets. Also, the permanent magnets have a novel directions of polarization defined as SNSN-NSNS (arrows in Figure 19 indicate the direction of the polarization). This type linear motor, with an adequate coil magnetization, can reach resolutions in position, better than 20 μm .

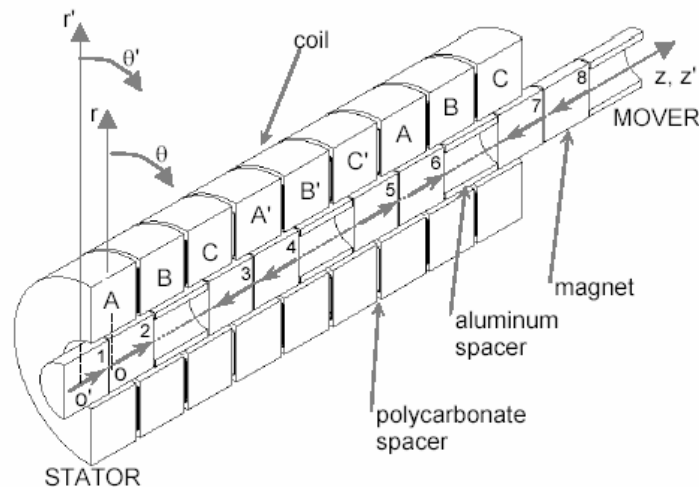


Figure 19: Tubular linear motor.

The objective of this section was to show variety of low power linear motors available. More exist, but these are representative designs that illustrate the plurality. Each one has something novel, advantages and disadvantages that allow them to be good solutions for some problems and bad solutions for others depending on the intended application.

2.4 Special application of Linear Motor

In this work, a case study of a linear motor as it applies to an elevator design will be used to perform the optimization of the parameters that govern its behavior. The traditional elevators have some disadvantages that limit new buildings architecture.

Today new buildings are very tall and designs exhibit more complex configurations than the single box form used in the past. Also today, the elevator is an integral part of the building and is used to accent the building's design and the view from the building. For this reason, the traditionally location of the elevators in the middle of the building floor plan is replaced by more non-conventional locations. Figure 20 shows some examples of modern elevator arrangement.

When the building is very tall, the traditional design has the problem of the excessive weight of the cable in addition, the traditional system is not able to adapt to variations in the form of the build. For example the case when the elevator is located on the exterior of the building and the build has a reduction in its dimensions at some level.

Furthermore, in a commercial building where various elevators are necessary to supply the traffic, this design needs a considerable space compared with the dimensions of the building. For that reason, the study of a novel elevator system is selected.

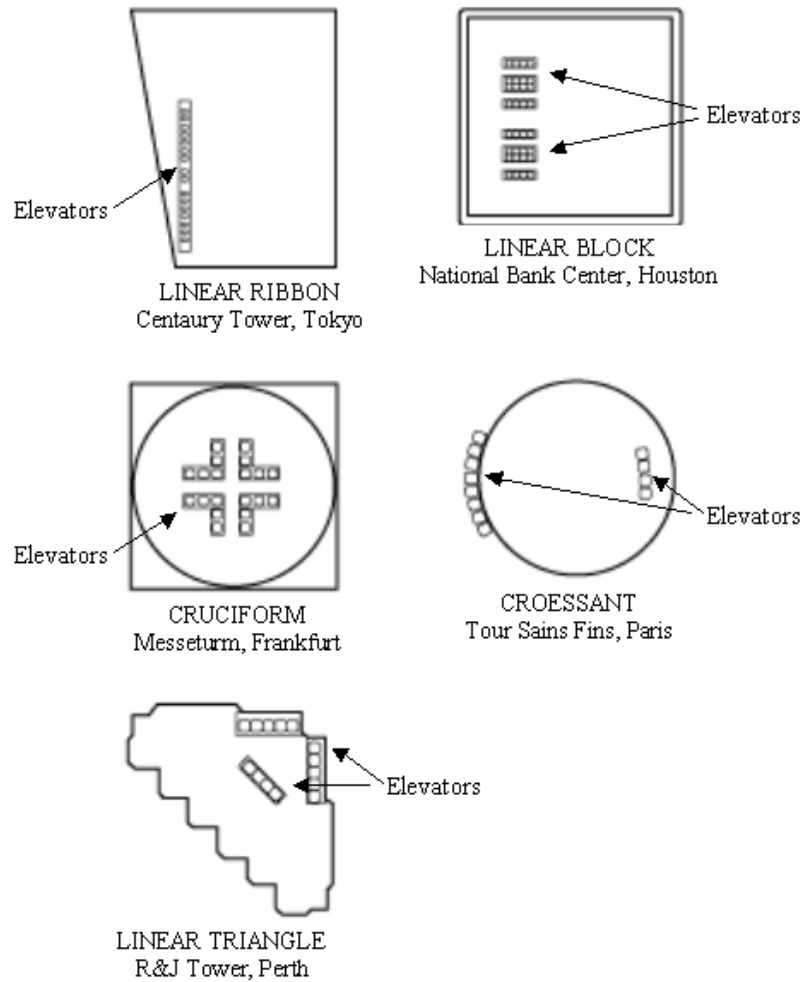


Figure 20: Example of location of the elevators (floor plans).

One of the new elevator designs is the helical elevator [25]. This type of elevator was developed in order to offer one more degree of freedom to building designers and architects. This elevator differs from the traditional in that the cabin is cylindrical. Then, when the elevator it is moving into the shaft (the shaft wall and cabin wall are transparent) it moves in two directions at the same time: vertical displacement and rotation over its axis. A hydraulic piston usually moves this elevator. This system of propulsion only allows low speed and short rise distances.

Another new elevator design is the twin elevator system developed by the ThyssenKrupp Elevator Company [26] based on the originally patent from the nineteen thirties. This design has two cars in the same shaft. This arrangement has the advantage of allowing more traffic in equal space. Figure 21 shows both systems: the traditional and the Twin. In this Figure it can be appreciated that in the same space the twin system has almost twice the transport capacity of the traditional design.

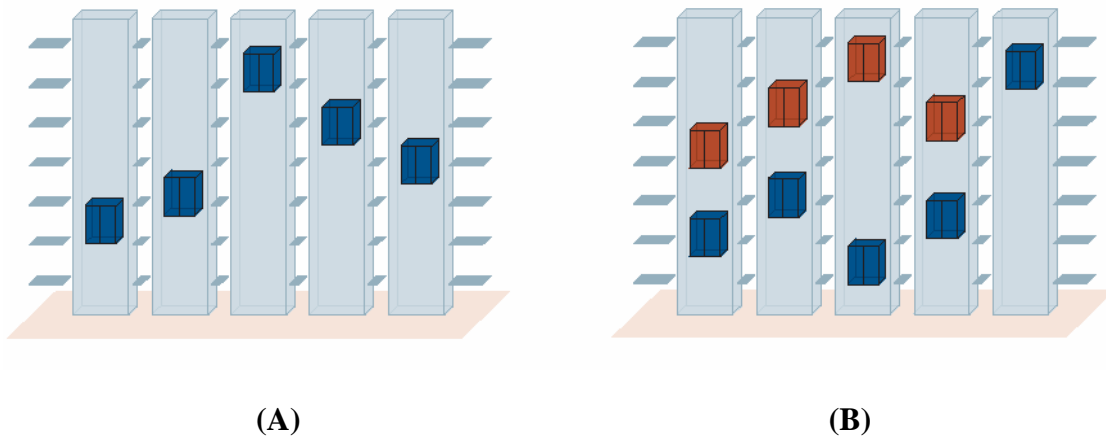


Figure 21: Comparison between: (A) Traditional and (B) Twin elevator System.

The additional car has its individual propulsion machine. With an appropriated control system the traffic can be optimized. Figure 22 (A) shows the model and the location of the components in the Twin system. Also, ThyssenKrupp Elevator Company designed another new elevator system that does not require the machine room (shaft pit room and headroom). This design, named Evolution, occupies less space than the traditional elevator. Figure 22 (B) shows the model of the Evolution elevator system.

T Dünser [27] proposed another new technology for elevator design. In his work, he studied the advantages of an elevator without cables and with flexible rails that would

allow horizontal translations as well. The advantages of this new system, compared to conventional elevators are:

- No need for cables. This is a very important issue because cables are limiting factor in the design of elevators when the building is very high.

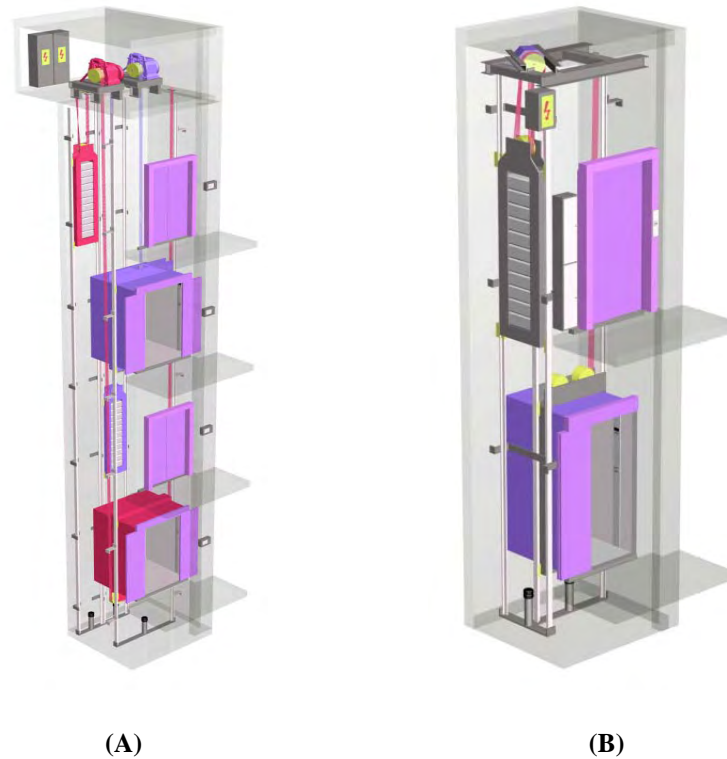


Figure 22: ThyssenKrupp Elevator Company designs: (A) Twin (B) Evolution.

- The possibility to use several cabins on the same rail with the net effect of reducing the area necessary for the traditional elevator.
- Easily change from vertical motion to lateral motion, which also allows changes in the rail and traffic optimization therefore, reducing the total time and number of cabins, see Figure 23.

- The possibility to store the cabin in another place different from the rail. That is, in the traditional elevator the cabin, when it is not in use, can only be stored underground. In this proposed elevator, because it can move in the horizontal direction, it can be stored in other places such as in the center, in the first level or into one side, see, Figure 24 .

The author, only describe the advantage of an elevator system with these capabilities but he does not mentioned any mechanical system able to do these movements.

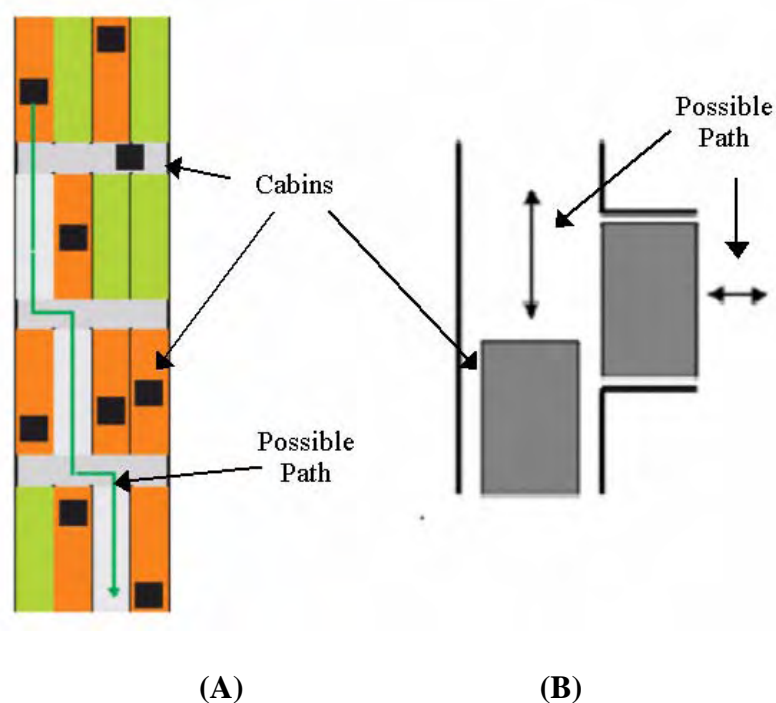


Figure 23: Elevator advantage (A) Traffic optimization (B) easy change of direction.

The previous elevator systems were intended for transporting people but applications to moving objects in general are also of interest. In this line, an attractive

example is the system of elevators used in the Robotic Parking [28] in New Jersey, Figure 25. This system of elevators formed by an array of electromechanical elements allows to optimize the space occupied in the building. This system of elevators has, platforms on which the car is mounted, that can be moved in vertical and horizontal directions and also capable of rotations of 180° . With these degrees of freedom the space can be optimized.

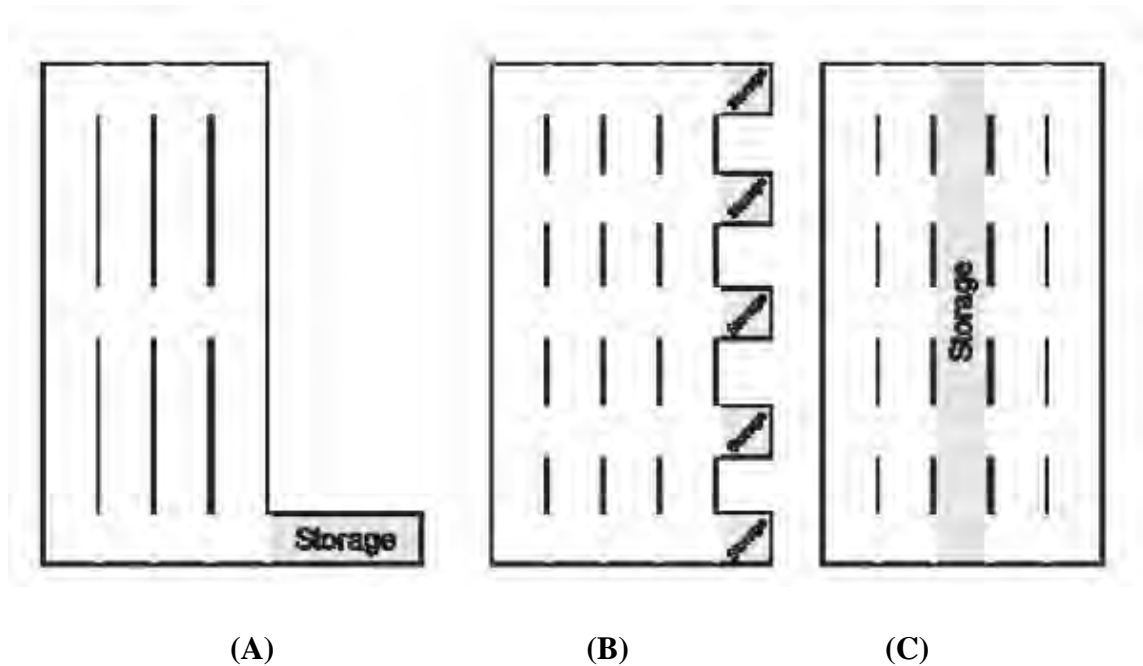


Figure 24: Storage possibilities.

The working principle of this system consists of several platforms, which are moved by electric motors along the vertical and horizontal rails. Platforms have specific movement. There are platforms to mount cars only; for instance these platforms are mounted over others platforms that move only in the vertical or horizontal directions (in each floor level, some of the platforms can be moved only in the vertical rails and the

others in the horizontal rails). The movements of each platform are controlled by a computer software.



Figure 25: Artistic view of the robotic parking

Potential use of linear motor technology in people and cargo transport may impact the future of elevator designs, buildings architecture and resource optimization. This work proposes a new elevator system based on the Berdud Linear Electrical Motor to allow improvements in the car traffic and location.

CHAPTER III: Mathematical Formulation

The system considered in this research is shown schematically in Figure 26. The motor has two rails, which are built with permanent magnets with the ‘T’ poles between each magnet that concentrate the magnetic field. The rails are stationary (stator) and the coil is moving. The coil is formed by an array of electro-magnets. When the current passed through the coil a magnetic field is induced. The magnetic field is concentrated in the nucleus by the effect of iron magnetization. Then, when coil passes between the rails with a certain velocity, the magnetic field of the permanent magnet is perturbed and a force on the coil is generated as the coil magnetic field switches.

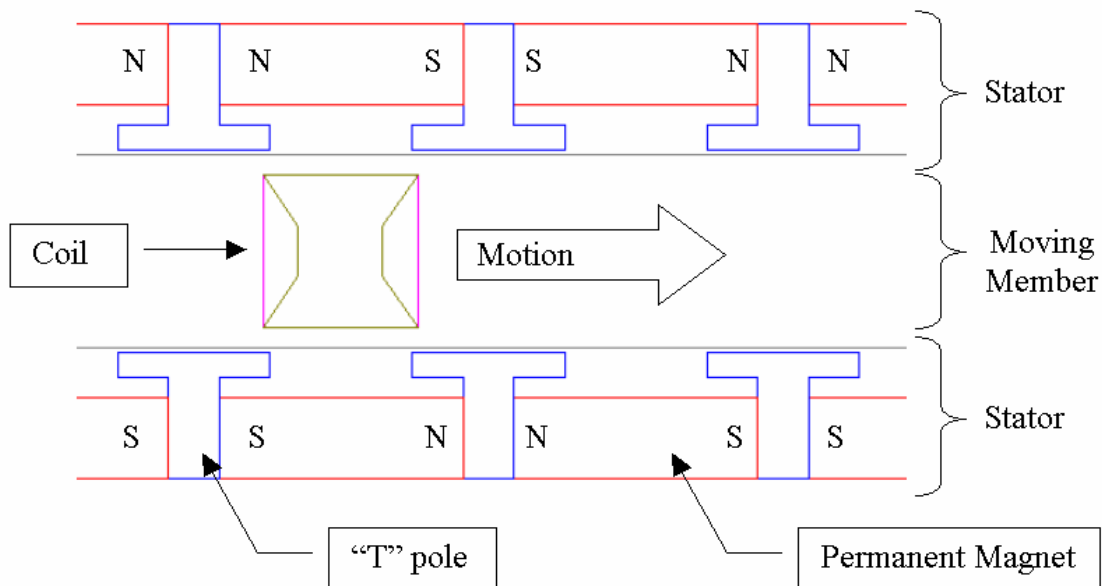


Figure 26: Diagram.

With an appropriate control of the current direction, it is possible to obtain force acting always in the same direction. As the coil moves from one set of poles to the next

the current in the coil must be switched in order to maintain the reaction force in the same direction. Similarly, the current may be controlled to obtain accelerations, steady state operation and regenerative braking. The governing equations necessary to describe the behavior of the motor are Maxwell's equations, coupled with Newton's second law. In this chapter, the governing equations will be analyzed and the boundary and initial conditions will be established. Also, the finite element formulation of the problem will be presented. In addition, because efficiency is the principal parameter to compare different electrical motors, the sources of power loss will be explained to show how they enter into the numerical model.

3.1. Governing Equations

The basic physical equations that describe the electromagnetic fields are given by Maxwell's equations [29]:

$$\nabla \cdot B = 0 \quad (1)$$

$$\nabla \cdot D = \rho \quad (2)$$

$$\nabla \times E = -\frac{\partial B}{\partial t} \quad (3)$$

$$\nabla \times H = J + \frac{\partial D}{\partial t} \quad (4)$$

Where ∇ is the Del-operator, B is the magnetic field, D is the current displacement, ρ is charge density, E is the electric field, H is the magnetic field intensity, J is the current density and t is time. The first equation establishes the absence of a magnetic isolated pole (in other words a north pole can not exist without a south

pole) and the second equation relates the total charge in the domain to the electric field.

For our analysis, the first two do not contribute with any new relationships.

The electrical constitutive equations are:

$$D = \varepsilon E \quad (5)$$

$$H = \frac{B}{\mu} - M \quad (6)$$

$$J = \sigma(E + \dot{x} \times B) \quad (7)$$

Where ε is the dielectric constant, μ is the magnetic permeability, M is the magnetization, σ is the electric conductivity and \dot{x} is the velocity vector. Equation (7) is usually referred to as Ohm's law. Combining equation (4) with equations (5) and (6) yields:

$$\nabla \times B = \mu J + \mu \nabla \times M + \mu \varepsilon \frac{\partial E}{\partial t} \quad (8)$$

The term $\nabla \times M$ is sometime called the magnetization current and is designated by J_m . In the term $\mu \varepsilon \frac{\partial E}{\partial t}$ by definition $\mu \varepsilon = \frac{1}{c^2}$ where c is the light velocity. This term is important when the change in the time of electric field is in the order of light velocity and it is not the case study in this thesis and the term is neglected:

$$\nabla \times B = \mu J + \mu \nabla \times M \quad (9)$$

Equations, (1)-(9), are presented in terms of the vector field variables E , D , B and H , but usually these equations are solved using vector potential formulation. The magnetic vector field B can be written in the term of the vector potential A as:

$$B = \nabla \times A \quad (10)$$

With this form to express the magnetic field, the first of Maxwell's equation (1) is automatically satisfied:

$$\nabla \cdot B = 0 \quad (11)$$

$$\nabla \cdot (\nabla \times A) = 0 \quad (12)$$

Then, the electric field is expressed in function of the scalar potentials v and vector potential A substituting equation (10) in equation (3):

$$\nabla \times E + \nabla \times \frac{\partial A}{\partial t} = 0 \quad (13)$$

Or:

$$\nabla \times (E + \dot{A}) = 0 \quad (14)$$

The vector, $E + \dot{A} = 0$, thus has zero curl and can be written as the gradient of a scalar v :

$$E = -\dot{A} - \nabla v \quad (15)$$

Then, substituting these relations (7), (10) and (15) into the fourth Maxwell's equations, (9), and operating, an equation in terms of the magnetic vector potential is obtained [30], [31]:

$$\nabla \times \nu \nabla \times A = J_s - \sigma \dot{A} - \sigma \nabla v + \nabla \times M + \sigma \dot{x} \times \nabla \times A \quad (16)$$

where ν is the magnetic reluctivity defined by $\nu = 1/\mu$. The physical interpretation of each term is a follow:

J_s Represents any other current source.

$\sigma \dot{A}$ Represents the induced eddy currents due to skin effects. For example when an electromagnet is subject to an AC current, a current appears in the core. This current is known as an eddy current.

$\sigma \nabla v$ Represents the current that passes through a conductor when it is under the effect of an electric field.

$\nabla \times M$ Represent the equivalent current that is originated by the change of the magnetization.

$\sigma \dot{x} \times \nabla \times A$ Represents the interaction in the system resulting from the motion of a DC source, such as a magnet, near a conductor. For example when a conductor and permanent magnet have a relative motion, a current is induced in the conductor (for example in the coil of generator).

On other hand, applying conservation of linear momentum over a rigid a body leads to Newton's law, which can be written, has:

$$m\ddot{x} + C\dot{x} + kx = F \quad (17)$$

Where F is considered a body force and is the sum of forces originating from the electro-magnetic field and also from external forces such as drag, gravity and others. Here, m is the mass of the moving body, C is the damping coefficient, k is the stiffness and x represents the positions of the body with respect to an inertial reference system and the dot over the x represent the rate of change in time.

The electro-magnetic problem and the mechanical problem are coupled through Lorenz's force. Lorenz's force, F_l , is the net force produced from the electric and magnetic field:

$$F_l = \rho(E + J \times B) \quad (18)$$

Lorenz's force is the force that appears when a electric charge is moving (J) into a magnetic field (B). Also the term F_l includes the force that appears over an electric

charge when it move into an electric field E . Substituting E using equation (14) and B by its equivalent vector field potential (10):

$$F_l = \rho(J \times \nabla \times A - \nabla v) \quad (19)$$

If the only force acting on the coil is Lorenz's force, then, the equations of motions yields:

$$m\ddot{x} + C\dot{x} + kx = \rho(J \times \nabla \times A - \nabla v) \quad (20)$$

Finally in order to solve a time dependent problem for example the transient behavior of an electrical motor, the coupled equations (16) and (20) need to be solved. The link between both equations, (16) and (20), are the velocity \dot{x} , the vector potential v , the current J and the vector magnetic potential A :

$$\left\{ \begin{array}{l} m\ddot{x} + C\dot{x} + kx = \rho(J \times \nabla \times A - \nabla v) \\ \nabla \times v \nabla \times A = J_s - \sigma \dot{A} - \sigma \nabla v + \nabla \times M + \sigma \dot{x} \times \nabla \times A \end{array} \right\} \quad (21)$$

In this system of partial differential equations the physical parameter m , C , k , ρ , v , J_s , v , and M are specified, and A and x , will be calculated. In addition to solve these coupled equations a set of initial and boundary condition are needed. In the next section these will be explained.

3.2. Boundary and Initial Conditions

In order to solve the systems of equations, it is necessary to impose appropriate initial and boundary conditions. The boundary conditions for Maxwell's equations can be: Neumann or natural boundary conditions, Dirichlet or value boundary conditions or balloon boundaries, [30].

3.2.1 Neumann Or Natural Boundary Conditions

The Neumann boundary condition for the magnetic field B can be obtained integrating the first of Maxwell's equations (1) over a cubic control volume that encloses the interface between two materials, obtaining:

$$B_{1n} = B_{2n} \quad (22)$$

Where the subscript 1 and 2 are reference to both materials at the interface and n is reference to the normal direction to the interface surface. That is, the magnetic field B can be continuous along the normal direction of the interface between both materials.

The Neumann boundary condition for the magnetic field intensity H is obtained integrating the fourth Maxwell equation (4) over the surface bounded for a rectangular loop that includes the interface between both materials, obtaining:

$$H_{1T} - H_{2T} = j_{s\perp} \quad (23)$$

Where the subscript 1 and 2 are reference to both materials at the interface and the subscript T is reference to the tangential direction to the interface surface. The term $j_{s\perp}$ represents the component of the current density in a perpendicular direction with respect to H , but this current is zero for finite conductivity [30], hence:

$$H_{1T} = H_{2T} \quad (24)$$

That is, the magnetic intensity field H can be continuous through the tangential directions of the interface of the materials.

In equation (10) the value of the magnetic field B in cartesian coordinates can be written in terms of A as:

$$B = \nabla \times A = \frac{\partial A}{\partial y} \hat{i} + \frac{\partial A}{\partial x} \hat{j} \quad (25)$$

Where \hat{i} and \hat{j} are versors that represent the direction of the x and y axes. In component form:

$$B_x = \frac{\partial A}{\partial y} \quad (26)$$

$$B_y = \frac{\partial A}{\partial x} \quad (27)$$

For example for a horizontal boundary condition if A is constant along the x axis, then from equation (12):

$$\nabla \cdot (\nabla \times A) = \frac{\partial^2 A}{\partial y^2} + \frac{\partial^2 A}{\partial x^2} = 0 \quad (28)$$

Because $\frac{\partial^2 A}{\partial x^2} = 0$, then $\frac{\partial^2 A}{\partial y^2} = \frac{\partial B_y}{\partial y} = 0$ which automatically satisfies relation

(22). If the boundary condition is a boundary value in terms of H , it can be transformed into a boundary value in terms of B using the electrical constitutive equations (6) and then in terms of A using equation (25).

3.2.2 Dirichlet Or Value Boundary Conditions

The Dirichlet boundary condition for the magnetic field and the magnetic field intensity are a set of values at the boundary. That is:

$$B|_{\Gamma} = B_0 \quad \text{and} \quad H|_{\Gamma} = H_0 \quad (29)$$

Where Γ is the boundary zone B_0 and H_0 are specific constant values. In equation (10) the value of the magnetic field B in cartesian coordinates can be written in terms of A as:

$$B = \nabla \times A = \frac{\partial A}{\partial y} \hat{i} + \frac{\partial A}{\partial x} \hat{j} \quad (30)$$

Where \hat{i} and \hat{j} are vectors that represent the direction of the x and y axes. For example, for a horizontal boundary condition, the partial derivate of A respect to x will be zero forcing B to have an x component equal to the derivative of A respect to y .

If the boundary condition is a boundary value in term of H , it can be transformed into a boundary value in terms of B using the electrical constitutive equations (6) and then in terms of A using equation (30).

3.2.3 Balloon Boundaries

When a balloon boundary is applied to a zone, it is equivalent to isolating this zone from other sources of current or magnetic fields. The effect of the balloon boundary is that the background of the zone is extended to the infinity. Mathematically, this type of boundary is expressed as the magnetic vector potential A equal to zero at infinity.

3.2.4 Initial Conditions

The initial conditions for the magnetic field are selected according with Maxwell's equations and the array of permanents magnets. The initial conditions for the mechanical equations of motion specify the initial position and initial velocity.

3.3. Source Terms

The magnetic field generated by the permanent magnets is modeled as an equivalent current sources. The known equivalent currents densities are defined as:

$$J_m = \nabla \times M \quad (25)$$

$$(26)$$

$$K_m = M \times \hat{n}$$

Where M is the magnetization, \hat{n} is the normal direction of the surface of domain, J_m is an equivalent volumetric current density originated by the magnetization and K_m is an equivalent laminar current that travels on the surface of the magnet as shown in Figure 27.

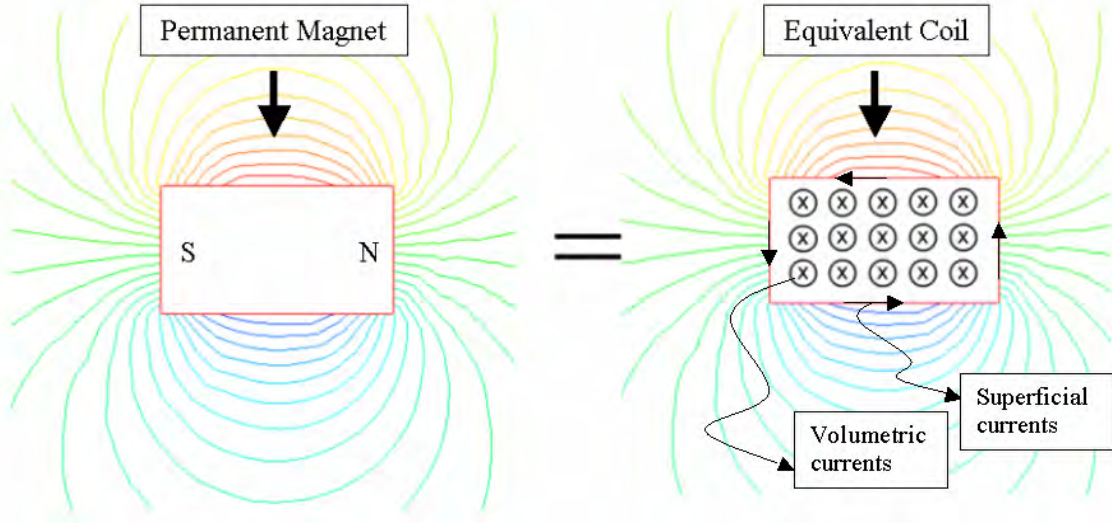


Figure 27: Equivalent magnet field of current density.

According to Plonus [32], these two equivalent currents are equivalent to the following magnetic field:

$$B = \frac{\mu}{4\pi} \iiint_{\Omega} \frac{J_m \times R}{|R|^3} d\Omega + \frac{\mu}{4\pi} \iint_S \frac{K_m \times R}{|R|^3} dS \quad (28)$$

Where Ω is the domain of the permanent magnet, S is the surface of the domain of the permanent magnet and R is the vector position where the equivalent current J_m and K_m are calculated. Also, it is necessary to add another current source in the zone where the coil windings are.

3.4. Numerical Analysis

The partial differential equations (20), are nonlinear and coupled and there is no analytical solution available. To solve them a numerical technique is necessary. Many techniques are available, the most common techniques used are Finite Difference Methods (FDM), Finite Element Methods (FEM), and Boundary Element Methods (BEM). In this work, the finite element method is chosen. The commercial software selected for this study was Maxwell[®] [33,34,35], because it is able to solve the coupled electromagnetic and mechanical dynamic equations. This software is also able to solve two and three-dimensional transient electromagnetic problems. In order to solve the model developed in this thesis, the two-dimensional version was used.

This software required four basic steps to arrive to the problem solution. In the first step the model is drawn and the material and mechanical properties set. Second, the domain is meshed and the boundary conditions are set. Third, the resulting matrix system for the problem is solved and fourth, the post processing analysis is performed. Figure 28 shows these steps for the linear motor problem.

The Maxwell software only uses a triangular element to mesh the domain and linear interpolation functions to approximate the solution. The linear interpolation function for triangular elements is:

$$\psi_i = \frac{1}{2Ae} \{ (x_j y_k - x_k y_j) + (y_j - y_k)x + (x_k - x_j)y \} \quad (29)$$

Where ψ_i is known as a polynomial weight function, Ae is the element area, x_{ijk} and y_{ijk} are the coordinates of the triangle's vertices and x and y are any point in the domain of the element.

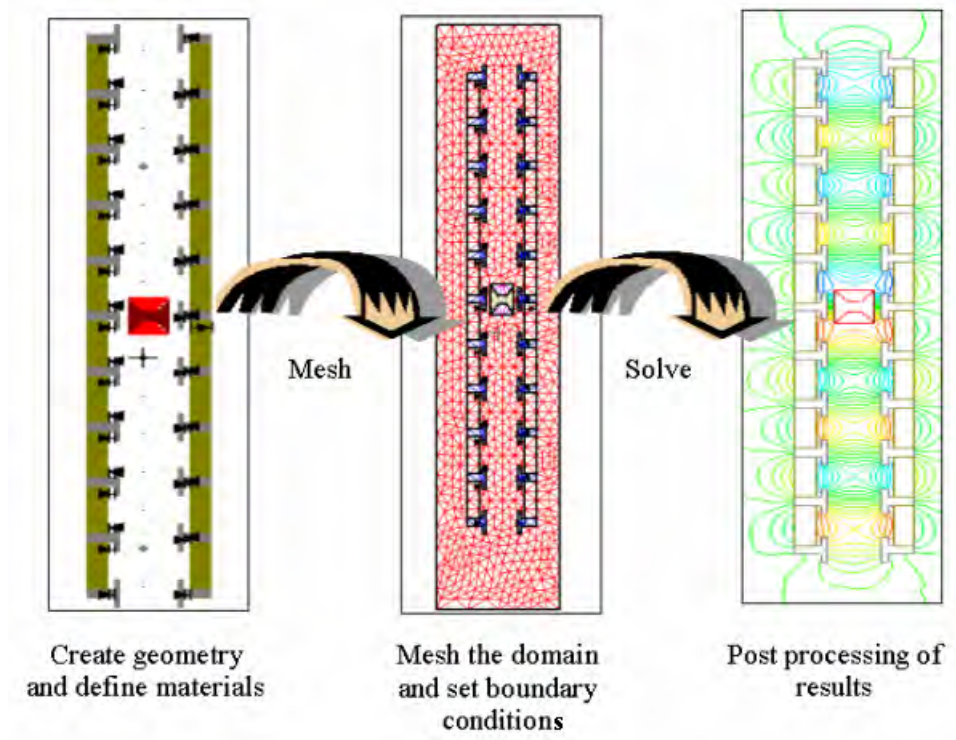


Figure 28: Steps in solving the model.

The unknown vector potential A is approximated in a particular element e by this interpolation function as:

$$A^e(x, y, t) = \sum_{i=1}^3 a^e(t) \psi_i^e(x, y) \quad (30)$$

Since the reluctivity ν depends on the magnetic flux B and the material properties, in order to simplify the problem, it is assumed constant with in each element. Then, substituting the approximation (29) into equation (30) and then into equation (16)

and integrating over a generic element e ; equation (16) can be rewritten as an ordinary differential equation:

$$[C]^e \dot{a}^e(t) + [K]^e a^e(t) = \{J\}^e \quad (31)$$

Where:

$$[K]^e = \nu \int_{\Omega} (\nabla \times \psi^T)^T (\nabla \times \psi^T) dxdy - \sigma \int_{\Omega} \psi (\dot{x} \times \nabla \times \psi^T) dxdy + \sigma \int_{\Omega} \psi (\nabla \psi^T) \nu dxdy \quad (32)$$

$$[C]^e = \sigma \int_{\Omega} \psi \nabla \psi^T dxdy \quad (33)$$

$$\{J\}^e = \int_{\Omega} J_s \psi^T dxdy + \int_{\Omega} (\nabla \times \psi^T)^T H_c dxdy \quad (34)$$

Thus in the last equations, to evaluate the $[K]^e$ and $[C]^e$ matrices and the vector $\{J\}^e$; the reluctivity ν and the conductivity σ are assumed constant and can be taken out of the integral, therefore assuming the same type of solution to it's linear counterpart. ν is constant within each element but changes in value from element to element.

To solve both coupled equations (31) and (20), the first order ordinary differential equation in time for the magnetic vector potential A and the second order ordinary differential equation in time for the dynamics, it is required to set which parts of the model are moving. The section of the model that moves is outside. This part is called the “band” and all the motion constrained to occur within the band. The mesh outside the band and inside the band containing the moving objects is maintained constant during the simulation. Whereas, the mesh between the outside of the band and the moving part, is updated and displacements recalculated at each time step, Figure 29.

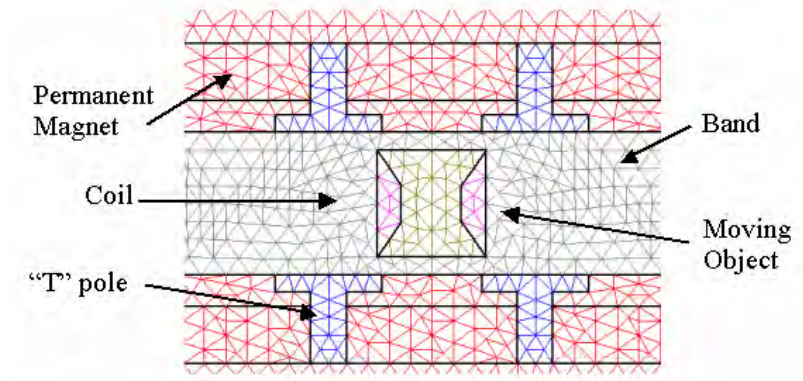


Figure 29: Maxwell mesh.

This update is done computing the residuals and comparing with the maximum residual permissible. In Maxwell's software the residuals are computed using the total field energy. Figure 30 shows the logic diagram that Maxwell software uses to iterate and minimize the residuals at each time step [35].

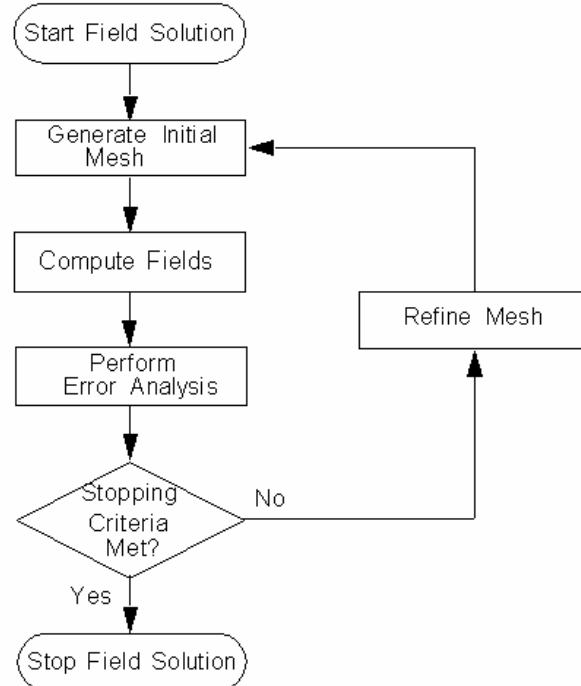


Figure 30: Logic diagram of iteration in each time step.

The finite element solution at any point in an element is defined in (28) as

$A^e(x, y, t) = \sum_{i=1}^3 a_i^e(t) \psi_i^e(x, y)$. Then, the derivatives are computed in the following form

$$\frac{\partial A^e}{\partial x} = \sum_{j=1}^n a_j^e \frac{\partial \psi_j^e}{\partial x}, \quad \frac{\partial A^e}{\partial y} = \sum_{j=1}^n a_j^e \frac{\partial \psi_j^e}{\partial y} \quad (35)$$

It should be pointed out that the derivatives of A^e will not be continuous at interelement boundaries, because continuity of the derivatives is not imposed during the assembly procedure. In practice the discrepancies of the derivatives from one element to the next can be reduced either by increasing the number of elements or increasing the order of the polynomial weight function ψ_i (equation (27)).

In Maxwell's software the polynomial weight function is fixed to a first order interpolation. Utilizing the definition of ψ_i in equation (27) and combining with equation (33) yields:

$$\frac{\partial \psi_j^e}{\partial x} = \frac{1}{2Ae} (y_j - y_k), \quad \frac{\partial \psi_j^e}{\partial y} = \frac{1}{2Ae} (x_k - x_j) \quad (36)$$

$$\frac{\partial A^e}{\partial x} = \sum_{j=1}^n \frac{a_j^e}{2Ae} (y_j - y_k), \quad \frac{\partial A^e}{\partial y} = \sum_{j=1}^n \frac{a_j^e}{2Ae} (x_k - x_j) \quad (37)$$

With this equation and the definition of magnetic vector potential equations (10) it is possible to obtain the magnetic flux density B in a post processing operation.

3.5 Power Loss

The most important power losses are originated by the eddy currents in the core of the coil and hysteresis cycle as a consequence of the ferromagnetic properties of the core.

Another area of power loss is friction; this is present if power to the coils is transmitted using brushes.

When alternating electrical current is applied to an electromagnet an electromagnetic force (EMF) is generated. In addition, the core of the coil is generally made of high electric conductivity materials, therefore, a current is generated by this EMF. This current is known as an eddy current, and it is capable of fusing the core. The total power dissipated by the eddy currents can be approximated as [32]:

$$P_e = K_e \sigma \omega^2 B^2 \quad (38)$$

Where K_e is a constant that depend on the geometry, σ is the electric conductivity, ω is the frequency of the applied electromagnetic field, B is the intensity of electromagnetic field. For that reason techniques to reduce the conductivity of the core are used. One technique uses materials with low electric conductivity and hard magnetic properties such as silicon-steel alloy. It has an electric conductivity of $1.66 \cdot 10^6$ S/m (steel has an electric conductivity of $13.5 \cdot 10^6$ S/m). But, the most popular technique uses a laminated core. The numerical strategy to simulate a laminated core recommended by the Ansoft's Maxwell software® [36] is through the use of an equivalent electric conductivity:

$$\sigma_{eff} = \frac{\sigma SF}{N^2} \quad (39)$$

Where σ_{eff} is the effective electric conductivity, SF is the stackin factor and N is the number of laminations. For the simulations done in this work a SF of 0.95 and N of 15 are used. With these values, an effective electric conductivity σ_{eff} of 4.35×10^4 [S/m] is obtained for the core material.

The second important point of losses is the hysteresis cycle in the ferromagnetic materials. When an external cyclic magnetic field is applied to a ferromagnetic material, it should be magnetized and demagnetized in the same form in each cycle. In practice this is not true, the presence of inclusions, cavities and crystallographic imperfections originate friction in the alignment process of the magnetic particles in the direction of the applied field. After the first time, in each cycle of charge and discharge energy is dissipated through this mechanism. Figure 31 shows a typical curve of charge and discharge of a ferromagnetic material. Also, in the same figure the dashed curves represent the first time the magnetic field is applied.

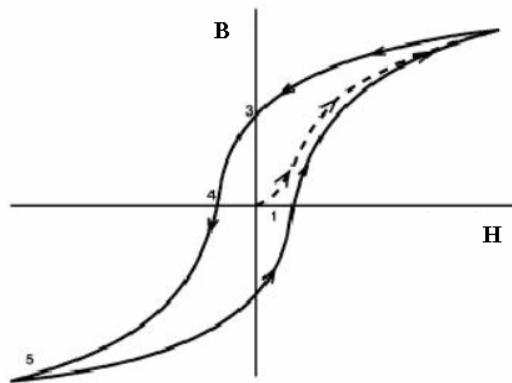


Figure 31: Hysteresis loop

The total energy dissipated in each cycle is proportional to the area between the charge and discharge curves. Usually, with the objective to simplify this curve for numerical purposes, it can be approximated using the H-B curve relation such as it is shown in Figure 32. This curve is easier to implement and it is set only for a quarter of the curve. The other part of the curve is calculated by symmetry. The reference points in

these curves are the parameters used to set the numerical model such as the coercivity H_c and the magnetic retentivity B_r and the relative permeability μ_0 .

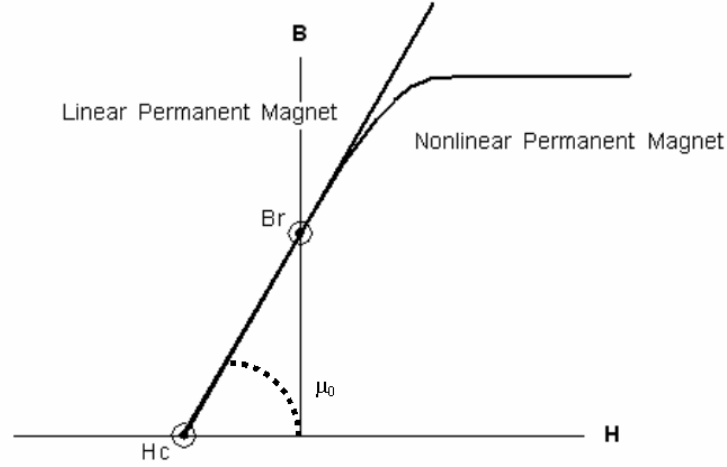


Figure 32: Normal B-H Curve

For linear materials only two of the three quantities (μ and magnetic coercivity H_c or magnetic retentivity Br) but for nonlinear materials it is necessary to set the curve point to point based on experimental results or as provided by the manufacturer. Figure 33 show a typical B-H curve for the permanent magnet known as Ceramic 5. This is a low cost magnet considered in the design of linear motor. For other materials such as iron, it can be approximated using a linear behavior and it is only necessary to specify the relative magnetic permeability μ , which for the iron is 4000 and the magnetic coercivity H_c which is 0.

The power dissipated by the hysteresis cycle may be also computed using the empirical relation know as Steinmetz equations [32]:

$$P_h = K_h \omega B^{1.6} \quad (40)$$

Where K_h is the hysteresis coefficient ω is the frequency of the cycle and B is the maximum amplitude of the flux density. K_h is a constant obtained experimentally for each case. For high quality steel alloys containing silicon, K_h is usually 0.001 and for soft steel it varies from 0.002 to 0.004 for P_h in $[\text{w/m}^3]$ ω in $[\text{1/s}]$ and B in $[\text{Gauss}]$.

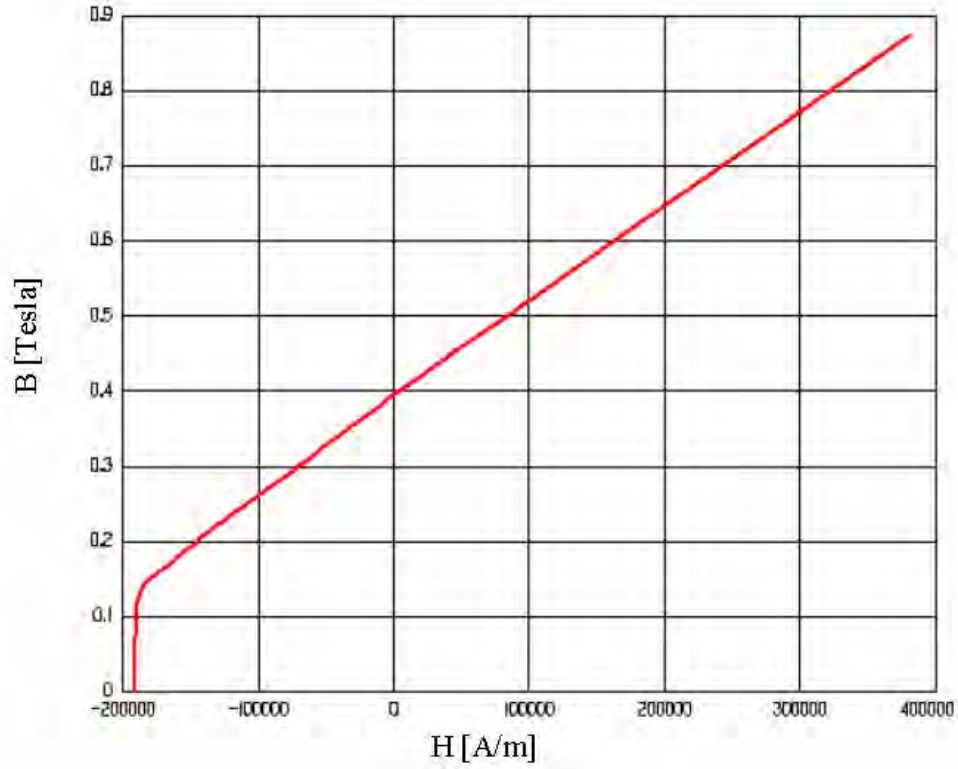


Figure 33: B-H curve for Ceramic 5

CHAPTER IV: Numerical Results

A prototype of the Berdut linear motor developed as a proof of concept model was selected as a reference point for validating the numerical model and starting configuration for the optimization.

In this chapter a numerical model is developed based on the theory presented in the previous chapter. The next chapter presents a validation of the model developed in this chapter with experiments using the physical prototype.

4.1. General Analysis

The analysis in this chapter is done for a motor with one coil. The effect of more than one coil is studied in section 4.3.4. Figure 34 shows the dimensions and properties of the reference motor. Ceramic 5 permanent magnet are used for the stator magnets. 1010 steel “T” poles are used between the magnets as shown in the Figure. As the coil travels the current in the coil will be switched such that a net force on the coil is produced.

First, the correct location to perform the current switching in the coil is determined. For this purpose, a simulation of the motor without considering the velocity of the coil (static analysis) and with the same polarization of the coil is used in all the positions studied. The force reaction on the coil is saved as a function of longitudinal position. The results, axial force versus position, are show in Figure 35.

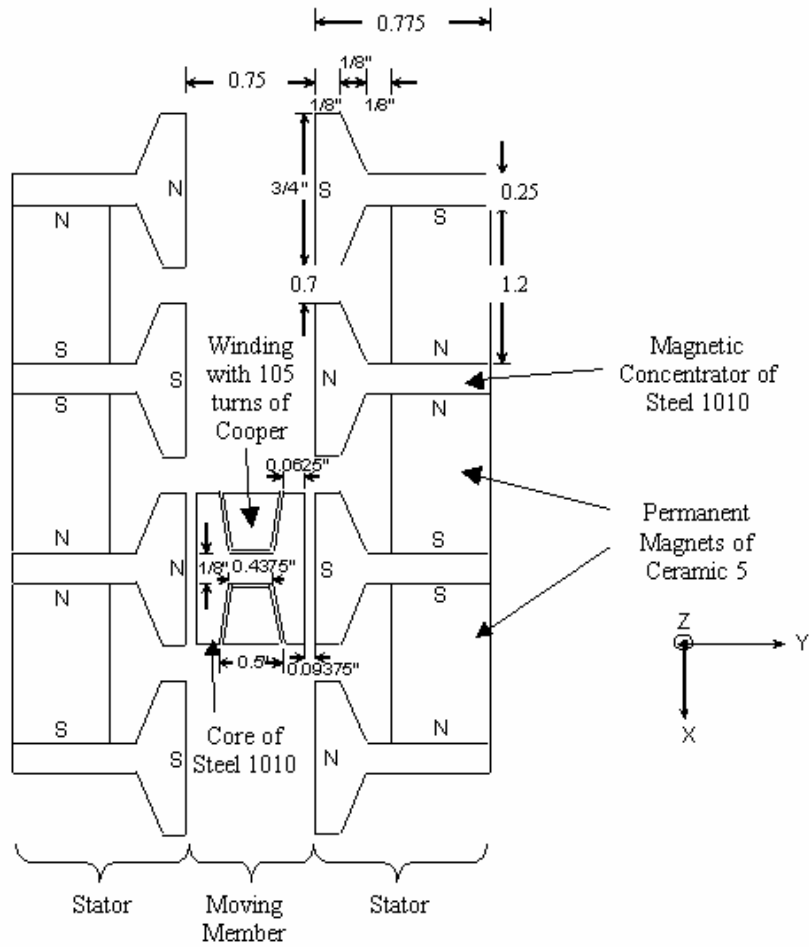


Figure 34: Motor dimensions and material properties

The point “zero” was chosen with coil centered with the “T” pole, such as is shown Figure 34. Then, with this result, the location where the current in the coil should be switched to change the negative axial force in a positive axial force can be determined. Note that the specific point where the axial force changes negative to positive is when coil is passing centered in front of the next “T” pole. This implies that the current in the coil should be such that the coil is in attraction with the pole that it is approaching and then, when it arrives to the pole it should switch polarity such that it is now attracted to the next pole after that.

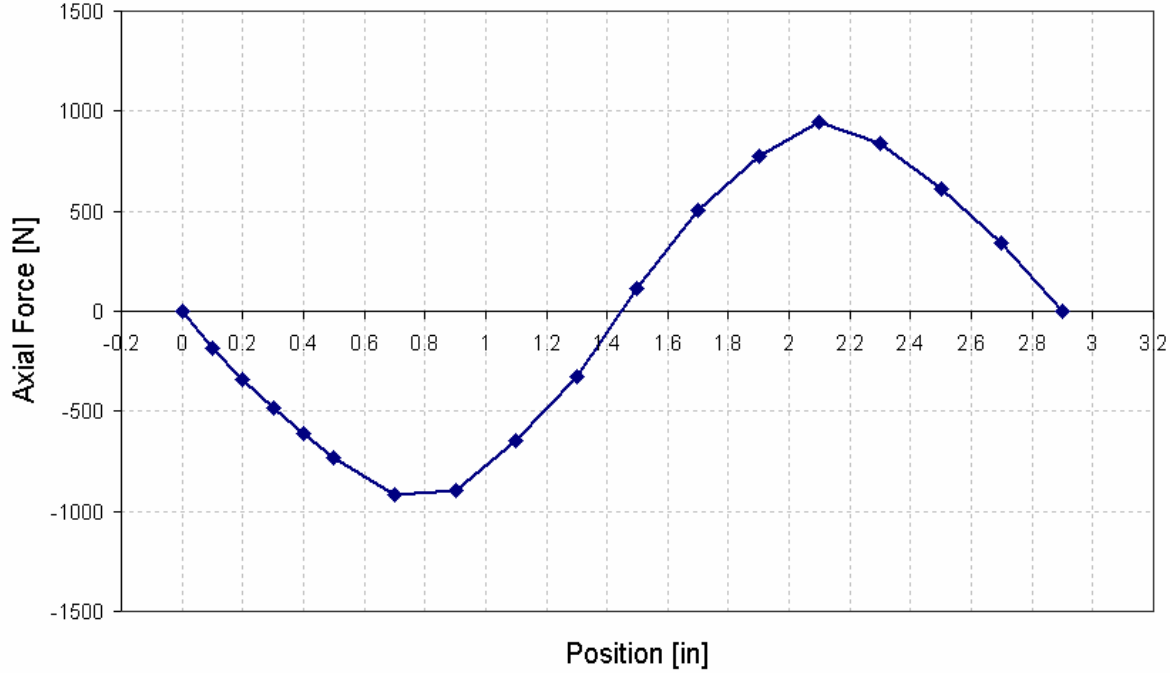


Figure 35: Force Diagram and Motor dimensions.

Next, the effect of the net force on the coil is analyzed for different current profile. Under the conclusion obtained in the previous paragraph, the current profile was first analyzed as periodic rectangular wave as shown in Figure 36 (A). A rectangular wave with zero current time interval (dead time) it was also studied, see Figure 36 (B). The dead time is a zone where the coil is not energized. This dead time is set when the coil is exactly passing in front of the “T” pole. This period is not the same length as the “T” pole.

In the previous static analysis the speed of the coil was not considered, but now the motion dynamic of the motor are included. The required current switching strategies are presented as a current profiles in time such as those shown in Figure 36.

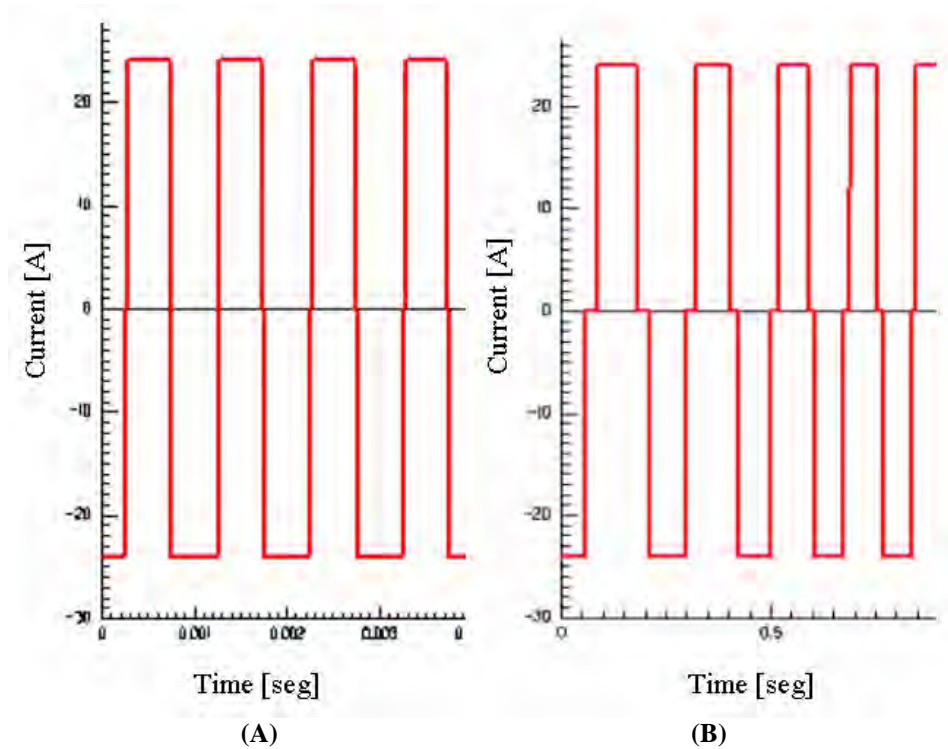


Figure 36: Rectangular wave (A) without dead time (B) with dead time

Because the current was plotted versus time, the period of the wave decreases. This is due to the acceleration of the coil, which causes the coil to pass subsequent pole in shorter time periods.

The simulations result obtained indicates that the axial force decreased as the distance (dead time), where the coil is not energized, is increased. Also, effect of the current intensity was studied. As the current intensity was increased the axial force also increased. These results are shown in Figure 37. The current used in the simulation was 24, 36 and 48 amperes.

The effect of a relative shift in distance “ δ ” between facing poles in the stator was also studied. Another important result obtained from the simulations is that the small shift between the positions of the stator or rails, Figure 38, generates an impulsive axial force and as well as a lateral force.

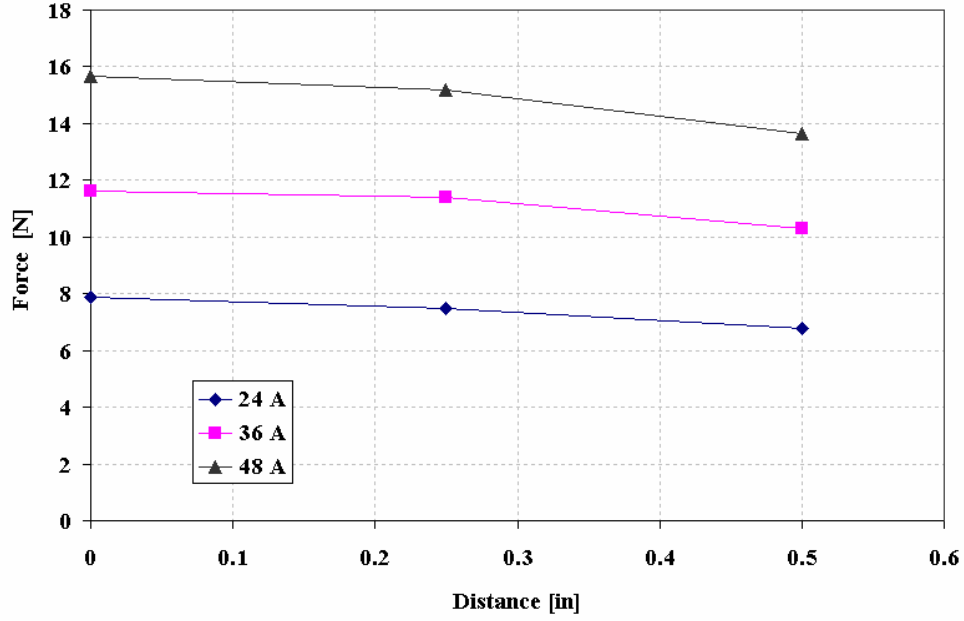


Figure 37: Force decrement as a function of current profile

The result of the simulations performed with a static coil (always in the same place) and constant current (36 ampere), are summarized in Figure 39.

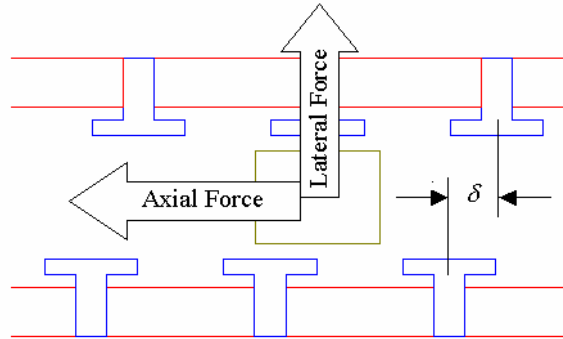


Figure 38: Model used for relative rail displacement

From Figure 39, it can be concluded that for small δ displacement the coil experiences an axial force, larger than the lateral force. As δ increases, both forces increase but there is a point where the lateral force increases in the magnitude beyond the axial force. This last effect is undesirable yet at small values of δ an initial force

favorable to starting the motor is presented and may be exploited in future design if necessary.

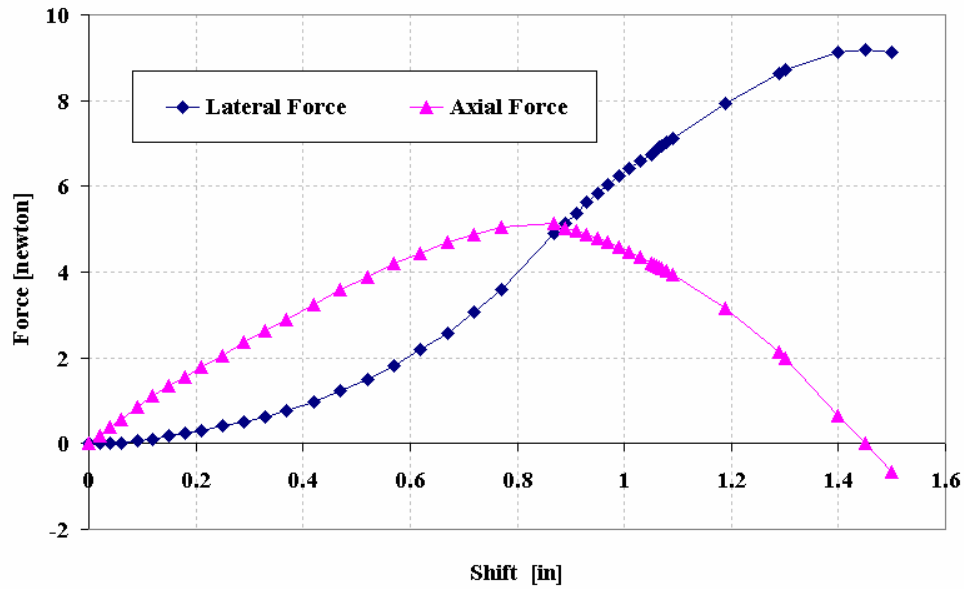


Figure 39: Relative guide displacement effect

4.2. Efficiency Analysis and Thrust Force

Two of the most important parameters in the design of linear motor are the efficiency and the thrust force. The efficiency and thrust force are calculated as a function of the velocity for different configurations of the linear motor. The configurations changed in each analysis were:

1. The dimensions of the “T” poles.
2. Input power.
3. Shift in time of the current switching.

In order to determine the operating point an approach similar to that used by a dynamometer was used. First a load is applied to coil (in the opposite direction to motion) and the simulations are run to determine the velocity (constraint) at which the motor can

sustain this force (equilibrium). This data corresponds to a point in the thrust force-velocity curve of the motor, by evaluating the output power as $P_{out} = F\dot{x}$ (where F is the thrust load added to the numerical model simulation and \dot{x} is the final velocity reached by motor) and the input power as $P_{in} = P_{out} + P_{loss}$ (where P_{loss} is the total power dissipated) it is possible to obtain the theoretical efficiency as the ratio $\eta = P_{out} / P_{in} = F\dot{x} / (F\dot{x} + P_{loss})$. This efficiency corresponds to a point in the efficiency-velocity curve of the motor. The load is varied and new velocity and efficiency values are obtained and another point for each curve is computed. This procedure is repeated to generate the force-velocity curve and efficiency-velocity curve for a particular motor configuration.

4.3.1. Effect of Power

Power input has a special importance as a parameter because it is possible to obtain a wide variety of efficiency and thrust forces by changing it. When the design of the physically the model is well known, this information is required for the design and the operating point of the control system. For this study no shift in the stator is used $\delta = 0$ and the dimensions remain the same as those used in last section, Figure 34. Steel 1010 was used for the “T” poles and the core, cooper for the windings and ceramic 5 for the permanent magnets. Using the conclusions obtained in the first section of this chapter, a rectangular wave without dead time is used for the simulations. In order to simplify the problem, a model with one coil is used.

For this study the power range is varied by changing the current input from 24 to 110 amperes. Figure 40 and Figure 41 show the efficiency and thrust force curves for

different power levels (input current). From these results it can be appreciated that as the current increases the maximum efficiency is lower but the thrust force and maximum velocity are increased.

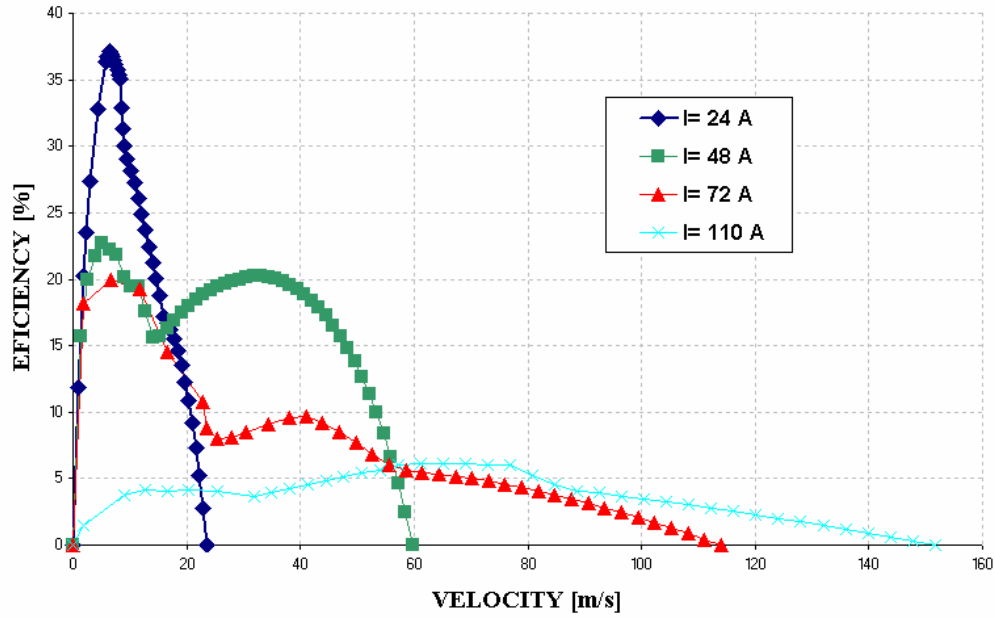


Figure 40: Efficiency curves for different input power levels

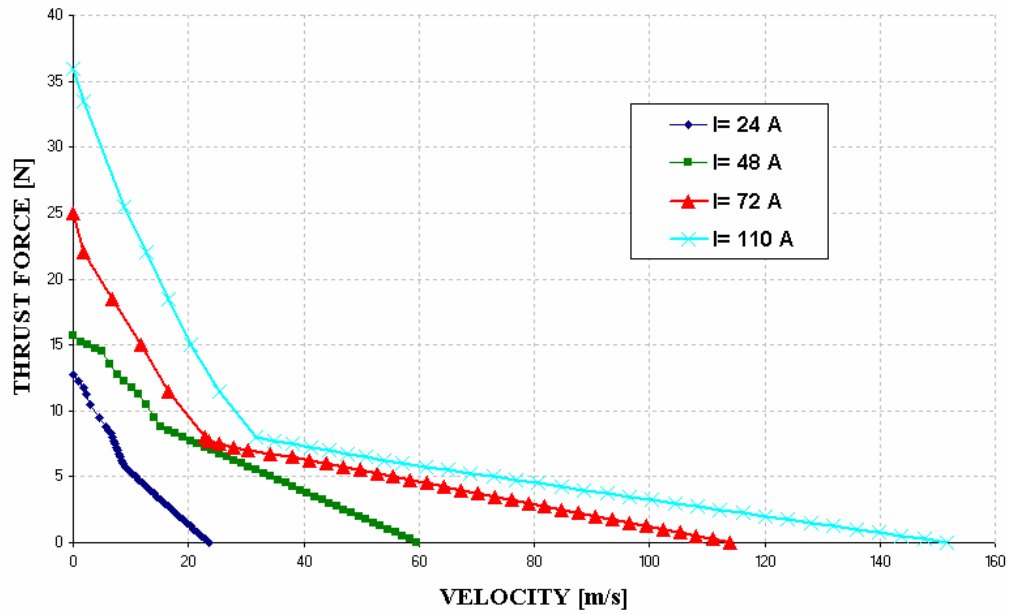


Figure 41: Thrust force for different input power levels

4.3.2. Effect of T Pole Dimensions

One of the components of the motor that most significantly changes the performance is the dimension of the “T” poles. The name of “T” to represent the magnetic concentrator has the origin in the original design, which uses poles of this shape. Various “T” configurations are studied, as listed in Table 1.

The two dimensions varied for the “T” pole were the flange and web width, see Figure 42. The arrays studied were:

1. Actual design.
2. Double flange length.
3. Without flange.
4. No flange and double web width.
5. Without magnetic concentrator (T pole).

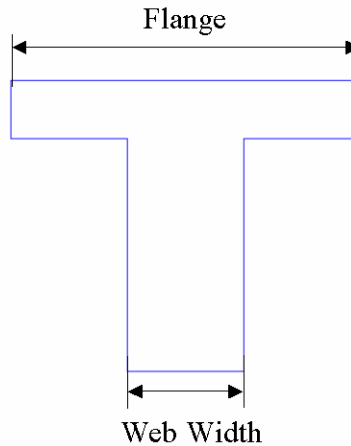


Figure 42: “T” pole parameters

For these analyses a current of 110 amperes is used because it corresponds to the least efficiency from the power level study. Table 1 show the model used. The case of 110 amperes from the last section was chosen as the current design configuration. No

shift in the stator is used and the dimensions remain the same as those in last section, Figure 34, except the dimensions of “T” pole. Steel 1010 was used for the “T” poles and the coil core, cooper for the winding and ceramic 5 for the permanent magnet. Also, rectangular wave without dead time is used for the current profile and one coil is used for the simulations.

Table 1: Concentrator Models

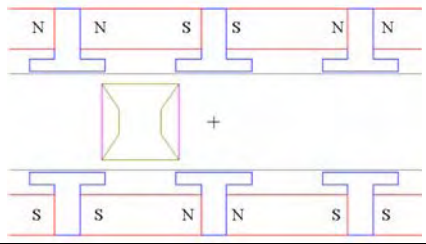
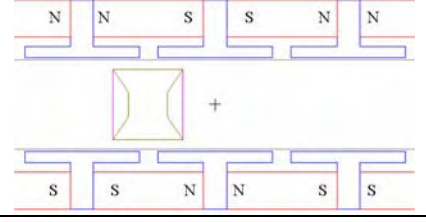
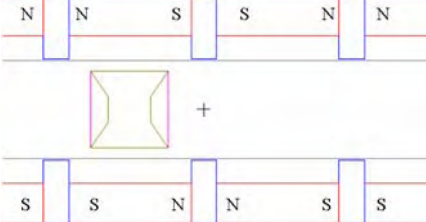
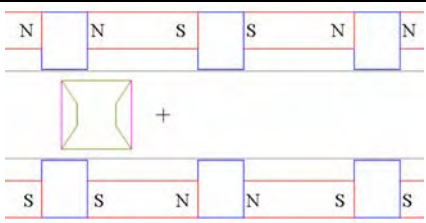
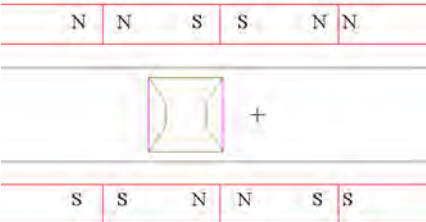
Model	Description
	Current Design
	Double Flange Length
	Without Flange
	No Flange and Double Web Length
	Without T Pole

Figure 43 and Figure 44, show the efficiency curves and thrust force for the different “T” arrays of Table 1. In these figures it can be seen that the model without “T” pole reaches the maximum thrust force over 35 N and also reaches a good maximum efficiency point, close to 7%, but this it is not the best performed.

The case with without flange and with a normal web width has the maximum efficiency point of 9.5% (28% better than not using “T” pole) but increasing the web width (and using no flange) the maximum efficiency decreases at 7%. Therefore an optimum value of web width is expected between zero and current web width. Also, the maximum force for all these cases is decreasing while the web width is increasing. For example, the maximum force for the case without “T” poles is 37N, for the case without flange is 36N and for the case with double web width is 22N. Then, the effect of increasing the flange dimension is counterproductive in all the cases and the case with double flange length has the poorest performance of all the studied cases.

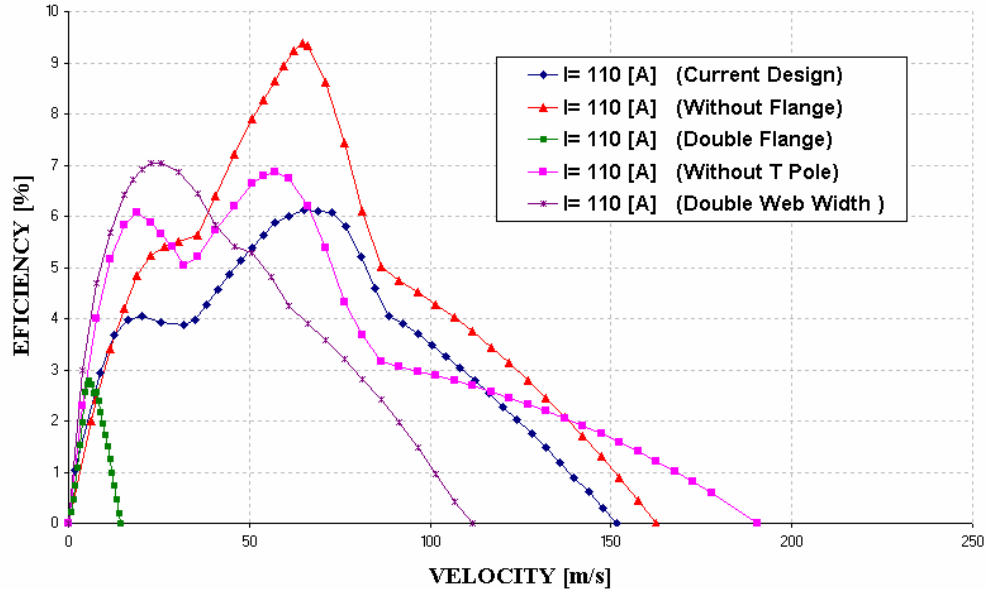


Figure 43: Efficiency curves for different “T” arrays

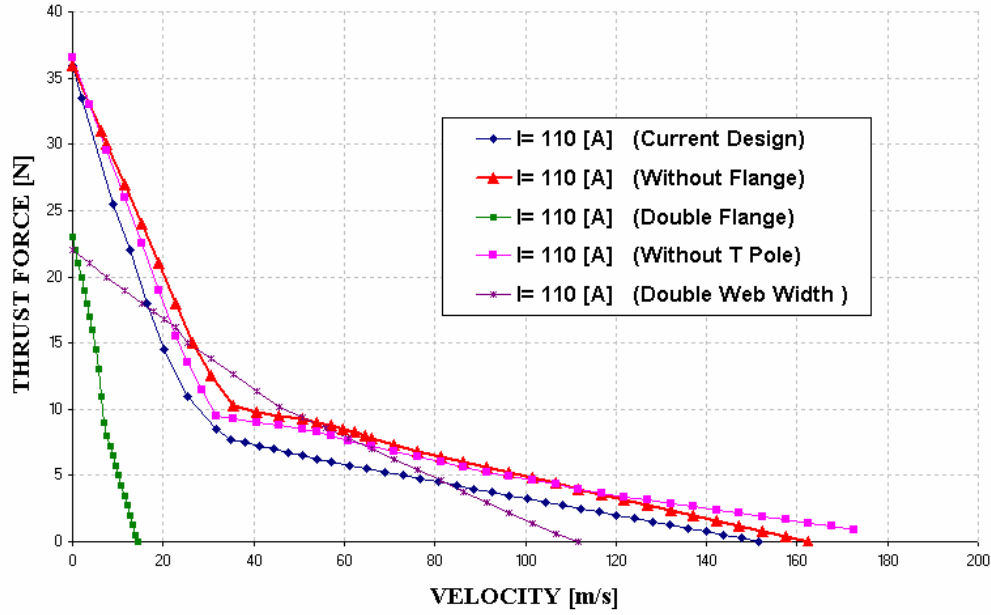


Figure 44: Thrust force curves for different “T” arrays

4.3.3. Effect of Materials

The study of the materials is focused on the material of the permanent magnets and the materials of the coil core. The materials analyzed for the permanent magnets are NdF35 and Ceramic 5. These permanent magnets are the most commonly used in similar devices such as electric motors and actuators.

For this analysis, a current of 24 amperes is used because it corresponds to the case with highest efficiency in Figure 40. The case of 24 amperes of the first section was performed using ceramic5 in the simulation. As before, no shift in the stator is used and the dimensions remain the same as that in Figure 34. In the case of “T” pole dimensions are the original dimensions. Steel 1010 was used for the “T” poles and the core and cooper for the windings. Also, a rectangular wave without dead time is used for the current profile and one coil is used for the simulations

Two types of permanent magnet materials were studied and their most relevant properties are shown. They are:

1. The Ceramic 5 is the most popular permanent magnet and it is also very economic. The ceramic 5 can reach a maximum magnetic field of 0.5 Tesla.
2. The NdFe35 has more magnetic capacity than the Ceramic 5 (maximum magnetic field approximately of 1.5 Tesla) but it is more expensive (4 times for the smaller size and 40 times for the bigger size).

Table 2: Magnetic properties of Ceramic5 and NdFe35

Property	Symbol	Ceramic5	Neodymium	Units
Magnetic Coercitivity	H_c	190985.9	890000	A/m
Magnetic Retentivity	B_r	0.39	1.23	Tesla
Magnetization	M_p	313967.7	978802.9	A/m

Configurations with both types of magnets are analyzed for different power levels inputs. In Figure 45 and Figure 46 the efficiencies and thrust forces for both permanent magnet materials and power levels are shown. In these figures can be appreciated that the NdFe35 improves the maximum efficiency and the maximum thrust force. Both curves have similar behavior, but it is important to note that for velocities greater than of 6.5 m/s Ceramic 5 has more efficiency than NdFe35.

In addition, NdFe35 has always more thrust force than Ceramic 5 except after a velocity of 17 m/s where they have similar behavior. Therefore in general higher forces are expected for similar motors at given speed when NdFe35 is used instead of Ceramic5. For similar motors in each case have a speed range better efficiencies than other.

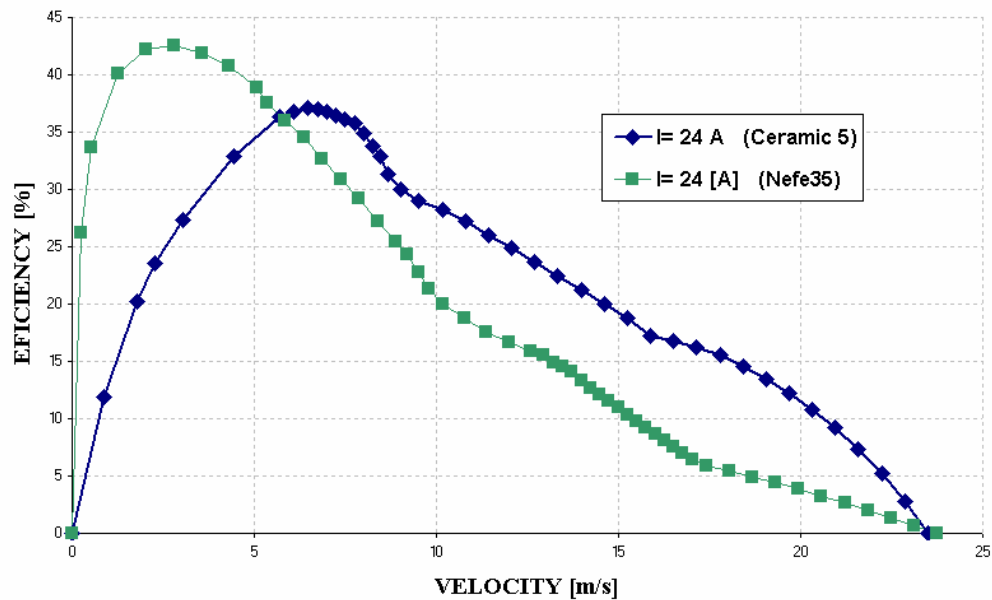


Figure 45: Efficiency curves for different permanent magnet material

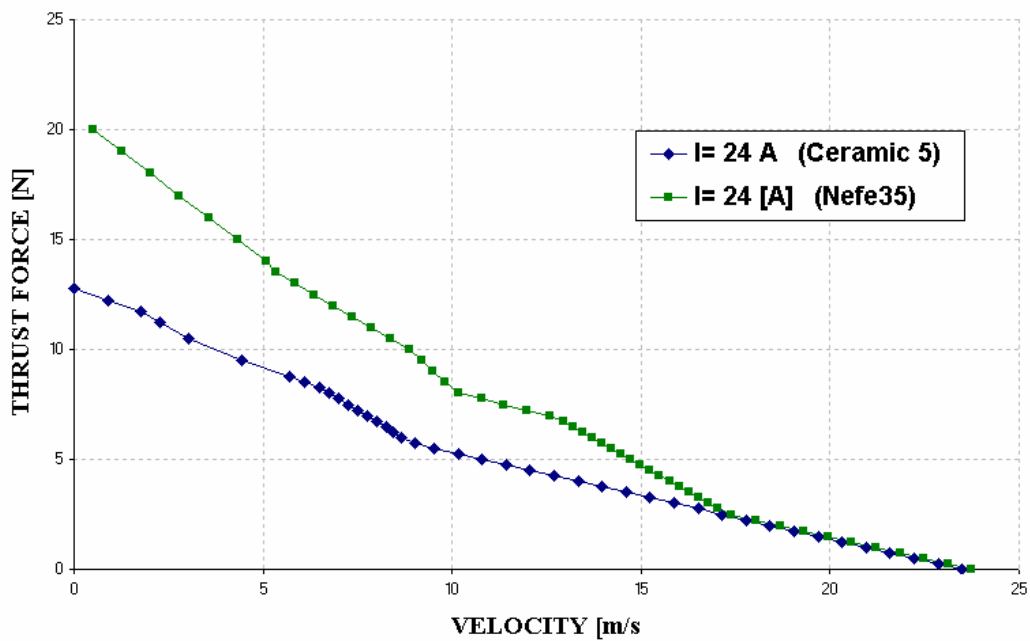


Figure 46: Thrust force curves for different permanent magnet material

4.3.4. Effect of Coil Connections

In this section, the effect of coil topologies on the performance is studied. Continuing with the same kind of analysis as in the previous section the efficiency and the thrust force curve as a function of the velocity are determined. Two coils topologies are studied, the first energizes all coils simultaneously and the coils are located in phase with the poles in the stator. The second topology has one coil located in front of a pole and the following coil is half way between the poles. Table 3 shows both designs. This connection can be interpreted as shifts in the current wave used to energize each coil. In the first case, the current wave energizing each coil is the same but in the second design there is a shift in the wave. For example, in the second topology the shift in the current wave for the case of two coils is 90° . Figure 47 shows the current versus time for the second case, the shift of 90° between each current wave can be appreciated.

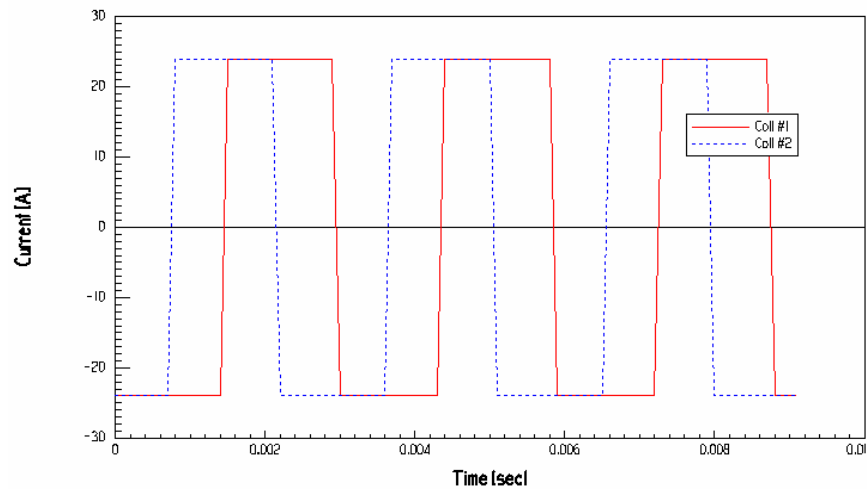


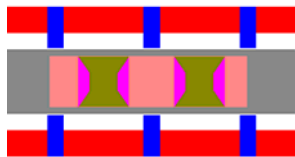
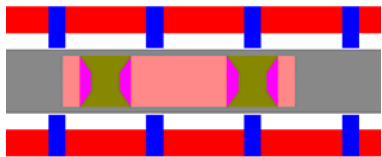
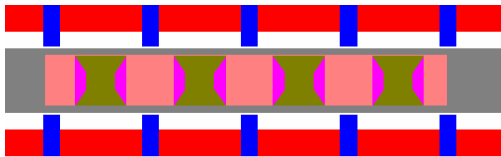
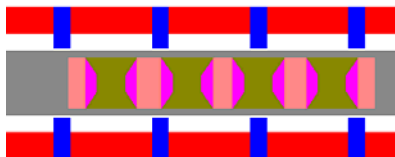
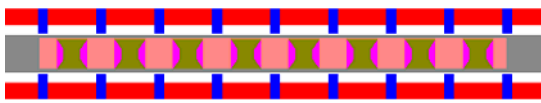
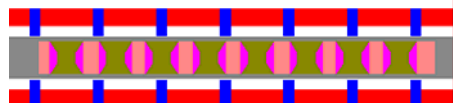
Figure 47: Current vs. Time

In general, this idea can be extended for a larger number of coils. For that reason, two four and eight coils in both types of connections are studied. Table 3 shows a list of

the models analyzed and the type of topology used. As before, the thrust force and the efficiency curves as a function of the velocity are generated for both configurations.

For this analysis, a current of 24 amperes is used. Rectangular wave without dead time is used for the current. Also, no shift in the stator is used and the dimensions remain the same that in Figure 34, except the for “T” pole. In this case the “T” pole dimensions correspond to a single bar (“T” pole without the flange) because according to previous results this has the highest efficiency.

Table 3: Coil topology analyzed

#	Simultaneous	Shift
2		
4		
8		

Steel 1010 was used for the poles, cooper for the winding and Ceramic 5 for the permanent magnets. The NeFe35 was removed from the analysis because of its high cost, which is significant when the stator is long, as the case for the application of concern to this thesis (i.e.: Maglev trains and elevators). Also, the material used for the core was laminated steel with fifteen laminations. This is the first simulation including the laminations. They are used to reduce the eddy current in the core. Commonly, in the electric motor and transformer design, the width of each steel layer is expect around

1mm. For the dimensions used in these simulations, the core has length approximately of 18 mm, which implies that each steel layer has a width of 1.2 mm. Then using equation (39), the effective core electric conductivity is $\sigma_{eff} = 4.35 \times 10^4$ [S/m].

The resulting curves are shown in Figure 48 thru Figure 50. In these Figures it can be appreciated that the effect of adding more coils always increases the efficiency and the thrust force. For example: for the case of simultaneously topology the efficiency increases from 57.7% to 80.5% when increasing from 2 to 8 coils, Figure 48. For the case of shift topology the efficiency increase from 71.7% to 88.3% when increasing from 2 to 8 coils, Figure 49. Also, the thrust increases with the number of coils from 13.7 N (for two coils simultaneous connection) to 74.75 N (for eight coils shift connection), Figure 50.

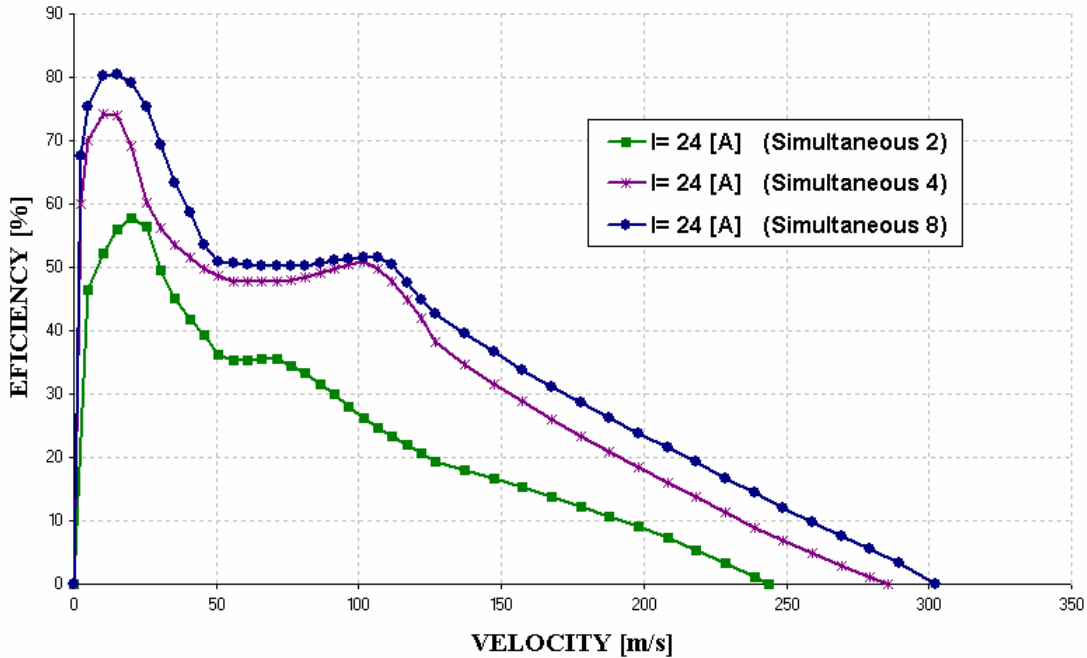


Figure 48: Efficiency curves for different numbers of coils for simultaneous coil connection.

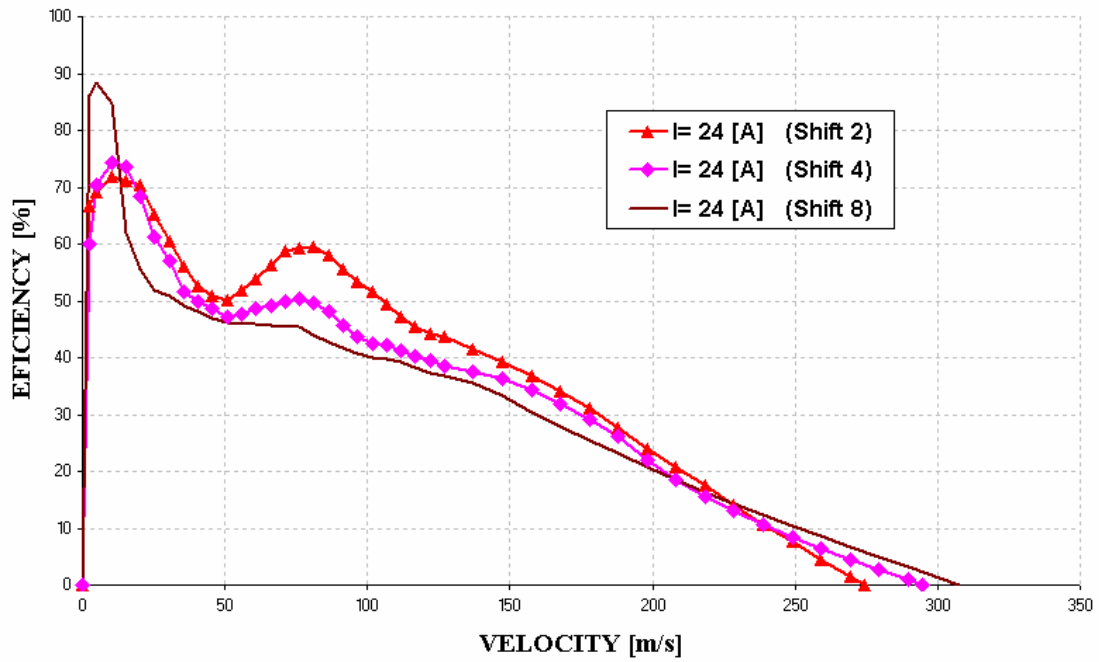


Figure 49: Efficiency curves for different numbers of coils. Shift connection.

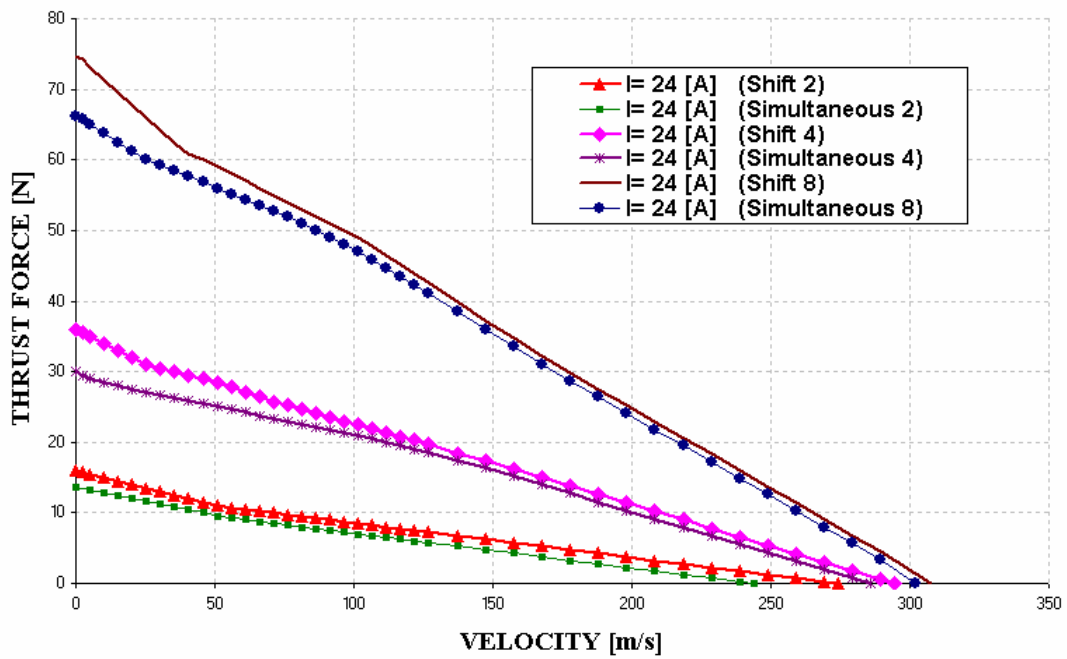


Figure 50 Thrust force for different numbers of coils

Another conclusion that can be obtained from these Figures is that the shift connection always has more efficiency and greater thrust force than the corresponding model in simultaneous connection. For example: for the case of eight coils with simultaneous topology the efficiency is 80.5% while for the case of eight coils with shift topology the efficiency is 88.3%. Also, for eight coils with simultaneously topology the thrust force is 66.25 N but for eight coils with shift topology the thrust force is 74.75 N.

CHAPTER V: Experimental Validation

In this chapter the results obtained from the proposed numerical model implemented using FEA are validated. Some prototype models of the Berdut system were used to obtain experimental measurements of their performance. The prototypes were modeled with Ansoft's Maxwell FE software using the model described in previous chapters. Then the results are compared to validate the models. The proof of concept prototype models built are two linear motors with 16 and 4 coils respectively and one orbital motor. The motor with 16 coils was used in a scaled prototype of a Maglev model and the instrumentation used was elementary. A second linear motor prototype was studied with data acquisition instrumentation in order to obtain performance measurements. Finally, an orbital motor prototype model was used to measure the torque and current and efficiency, because is more easy to obtain the efficiency experimentally for an orbital motor than for a linear motor. Both the linear and the orbital motors use the same Berdut arrangement and the result may be compared.

5.1. 16 Coil Linear Motor Experiment

The first experiment made to acquire experience with the behavior of the motor used a 16 coil linear motor. In this experiment the first part of the rail is used as a linear motor and then the second part of the rail is used to brake the prototype and it is used a regenerative brake. This model has the typical array proposed in the patent [1,2,3,4]. The dimensions are the same as those used in the numerical model. Figure 51 summarizes the dimensions and the material properties of the rail.

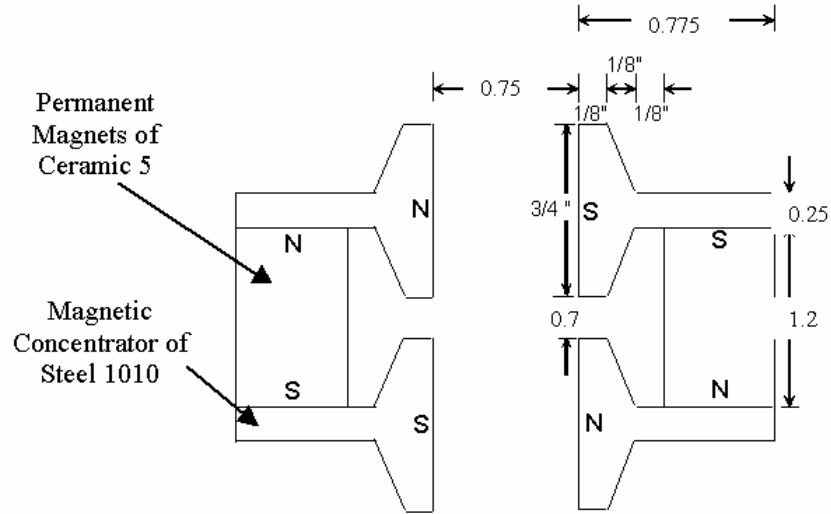


Figure 51: Motor dimensions and material properties

5.1.1. Experimental Setup

The model for this experiment has a rail of 10 m in length and also it has the same magnet array for the motor and the generator portion. Between each permanent magnet in the rail there is a magnetic concentrator with the form of a “T” named “T” pole. This rail is constructed with Ceramic 5 permanent magnets and steel 1010 for the “T” pole. Figure 52 A) and B) show the details of the rail. The prototype uses a power strip contact along the rail that provides the power to the coils via brushes. It is able to switch the polarity of the current to energize the coils adequately in the motor and switch the polarity of the current to obtain a direct current in the generator. The connection system used is described in detail in the next subsection.

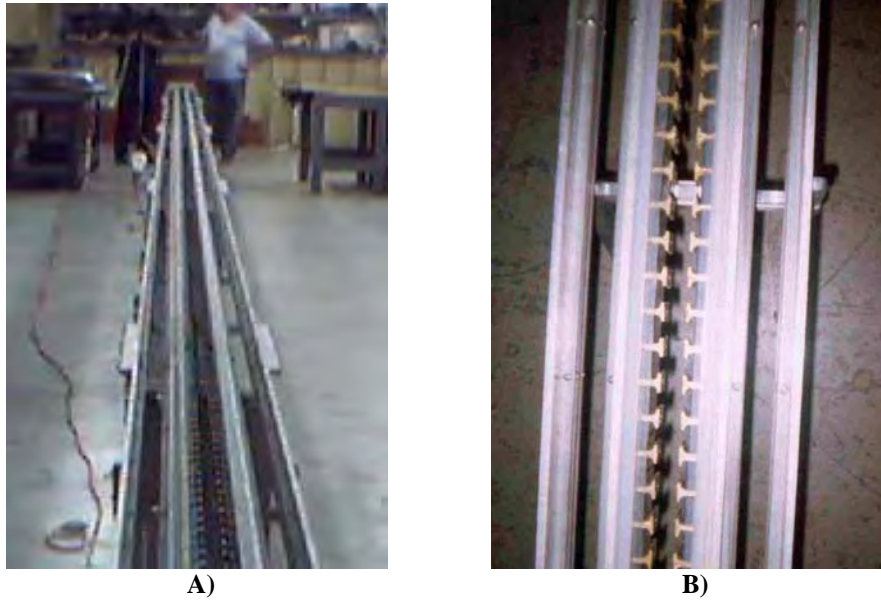


Figure 52: A) Complete view of the rail; B) Detail of the magnets and “T” arrays

The total height of the “T” pole is 0.45 in. The dimensions are shown in Figure 51. On the other hand the moving part or “car” has 16 coils with 105 turns for each coil. The connections of the coils are in parallel and the switching of the coils is done simultaneously. Figure 53 shows a picture of the car. The material for the core was laminated iron with 10 laminations and copper wire gauge 20 was used for the coils.



Figure 53: Details of the moving part

The mass of the car was 57 lb (25.8 kg) and the details of the dimensions of the car and rail were shown in the previous chapter in Figure 34. Tests were run at 24, 36 and 48 volts.

5.1.2. Test Results

The variable measured in this experiment was the velocity of the car. The velocity was obtained measuring the time taken by the car to travel the distance between each “T” pole along the rail. Then, dividing the distance between T-poles by this time the average velocity for each interval is obtained. Figure 54, Figure 55 and Figure 56 show the average velocity as a function of time for the three input voltages.

Integrating these curves in time the average acceleration is obtained. Then, multiplying the average acceleration by the mass of the car the average force is obtained. In Figure 57 the average thrust force over the car for the different power levels supplied is shown.

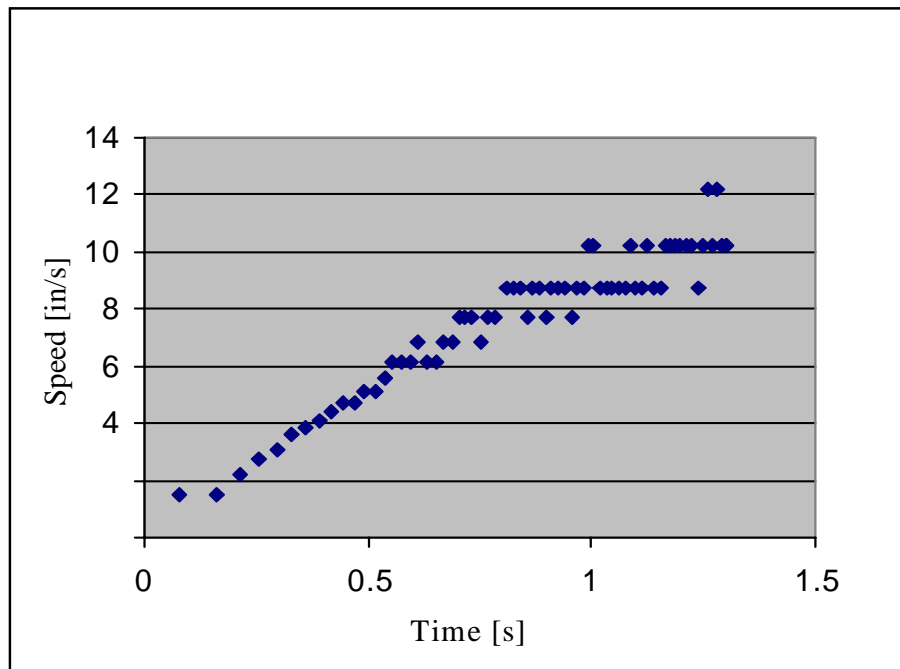


Figure 54: Speed vs. Time for 24 volts

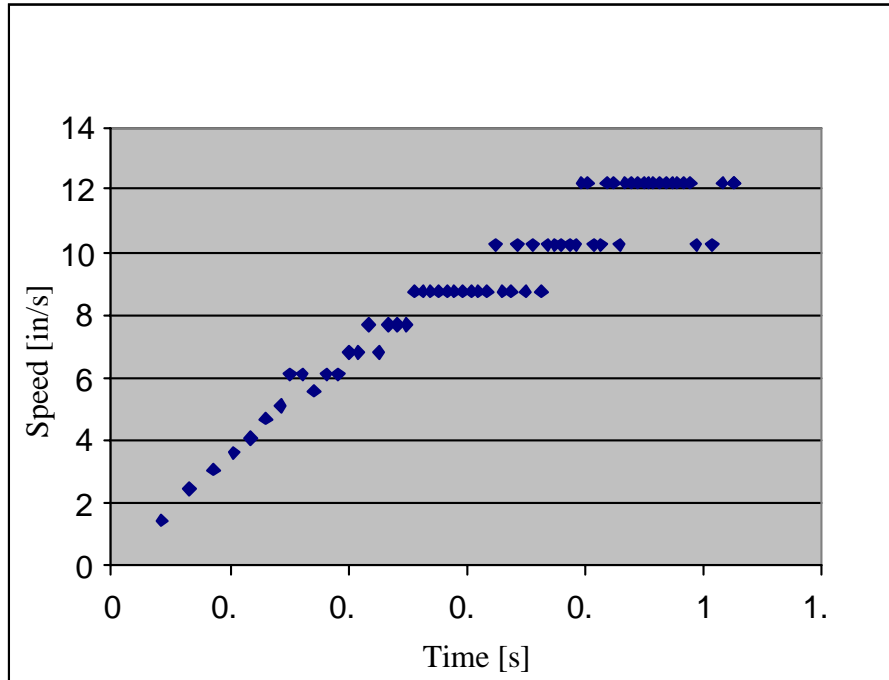


Figure 55: Speed vs. time for 36 volts

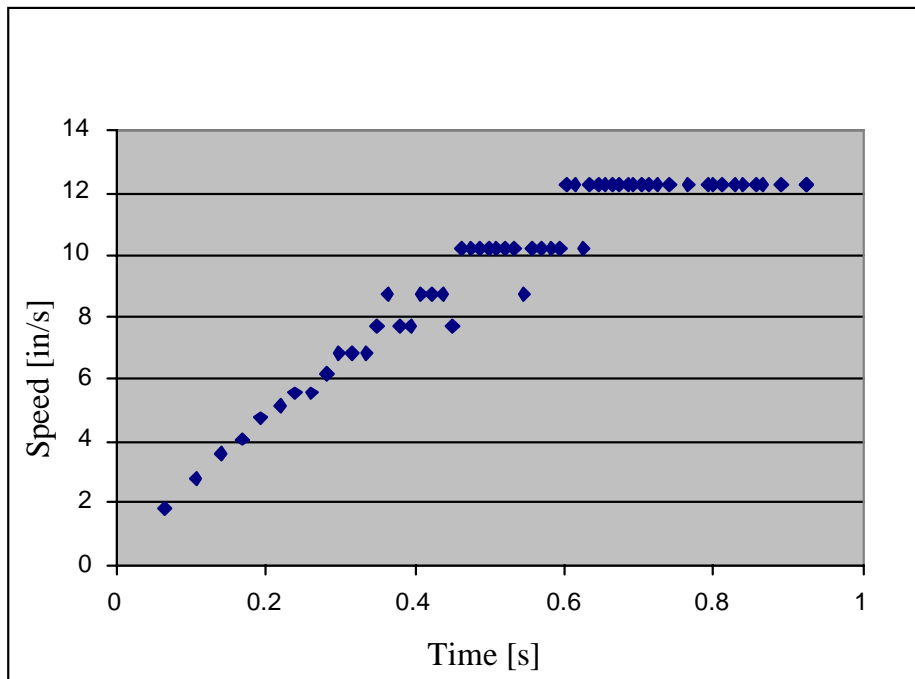


Figure 56: Speed vs. time for 48 volts

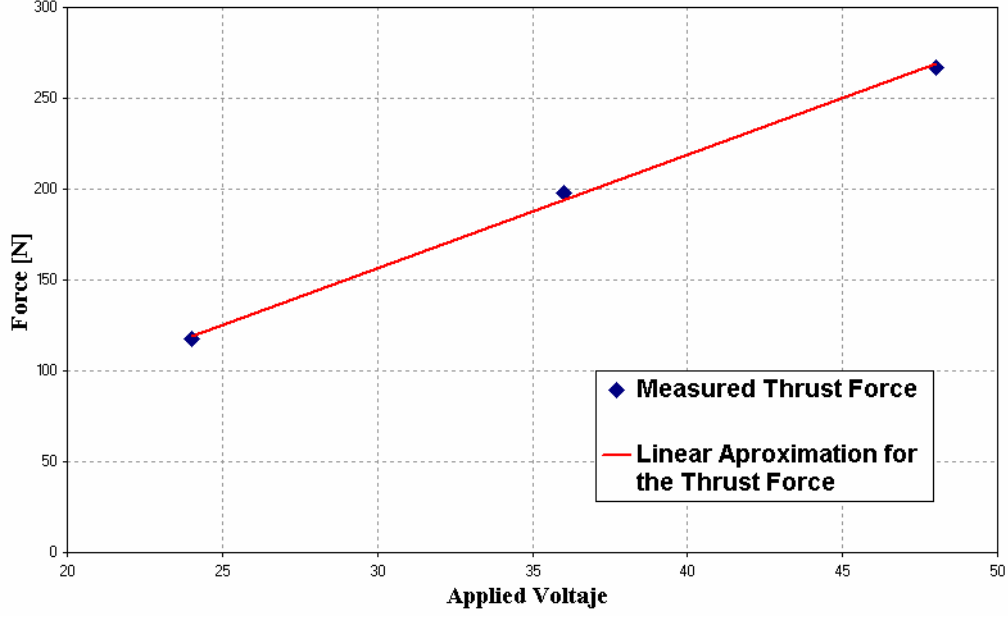


Figure 57: Average Thrust Force over the car

These data points for force are approximated by a linear regressions curve as:

$$F = 6.2315 \text{ Volt} - 30.23 \quad (40)$$

This linear regression has $R = 0.9979$. Then, the thrust force is divided by the number of coils and the thrust force for each coil is obtained. Maxwell is used to solve the numerical model for one coil motor with the corresponding data for this experiment. Then, the thrust force over the coil for both cases (experimental and finite element method) is compared. Figure 58 shows the results of the thrust force for each case. The maximum error between each procedure is obtained for the case of 48 volts and it is less than 6%, which is acceptable by engineering standards. The difference is due to factors such as friction in the prototype, manufacturing and measurement inaccuracies, exact material properties, losses in the contact brushes of the prototype among others, which can not be accounted for in the theoretical model. Therefore validating the numerical model, the solution technique and the boundary conditions used.

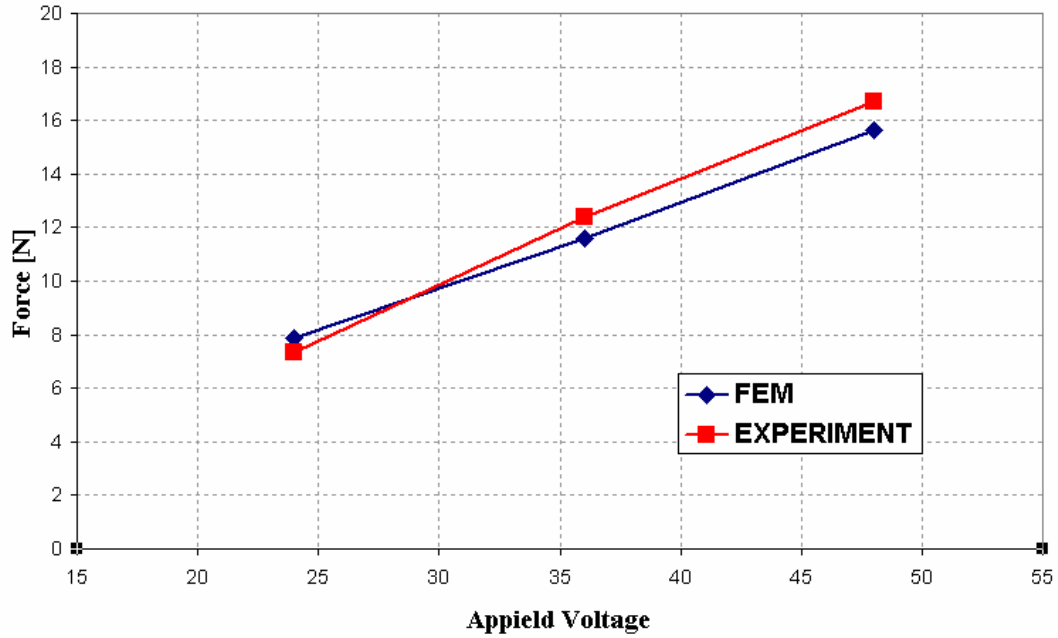


Figure 58: Average Thrust Force over each coil

5.2. Experiment 4 Coils

Another experiment to validate the theoretical model with more details in the form and magnitude of the force-time curve and current-time curve was performed using a 4 coil linear motor prototype. Then, the corresponding numerical model was simulated in Maxwell and the results obtained experimentally and theoretically are compared.

5.2.1. Experimental Setup

The model is a linear motor with a moving part with four coils that which are connected to the power supply through the brushes and a power strip with both current polarities. As in the previous prototype, the switching is achieved by alternating the position of the two strips carrying different polarities. As the brushes connected to the coils pass over the alternating strips the current polarity switches in the coils (Figure 60).

The Figure 59 A) and B) show the car view and the details of the brush connector and Figure 60 shows the alternating power strips used to power coils from the rails. This strip is located in one side of the rail.



Figure 59: (A) Car with the details of the brushes, (B) Lateral view of the car



Figure 60: View of the alternating power strip used to power the coils

When, the car is mounted in the rail (stator), both sides of the rail have an array of permanent magnets separated by a magnetic concentrator with form of “T”. This array generates the magnetic field that with the interactions of the magnetic field generated by the coils in the car originates the thrust force over the car. Figure 61 (A) shows the rail with permanent magnets, “T” poles and power strip. Figure 61 (B) shows the final assembly of rail (stator) and the car (moving part with coils).

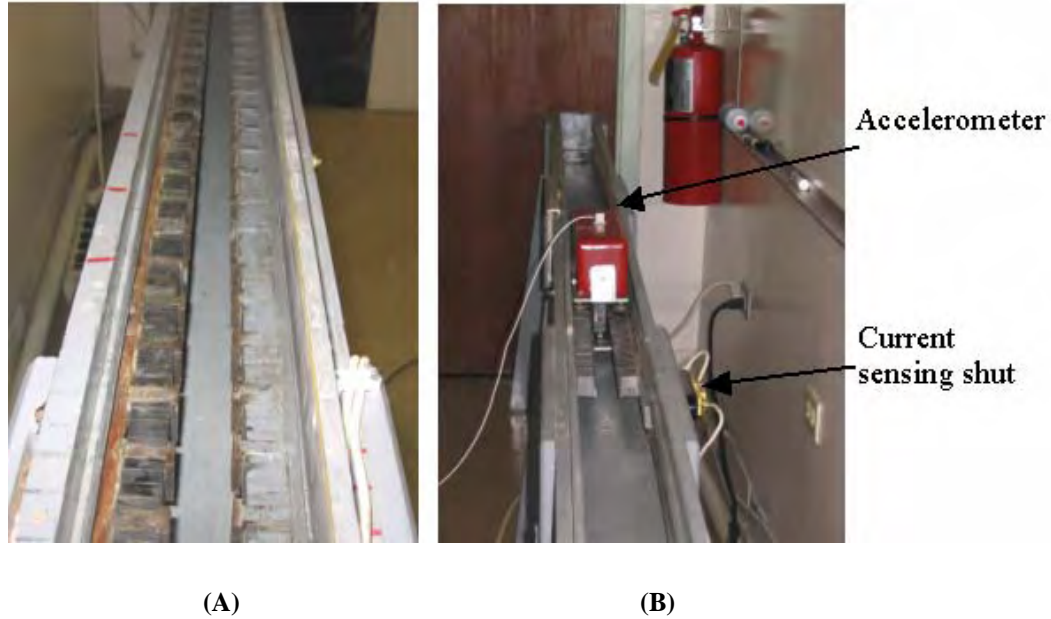


Figure 61: (A) Rail, (B) Final assembly of rail and car

To measure the force and the current, an accelerometer and a calibrated shunt resistor were used. The accelerometer used to measure the force can be seen attached to the car and current sensing shunt is attached to the rail (stator, Figure 61). The accelerometer is mounted to the car and it is connected to the data acquisition system. Figure 62 (A) shows the data acquisition system used for the experiment. The data acquisition system is a Siglab model. Figure 62 (B) shows the connectors used between the accelerometer and data acquisition system and Figure 62 (C) shows the calibrated shunt resistor that is connected in series with the coils and used to measure the current used by the coils.

The voltage difference in the shunt resistor is proportional to the current that passes through the coils, and this value of voltage is collected by the data acquisition system over time.

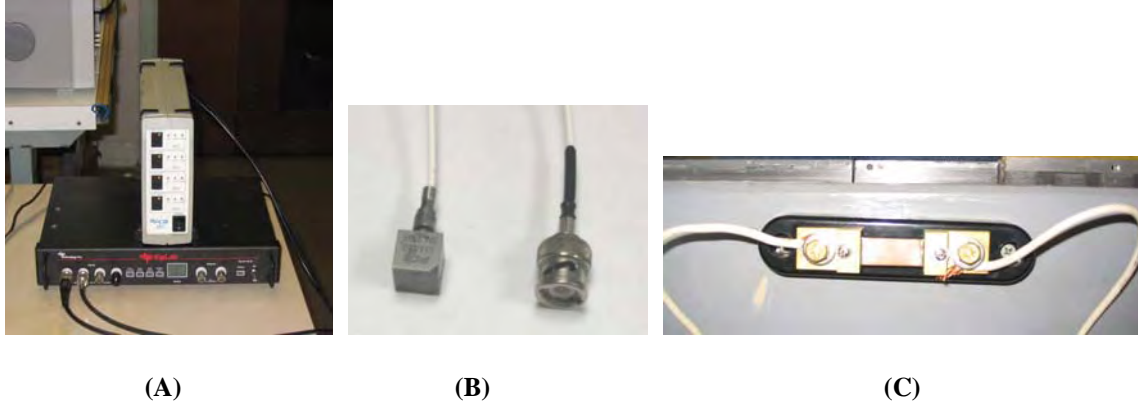


Figure 62: A) Data acquisition system B) accelerometer C) Calibrated resistor

The materials used for the prototype used in the experiment are ceramic 5 for the permanent magnets; steel 1010 for the “T” pole and the core of the coil is built with ten sheets of steel 1010. The coils are built with 100 turns of copper. The power supply used supplies 12, 24 and 36 volts. The coils are in parallel and switched simultaneously.

5.2.2. Results

The results obtained for each test using a different power level are converted with the corresponding constant for each sensor from volts to the corresponding units. An equivalent two-dimensional model is generated for simulation in Maxwell and the both results are compared.

The connection of the coils is in parallel; therefore the current measured in the supply line of the motor is four times the current passing through each coil. Figure 63 shows the electric circuit schematic. Including the calibrated shunt resistor R_c used to measure the current.

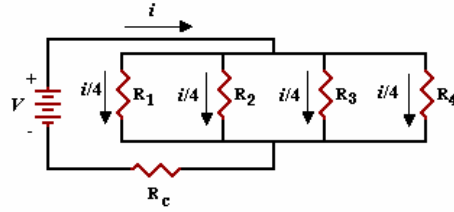


Figure 63: Electric circuit of the experimental motor

Figures 59, 60, 61, 62, 63 and 64 show the current and the force measured for each power supply setting. These figures show that at the start of the motion there is some fluctuations in the force that can be attributed to some blemishes in the assembled of the rail.

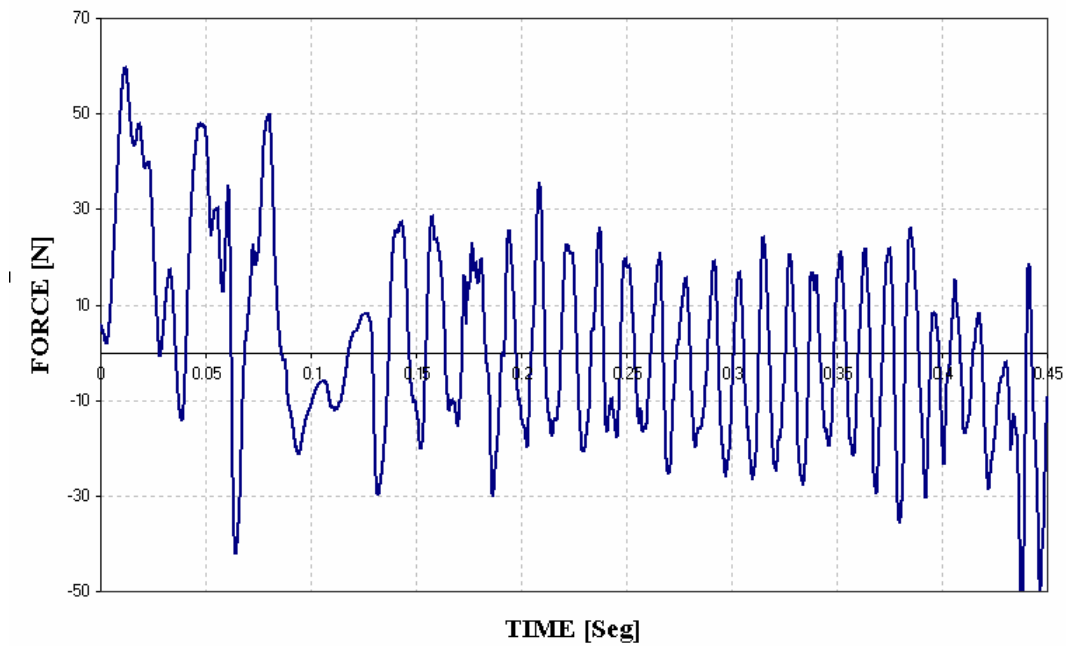


Figure 64: Thrust force for 12 volts

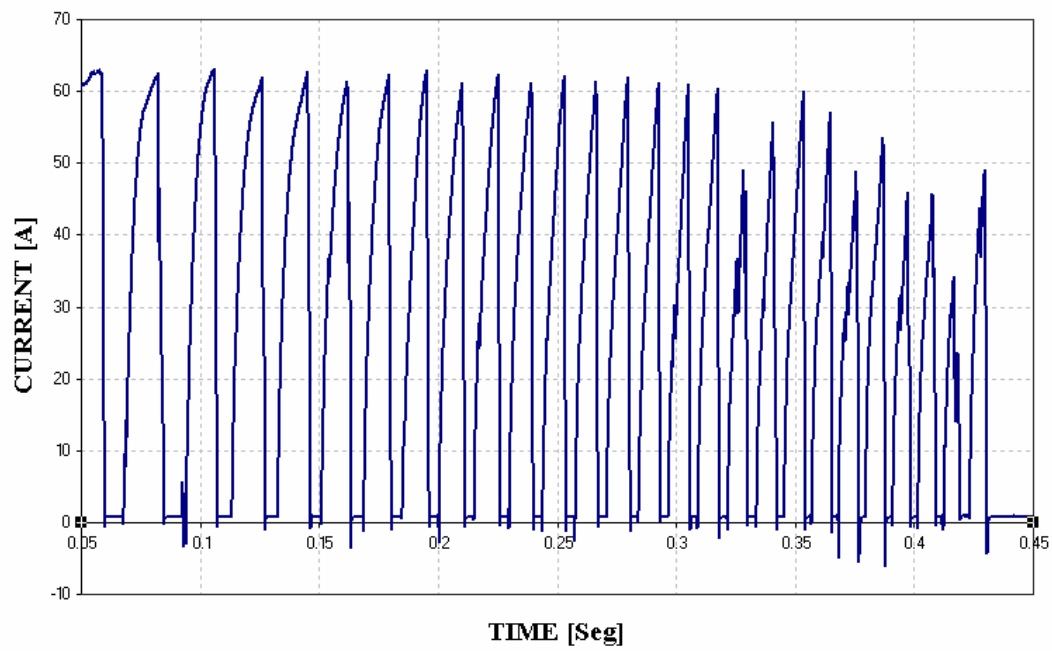


Figure 65: Current for 12 volts

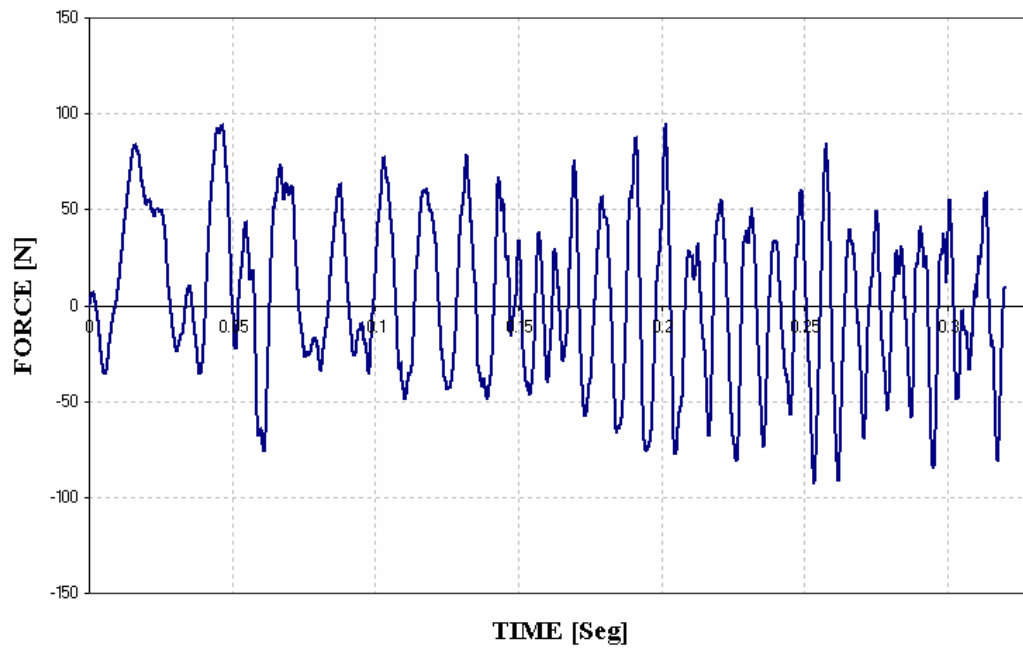


Figure 66: Thrust force for 24 volts

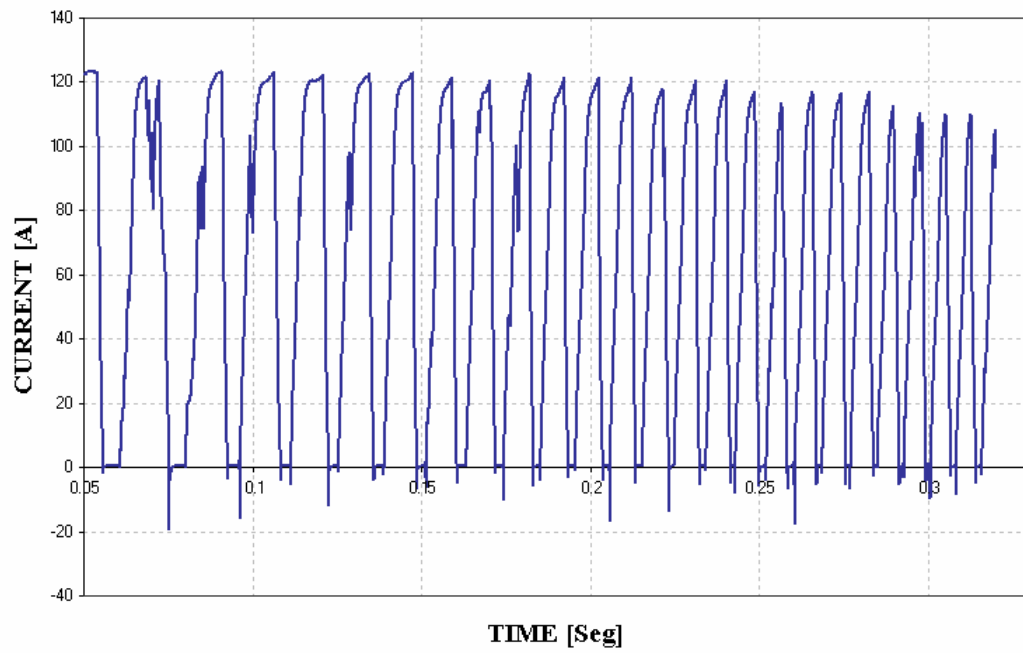


Figure 67: Current for 24 volts

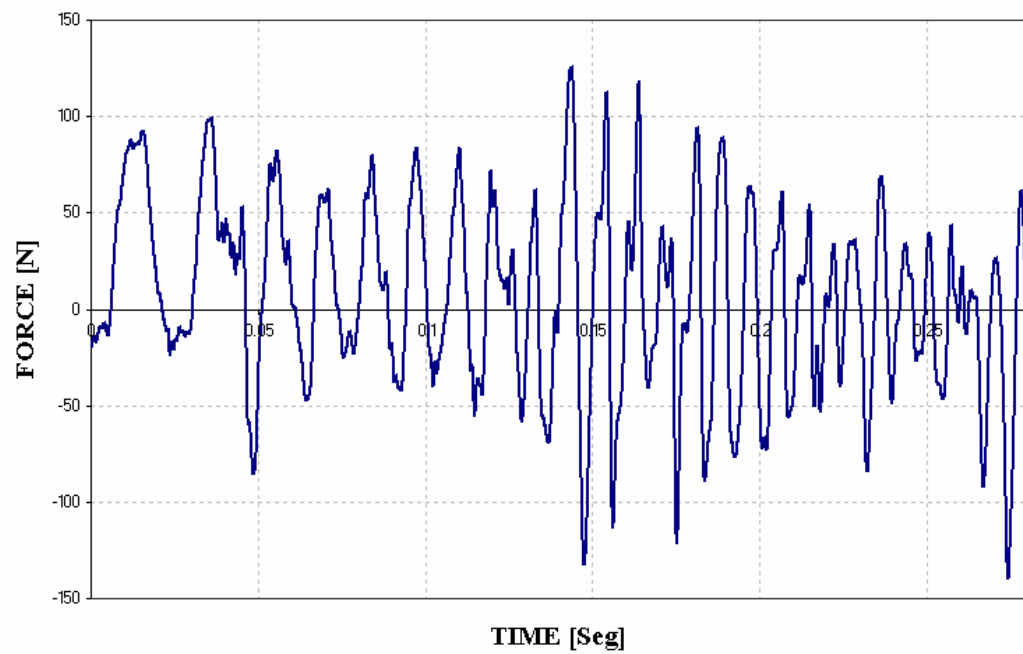


Figure 68: Thrust force for 36 volts

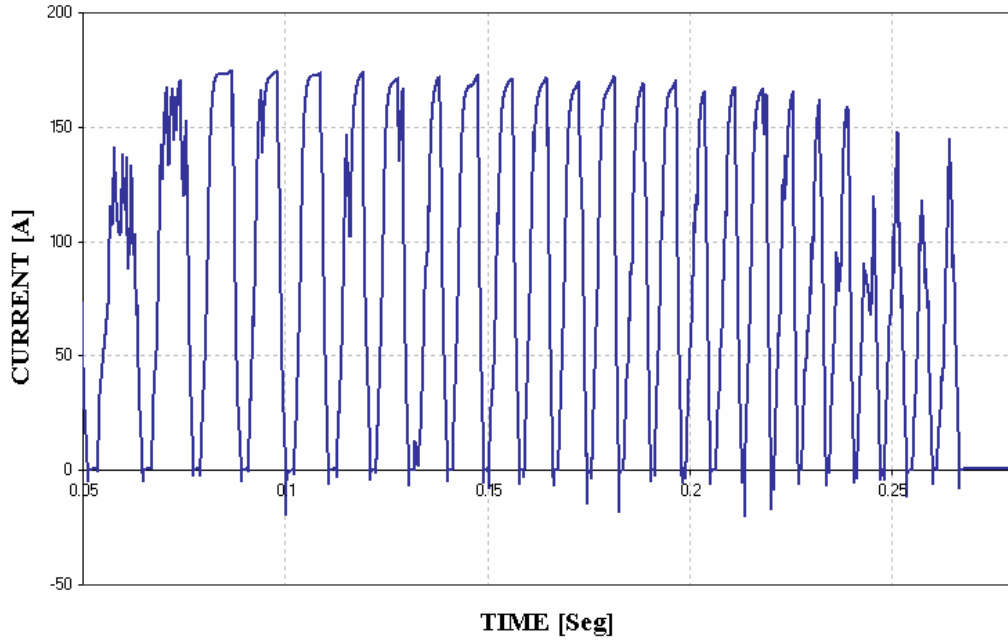


Figure 69: Current for 36 volts

The corresponding two-dimensional model simulated in Maxwell is shown in Figure 70. In order to simulate the motor in two-dimensions the most important assumption is the depth of the model; because this dimension has to be representative of the size of the coil in order to generate an equivalent electromagnetic field around the coil and therefore the equivalent thrust force. The depth used was the height of the coil.

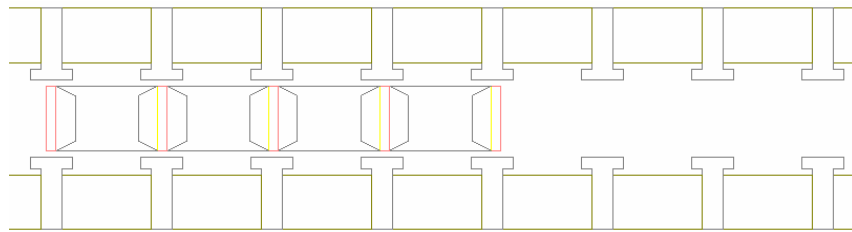


Figure 70: Schematic model used in Maxwell

The experimental results are compared with the numerical simulations in Figure 71 thru Figure 76. The Figures are organized showing the thrust force and current for a

power supply of 12v, then for 24v and finally for 36v. These figures show an important difference between the frequency of the current switching in the coils and therefore in the velocity of the moving part for experimental and numerical models.

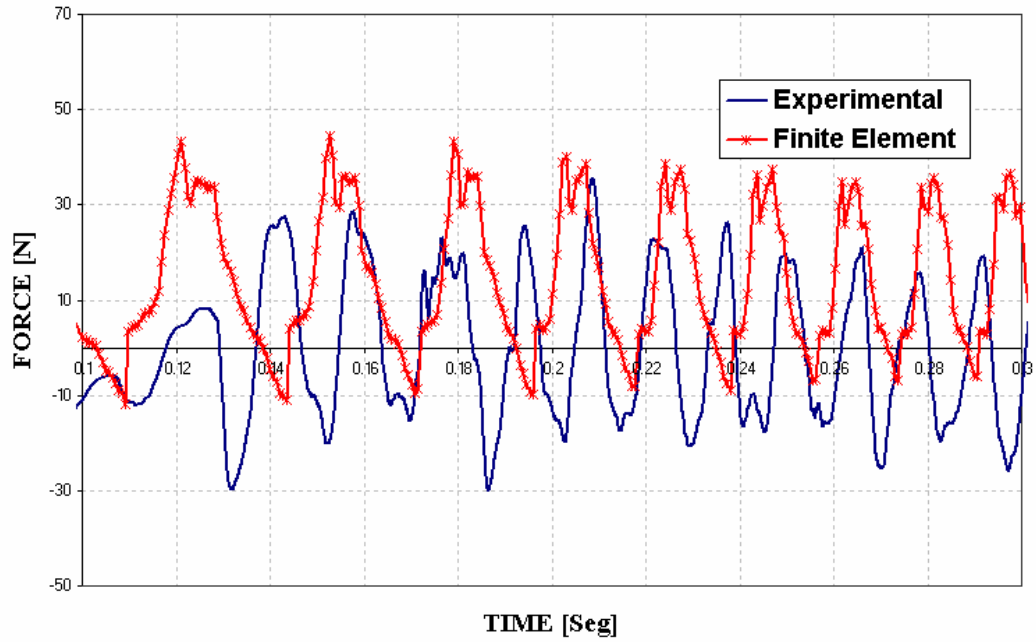


Figure 71: Comparison of thrust force between experimental data and FE simulation for 12v

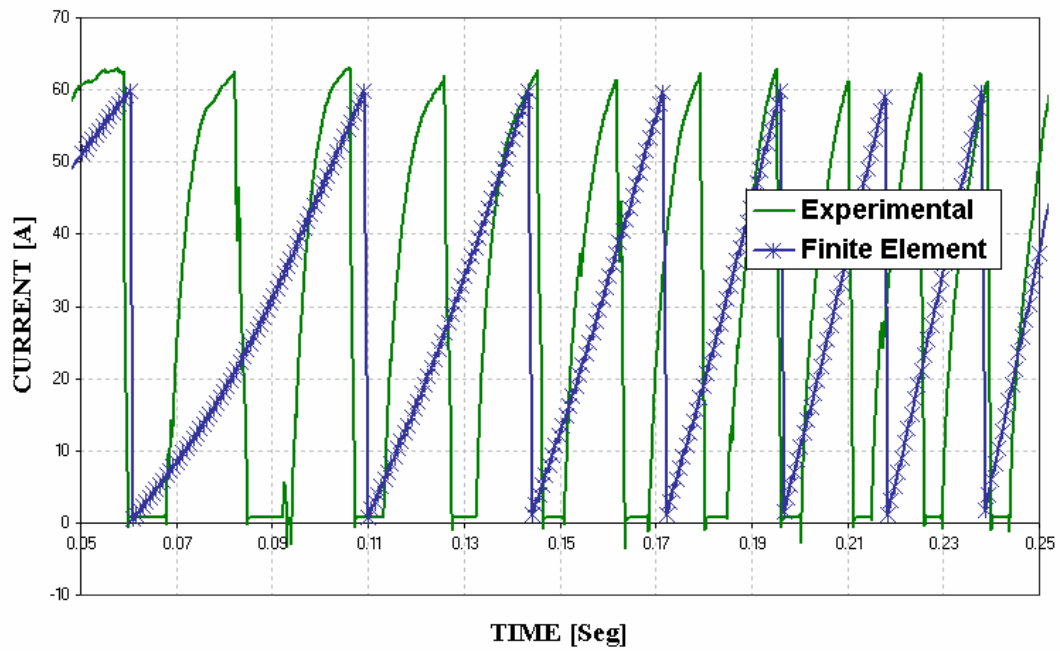


Figure 72: Comparison of current between experimental data and FE simulation for 12v

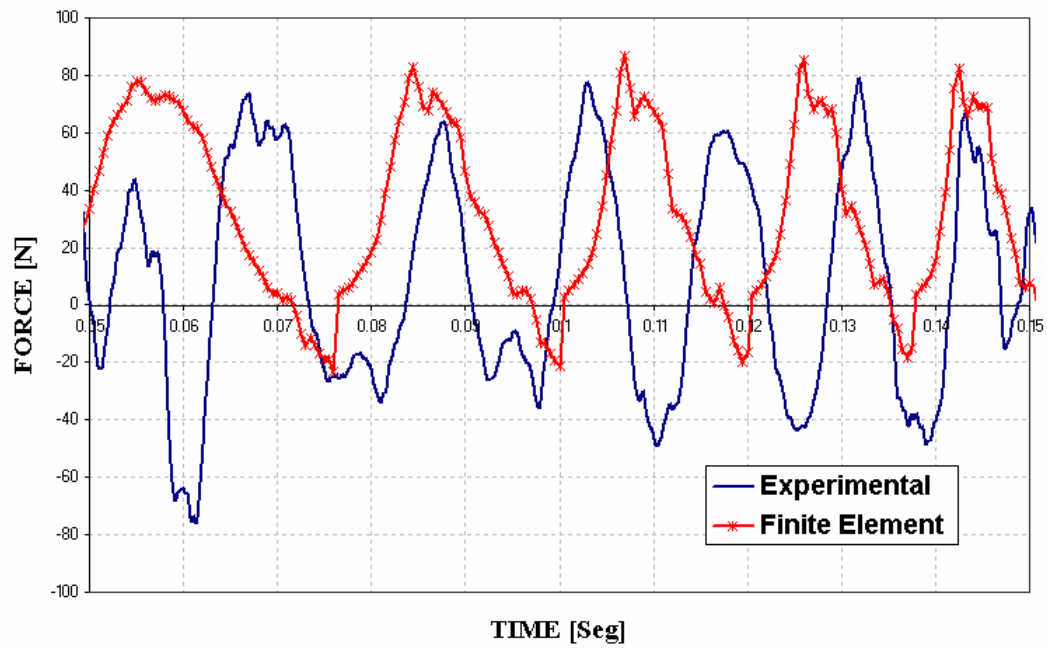


Figure 73: Comparison of thrust force between experimental data and FE simulation for 24v

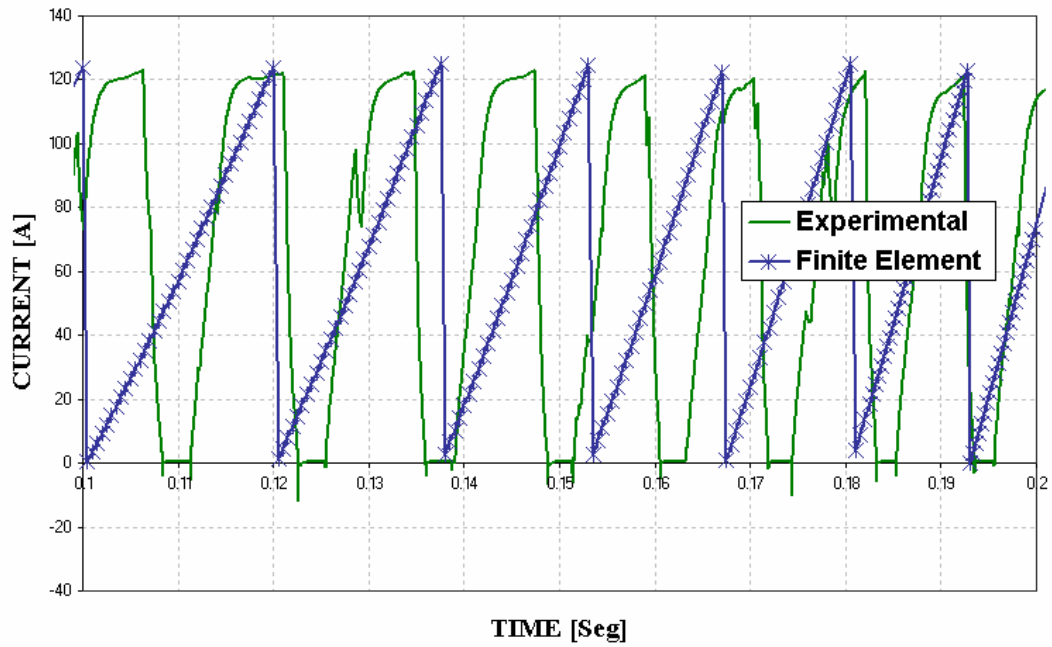


Figure 74: Comparison of current between experimental data and FE simulation for 24v

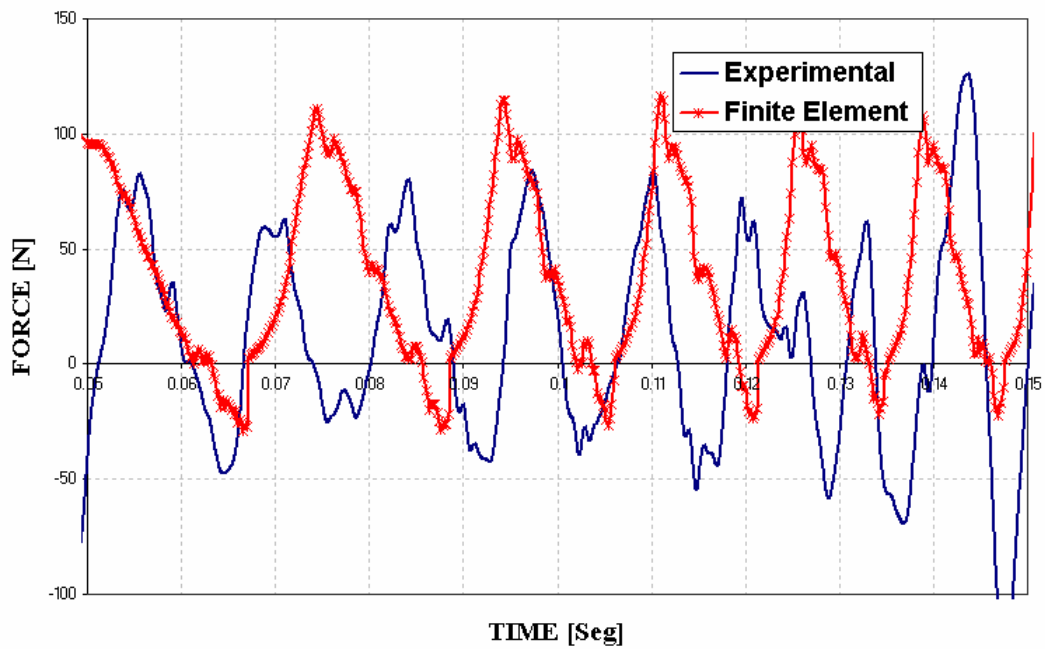


Figure 75: Comparison of thrust force between experimental data and FE simulation for 36v

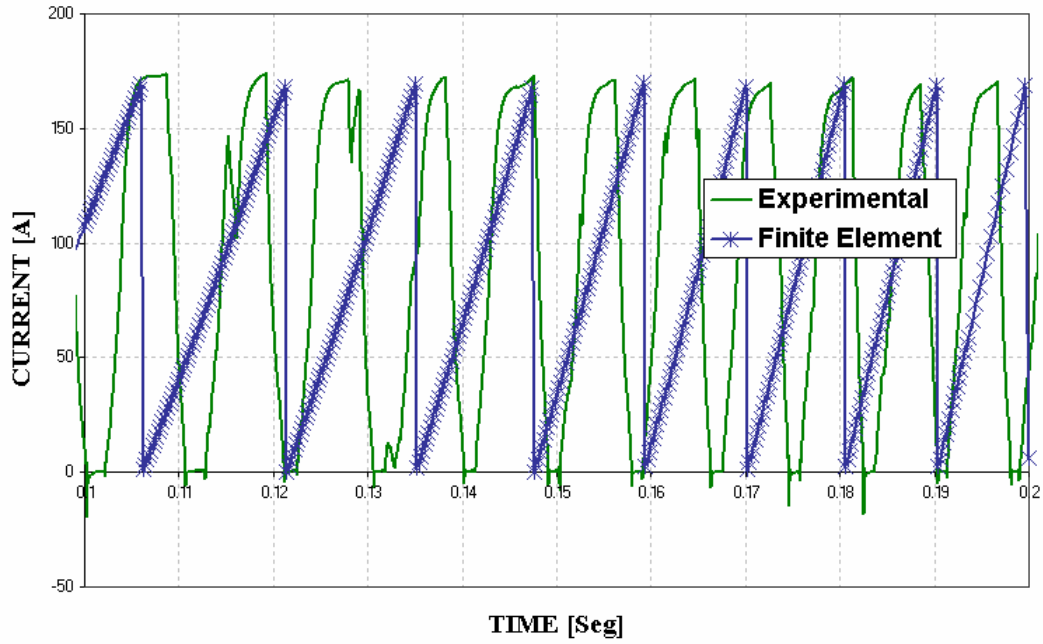


Figure 76: Comparison of current between experimental data and FE simulation for 36v

This difference is a consequence that the experimental model needs a small initial velocity to start running. This initial velocity cannot be measured and was not included in the numerical model but the effect is that in the experiment, the car has more velocity than that predicted by the finite element method. The other difference is the current input profile. In the numerical model a triangular wave was used to model the real current profile. In the experiment the current profile measured is a wave with exponential form. The exponential form is originated because the electric circuit of the moving part is basically an R-L circuit. Therefore the solution for the current in time for R-L circuits is an exponential described by:

$$I(t) = \frac{V}{R} \left(1 - e^{-t/L/R} \right) \quad (38)$$

The closest approximation to the profile allowed by the FE software was the triangular wave used. Another parameter that was not included in the numerical model was the friction between the rail and car. In addition the friction between the car and the rail is Coulomb friction or dry friction. This force is proportional to the normal force that there is between the car's guide wheel and rail:

$$F_R = \mu F_N \quad (41)$$

Where μ is the friction coefficient. Usually, this coefficient is obtained experimentally. At this point is important to note that the friction force does not dependent on the velocity of the car, therefore does not dependent on the power supplied used. This effect justifies the difference between the maximum and minimum force reached by both curves, experimental and numerical. For that reason, the average value of these curves was used and always a constant difference of approximately 15 N was obtained between each set of curves. The average force showing these difference are plotted in Figure 77, Figure 78 and Figure 79. This value representing the friction force was not accounted in the numerical simulation. After all these approximations, the thrust force obtained numerically has a good agreement with the thrust force obtained from the experiment. These comparisons are shown for each voltage supplied in Figure 71, Figure 73 and Figure 75.

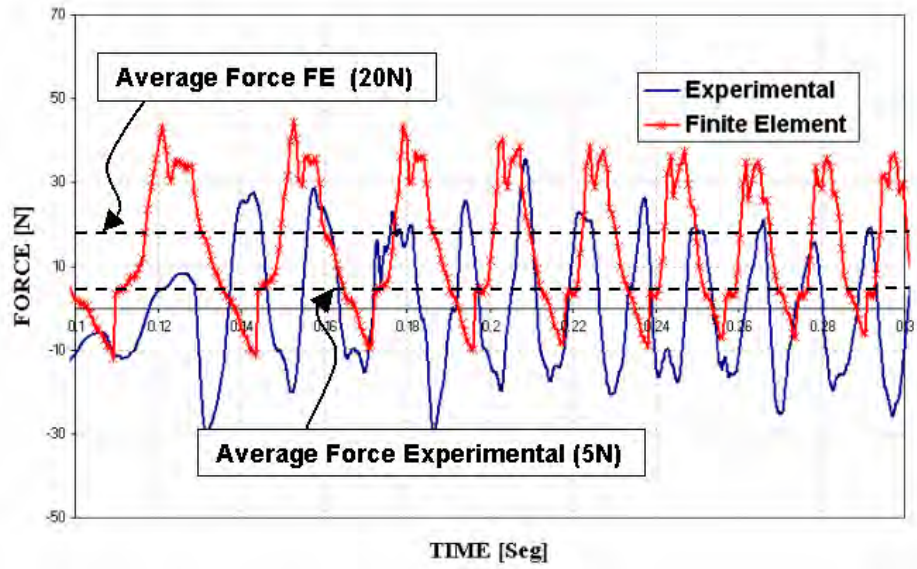


Figure 77: Comparison of the average thrust force between experiment and FE simulation for 12v

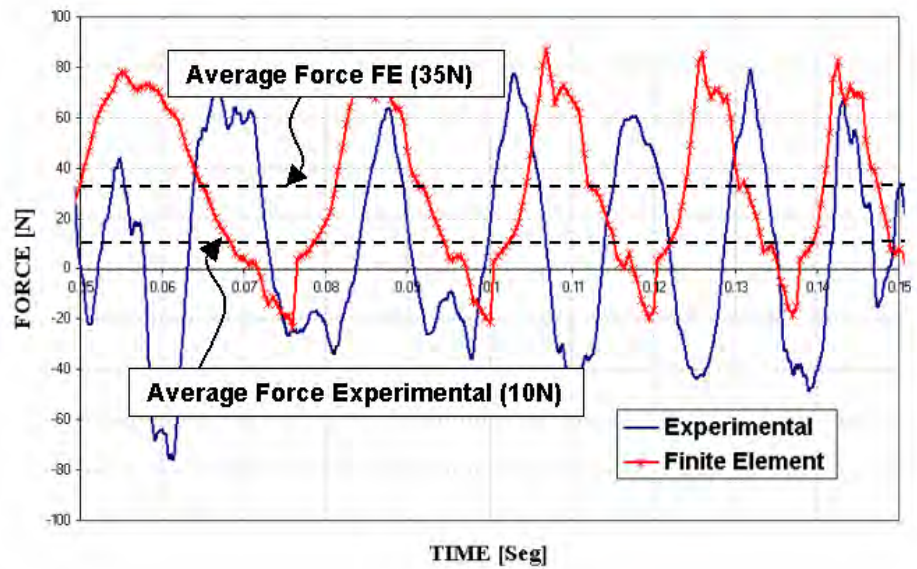


Figure 78: Comparison of the average thrust force between experiment and FE simulation for 24v

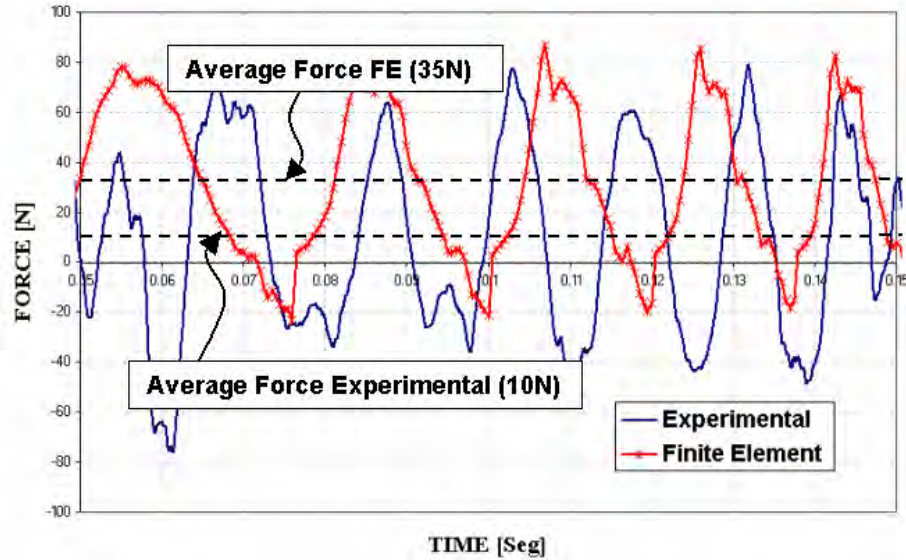


Figure 79: Comparison of the average thrust force between experiment and FE simulation for 36v

Another important parameter that is commonly used in the electric motor design is the ripple. The ripple is the amplitude in oscillation of the force profile around its mean value. For the cases studied here the ripple is 100%. This is not an accepted value for any design but with an adequate control system and more coils can be reduced to a value less than 20%.

5.3. Experiment Orbital Motor

A third experiment was performed with the same technology but using the orbital version of the motor. This experiment was performed to have more details on the behavior of this technology and also the orbital version has the advantage that it is easier to measure the efficiency-angular velocity curve and torque-angular velocity curve. These curves are equivalent to efficiency-velocity and thrust force velocity in the linear motor. This experiment was not simulated in the finite elements; as it would require a

different model (and is not within the scope of the thesis) the results are only used in qualitative form to show some correlations with the curves obtained for the linear motor.

5.3.1. Experimental Setup

The characteristics of the motor used in this experiment are similar to that used in the experiment of the linear motor. In this case the car is the rotor located between the arrays of permanent magnets with the magnetic concentrators. One significant difference with the 4 coil prototype is that the “T” pole does not have the form of “T”, on the contrary, it has the form of simple bar, in other words it is a “T” without the flange. The orbital motor also uses a power strip with alternating contacts and brushes connected to the coils. Figure 80 shows the orbital motor used in the experiment. The Figure shows the motor with a pulley on one end of the shaft and contact brushes on the other.

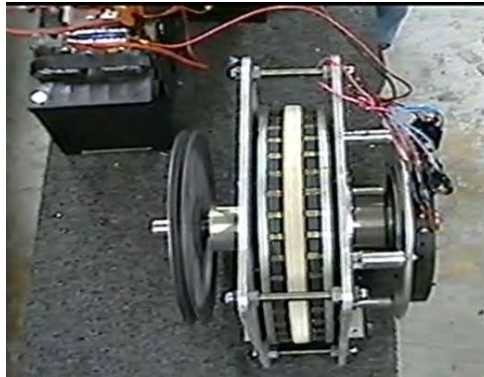


Figure 80: Orbital motor

The parameters measured in the experiment are the current used by the coils, the torque provided on the output shaft, and the voltage given by the power supply and the angular velocity. To measure the current an ampere meter is used, to measure the torque a torque meter is used and to measure the angular velocity a tachometer is used. The

material used for each component is the same as that in the linear motor and the power supply used provides 24 and 36 volts.

5.3.2. Results

The procedure used to obtain the efficiency required to obtain the mechanical power as the product of Torque and angular velocity:

$$P_m = T\omega \quad (42)$$

The electrical power is obtained as the product of the current and the voltage:

$$P_e = IV \quad (43)$$

The efficiency is the ratio of these:

$$\eta = \frac{\text{output}}{\text{input}} = \frac{T\omega}{IV} \quad (44)$$

The results obtained for both cases of supplied voltage are shown in Figure 81 and Figure 82. These figures plot together torque, electrical power and efficiency curves as a function of the angular velocity.

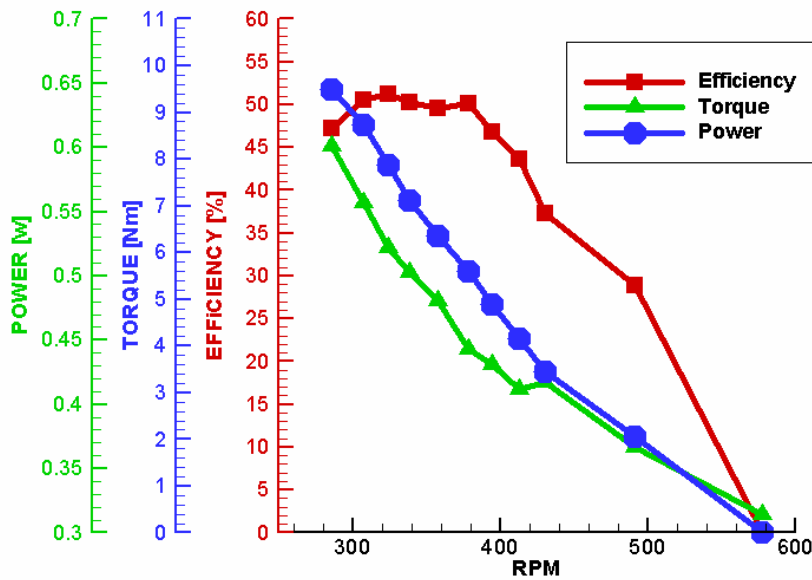


Figure 81: Motor performance at 24 volts

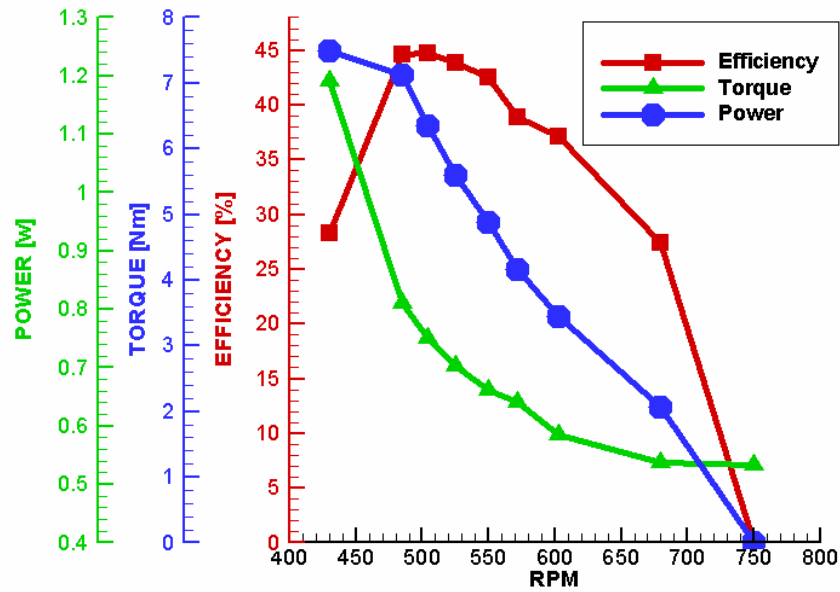


Figure 82: Motor performance at 36 volts

The result obtained in these experiment are not compared with theoretical data from finite element methods because, the scope of the thesis theoretical model is focused on the linear motor but these results can be easily extrapolated to the linear motor. These curves are useful to compare qualitatively with the efficiency obtained theoretically for the linear motor. For example, these curves can be compared with the theoretical data obtained from Chapter 4 for the section “type of connection”. The efficiency obtained from this experiment (between 50% for 24 v and 45% for 36 v) is similar to the second local maximum efficiency point showed in Figure 48 (50% for simultaneous connection with 8 coils which is also the connection used in the orbital motor experiment). The first maximum efficiency point was probably not reached in the experiment because of the measurement instrumentation was not accurate at low speeds and data in that range was not obtained. Also, with the radius of the rotor (0.075m) and the torque provided on the output shaft it is possible estimate the tangential force (the coils has practically the same

size that was used in the numerical study in the previous chapter). The tangential force at the maximum out torque of 9.5 Nm and 7.5 Nm for 24 and 36 volts respectively, is 126.66N and 100N. These values correspond to the tangential velocities of 3.3 m/s and 1.3 m/s respectively. Then, tangential forces per coil (18coils) are 7N and 5.5N respectively. These tangential forces can be compared with the thrust force obtained theoretically (using FEA) showed in Figure 41 for the case of 24 A (which is the mean current measured in the experiment). For the case of 24 A at the linear velocities in the range of 1.3 m/s to 3.3 m/s, the thrust force range is from 10.5 N to 11.5 N; which are in the order of the tangential force obtained experimentally.

CHAPTER VI: Case Study: Design Optimization

Once the analytical model was developed (Chapter 4) and validated (Chapter 5). A case study for with an innovative application of this technology could be examined as a test bed. As described in Chapter 2, elevator design is an innovative application for linear motors and therefore was selected for the case study. In this chapter an optimization analysis of the motor is performed. In the first part, details of the design variable selection and the procedure required to obtain the objective function are explained. The variables are described and the objective function is evaluated at each point. A one-dimension search in each design variable direction is performed in order to start the optimization search, which is refined around these points. This iterative process is used to obtain an optimum solution given the initial value, the constraints and the linear motor model used in the objective function.

6.1. Design Variable Definitions

In order to perform the optimization, the objective must be defined based on the model of the electrical motor subject to the unique constraints required for the elevator system case study. For that reason, some specifications for elevator design, which take into consideration the passenger comfort (as required by conventional elevators) are [37]:

- Maximum Velocity: 1 m/s
- Maximum Acceleration: 1 m/s²
- Maximum Jerk: 0.8 m/s³

These magnitudes can be reached in the range of 1 or 2 meters (that is typical in high buildings) and the time of 2 or 3 seconds. With these constraints, several displacement functions are possible solutions. To select an appropriate solution, a polynomial approximation function is used to interpolate values for velocity, acceleration and jerk modeling. Among the interpolations studied were constant jerk, linear jerk and quadratic jerk. By, integrating one, two, and three times respect to time the jerk; acceleration, velocity and position are obtained. Figure 83, shows these relationships for a maximum time to reach the steady state (acceleration equal to zero and constant velocity) of 2 and 3 seconds respectively.

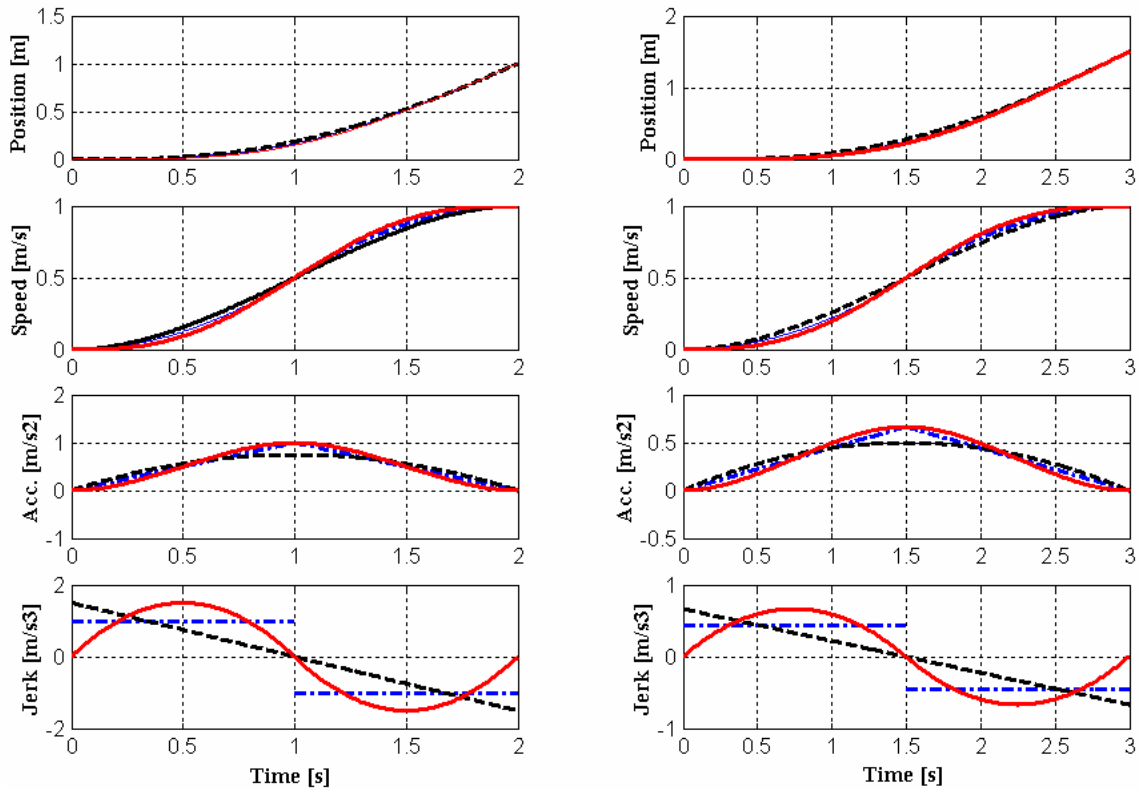


Figure 83: Elevator performance

Looking at these curves a maximum displacement of 1.5 meters with linear jerk was selected. The linear jerk is selected because it produces the lowest maximum acceleration. The maximum acceleration obtained with this assumption is 0.8 m/s^2 .

Then the maximum elevator capacity of six passengers was chosen. For six passengers, the load is approximately to 500 kg (80kg for each passenger) and another 500 kg for the cabin weight. The total maximum load that must be moved is 1000 kg (in the rise) with an acceleration of 10.6 m/s^2 (this is sum of maximum acceleration calculated plus gravity). Then, the total force that must to be supplied by the electrical linear motor is 10600 N. This value is also used as a constraint.

The design variables selected for the optimization correspond to the most significant mechanical parameters. The parameters related to the control of the motor are not included in of the analysis. That implies, that the effect of the RLC circuit on the current waveform is not taken into consideration, this is left for the future study. The current waveform is therefore assumed a rectangular wave. The selected design variables are:

- The permanent magnet dimensions (width -S1- and length -S2-).
- The magnetic pole concentrator dimensions (width -S3- and distance -S4- above the length of permanent magnet size -S2-).
- Dimensions of the coils nucleus (width -S5- and length -S6-).
- The number of total turns in the coil (S7).
- The depth of the model (S8).
- The current used (S9).

Figure 84 shows some of the geometric variables used in the optimization. In the figure, the geometric variable S9 is not showed because this variable represents the height of the model and it is perpendicular to the plane of the drawing.

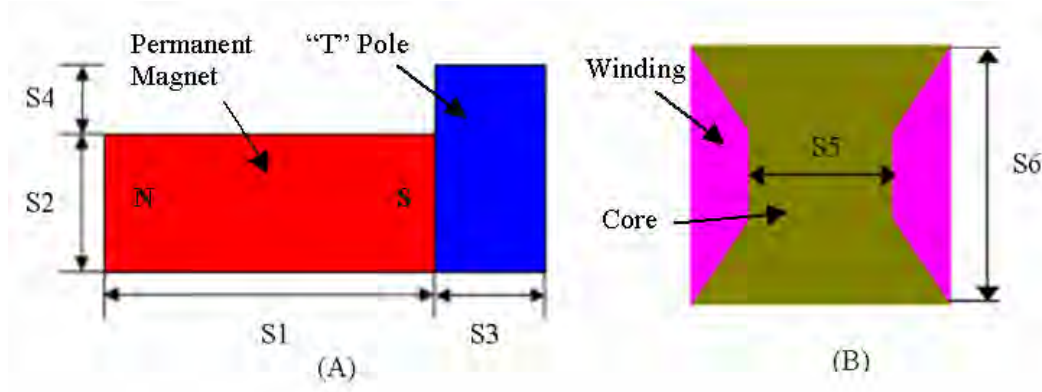


Figure 84: (A) Rail, (B) Coil

Appropriate limit constraints for each design variable are needed. The first constraints require that each design variable should not be less than zero. The others are obtained by maintaining the geometric assembly requirements for the motor. These are: S3 less than S1, S4 less than S2, S2 less than S1, S6 less than $2(S4 + S2)$, S5 less than $(S1 + S3)$ and S7 less than a reasonable number of turns such as 1000, S8 less than two times S1 and S9 between the maximum current of 110 amperes and the minimum of 12 amperes and the length of the motor less than length of the elevator cabin (L_{cabin}). The last constraint can be written as the length of each pole unit $(S1 + S3)$ time the number of coils (N_B) would not be more than the high of the cabin. Also, for stability reasons, the total thrust needed to move the cabin should be provided by an even number of motors (more than 4 because of it is easier to locate motors in each of the four rails located at each vertex of the cabin). Defining the vector of design variables \tilde{S} as:

$$\tilde{S} = \{S1, S2, \dots, S8, S9\}$$

The constraint vector \tilde{g} in term of the design variables can be written as:

$$\tilde{g} = \left\{ \begin{array}{l} 0 < S1 < 4 \frac{L_{cabin}}{N_B} - S3 \\ 0 < S2 < S1 \\ 0 < S3 < S1 \\ 0 < S4 < S2 \\ 0 < S5 < 2(S1 + S3) \\ 0 < S6 < 2(S4 + S2) \\ 0 < S7 < 1000 \\ 0 < S8 < 2S1 \\ 0 < S9 < 110 \end{array} \right\} \quad (45)$$

Where N_B is the number of coils required and depends on the others parameters.

The primary objective is to obtain the most efficient motor capable of performing the task. The objective is to maximize the linear motor's efficiency subject to the operation requirements and constraints. The objective function is therefore the motor efficiency ($f_{(\tilde{S})}$), which is defined by the ratio between the mechanical power output ($F_{Total} V_{elevator}$) and the power input supplied to the electrical motor. The power input is defined by adding the output power and the power loss (P_{loss}):

$$f_{(\tilde{S})} = \frac{P_{output}}{P_{input}} = \frac{P_{output}}{P_{output} + P_{loss_{(\tilde{S})}}} = \frac{F_{Total} V_{elevator}}{F_{Total} V_{elevator} + P_{loss_{(\tilde{S})}}} \quad (46)$$

Where, $V_{elevator}$ is the maximum velocity of the elevator, which is set to 1 m/s and

F_{Total} is the maximum load required by the elevator and is set to 10600 N. The total force provided by the linear motor can be approximately by the sum of the force provided by each coil. It is assumed that each coil provides the same force independently of the others. Given these assumptions, the number of coils can be calculated as:

$$N_{B(\tilde{S})} = \frac{F_{Total}}{F_{B(\tilde{S})}} \quad (47)$$

Where F_B is the force that can be provided by one coil. Then, the objective function (44) can be rewritten in terms of equations (45) as:

$$f_{(\tilde{S})} = \frac{F_{B(\tilde{S})} V_{elevtor}}{N_B \left(\frac{F_{B(\tilde{S})} V_{elevtor}}{N_B} + Ploss_{(\tilde{S})} \right)} = \frac{F_{B(\tilde{S})} V_{elevtor}}{F_{B(\tilde{S})} V_{elevtor} + N_{B(\tilde{S})} Ploss_{(\tilde{S})}} \quad (48)$$

There is no explicit function either for F_B or $f_{(\tilde{S})}$ in terms of the design variables \tilde{S} . The only tool to obtain a function for F_B is an interpolation of discrete values obtained from finite element analysis. It is important to note that Maxwell Software is not able to perform an optimization analysis for transient simulations automatically. Each point, where the design variables are evaluated requires an individual simulation. As a consequence, computational effort and much CPU time running are required for the optimization. The procedure in each simulation is similar to that presented in Chapter 4. For this case the velocity is prescribed. So, it is necessary to find the force that generates this steady state velocity of the motor for each simulation. The next section presents how the design variables range is set, how the interpolation is performed, and how the maximum point is selected.

6.2. Optimum Berndt Linear Motor for elevator design

The optimization method is based on a quadratic approximation of the objective function. Given an initial starting point in the design space \tilde{S}^0 two additional points are calculated taking $\tilde{S}^{new} = \tilde{S}^0 \pm \Delta h_i$ where Δh_i is a step in the i^{th} variable. Other variables

remain constant during that step. With the resulting three points a quadratic function is fitted for the objective function and the maximum is obtained for that variable. This optimum value \tilde{S}^* replaces the least optimum of the previous three points and the process is repeated until a convergence is obtained. The process is repeated for each design variable. When constraints are present then the optimum may either be an unconstrained optimum or a constrained optimum. For example, in Figure 85, the parabolic function $Y_{(x)} = -25x^2 - 10x + 5$ has a maximum at $x = -0.2$. This is true if it has only constraints g1 and g3, but if constraint g2 is added, the constrained maximum is now $x = 0$. This method of optimization is known as polynomial approximation [38].

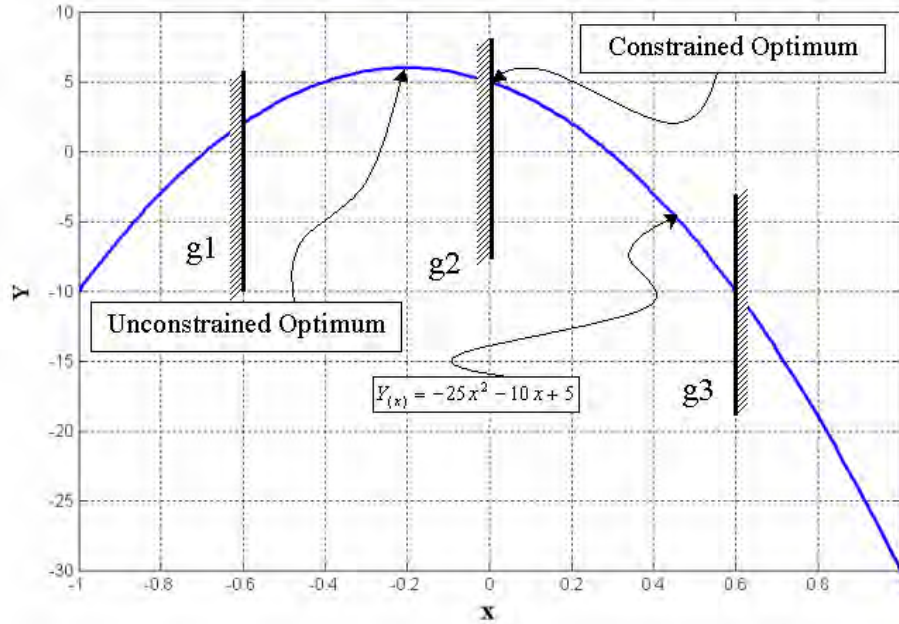


Figure 85: Example of quadratic objective function

This method can also be applied to an n-dimension quadratic surface and the optimum evaluated for the surface is used as the value for the one iteration. The \tilde{S}^* is

then used to replace a point in the surface approximation and another iteration is performed until convergence. The drawback of this approach is when too many design variables are used the number of function evaluations increases significantly. In the case when the function evaluation is expensive, such as when FEA is used, this is prohibitive. After the local maximum is calculated in one design variable it is fixed for that iteration and the procedure is repeated for each other design variable. One iteration is completed upon examining all design variables. The maximum point found for an iteration is not necessary the maximum of the objective function. For that reason, the procedure is repeated again, starting with the first design variable and continues with each one. The iterations are finished when an adequate minimum error is reached between successive maximum values of $f_{(\tilde{s})}$.

The initial starting point was selected using the parameter values shown in the second column of Table 4. For this study no shift in the stator is used and the initial values for the dimensions remain the same as those in the “current design” shown in Figure 34 chapter 4, except the for “T” pole.

In the optimization case the “T” pole used is a single bar (“T” without the flange) according to previous results. Steel 1010 was used for the “T” poles and cooper for the winding. Also, the material used for the core was laminated steel with fifteen laminations and Ceramic 5 for the permanent magnets. According to the assumptions presented in the first section of this chapter, a model with one coil is used. A rectangular wave profile without dead time is used for the simulations.

Table 4: Values for the Design Variables

Parameter	Starting Value	Unit
S1	0.85	in
S2	0.4	in
S3	0.15	in
S4	0.2	in
S5	0.75	in
S6	0.42	in
S7	105	-
S8	0.6	in
S9	110	Volts

For the simulation the discretized points for each parameter used to evaluate F_B , and therefore $f_{(\tilde{s})}$, in the first iteration are shown in the second, third and fourth columns of Table 5. The parameters S8 and S9 were not included as a parameters in the design variables for the initial set because of, from the previous iteration, the efficiency did not change significantly for these design variables, see Figure 95 and Figure 96 in the Appendix A. These two parameters were included in the second iteration.

The second and third iterations were performed and the values for each design variable used to evaluate F_B , and then $f_{(\tilde{s})}$, are summarized in Table 5. The procedure was to calculate F_B by finite elements, check whether the number of coils required to produce this force fit into the space available (constraints), and then calculate $f_{(\tilde{s})}$.

Table 5: Useful parameter values for the iterations

Iteration	Param. analyzed	Values used			Units
1st	S1	0.85	1.5	2	In
	S2	0.4	0.6	1	In
	S3	0.15	0.25	0.4	In
	S4	0	0.1	0.2	In
	S5	0.75	1	1.25	In
	S6	0.42	0.62	0.82	In
	S7	105	210	315	-
2nd	S1	1.45	2	2.3	In
	S7	105	210	315	-
	S8	0.6	1	1.4	In
	S9	110	36	14	Volt
3rd	S7	105	210	315	-
	S8	0.6	1.4	-	In
	S9	24	21	6	Volt
4th	S7	315	400	500	-
	S8	1.4	2	2.2	In
	S9	6	4	-	Volt

The results obtained from each design variable during the optimization are summarized in Table 6. This table present the value of motor longitude L_{motor} , force in the coil F_B and efficiency $f_{(\tilde{s})}$ for each design variable. Figure 86 shows the value of the efficiency $f_{(\tilde{s})}$ as a function number of optimization steps. The step number represents a computation (FEA) as a result of new value for the design variable. The values of $f_{(\tilde{s})}$ are plotted for each design variable in the order that they appear in Table 6. The maximum efficiency reached, under the constraints listed in the previous section, was 92.8%. Values for each design variable at the optimum $f_{(\tilde{s})}$ of 92.8% are listed in Table 7 and the complete details of the result are presented in the Appendix A.

Table 6: Results obtained for each variable design

ITER	Variable	Value	F_B [N]	N_B	L_{motor} [m]	$f_{(\tilde{s})}$ [%]	\tilde{S}^*
FIRST RUN	S1	0.85	3.2	843.75	21.43125	25	1.45
		1.5	35	77.14286	3.233057	58.33333	
		2	3	900	49.149	54.54545	
	S2	0.4	35	77.14286	3.135086	58.33333	0.6
		0.6	48	56.25	2.286	68.57143	
		1	70	38.57143	1.567543	59.32203	
	S3	0.15	48	56.25	2.286	68.57143	0.1
		0.25	52	51.92308	2.242038	63.41463	
		0.4	45	60	2.8194	47.36842	

SECOND RUN	S4	0	45	60	2.3622	70.3125	0.05
		0.1	43	62.7907	2.47207	69.35484	
		0.2	41	65.85366	2.592659	63.07692	
	S7	105	45	60	2.3622	73.77049	105
		210	75	36	1.41732	61.98347	
		315	105	25.71429	1.012371	57.85124	
	S5	0.42	45	60	2.3622	73.77049	0.42
		0.62	45	60	2.3622	70.3125	
		0.82	45	60	2.3622	66.17647	
	S6	0.75	45	60	2.3622	73.77049	0.75
		1	42	64.28571	2.530929	70	
	S1	1.6	45	60	2.5908	73.77049	1.45
		2	15	180	9.6012	42.85714	
		2.3	5	540	32.9184	25	
	S8	0.6	45	60	2.3622	73.77049	0.6
		1	70	38.57143	1.518557	72.16495	
		1.4	100	27	1.06299	71.94245	
	S9	110	45	60	2.3622	73.77049	36
		36	15	180	7.0866	89.28571	
		24	10	270	10.6299	92.59259	
	S7	105	15	180	7.0866	89.28571	105
		210	30	90	3.5433	81.08108	

		315	40	67.5	2.657475	72.72727	
THIRD RUN	S7	105	10	270	10.6299	92.59259	315
		210	20	135	5.31495	86.58009	
		315	30	90	3.5433	81.08108	
	S8	0.6	30	90	3.5433	81.08108	1.4
		1.4	70	38.57143	1.518557	81.39535	
	S9	24	70	38.57143	1.518557	81.39535	6
		12	35	77.14286	3.037114	89.28571	
		6	18	150	5.9055	94.24084	
FOURTH RUN	S8	1.4	18	150	5.9055	94.24084	2.2
		2	25	108	4.25196	94.21519	
		2.2	28	96.42857	3.796393	94.18096	
	S7	315	28	96.42857	3.796393	94.18096	500
		400	36	75	2.95275	92.8553	
		500	45	60	2.3622	91.46341	
	S9	6	36	75	2.95275	92.8553	6
		4	30	90	3.5433	94.04389	

It is important to note that in the second and third iterations the entire design variable set was not used. Some of them were not used because they did not affect significantly the efficiency as much as the others (for example the width of the “T” pole). The relative maximum point for some of the design variables did not change much when other design variables varied (for example the case of permanent magnet width with the

voltage applied). These situations are appreciated in more detail in Appendix A. Appendix A also shows the values of $f_{(\tilde{s})}$ for each design variable. Figure 86 shows the optimization history and convergence.

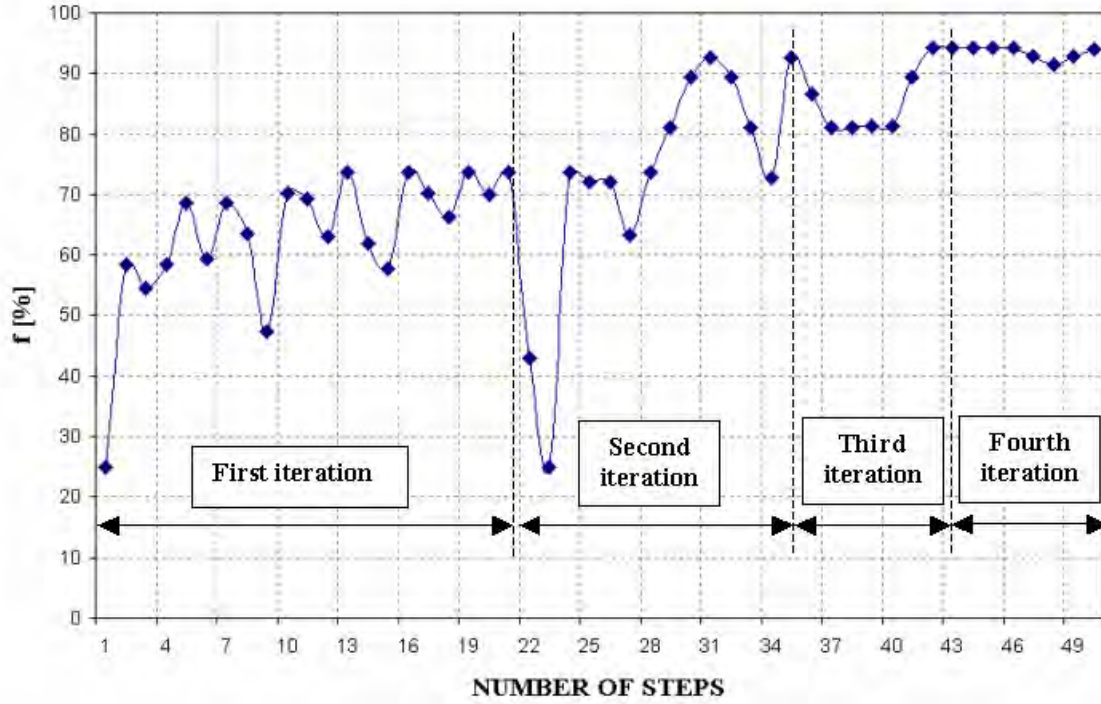


Figure 86: Optimization convergence

With these results the best motor to move the elevator has four motors with seventy five coils in each rail. The seventy five coils for motor can be provide a force of 2700 N, each and it has a total trust force of 10800 N. The operating point is at 6 amperes with 92.8 %efficiency. This is good operating point for the efficiency but it requires a large number of coils which represents a big volume of material. The seventy five coils of 2.25 in each in length total 2.9 m length for each rail motor. Table 7 summarizes the optimum values for the design variables.

Table 7: Optimum point

	S1	S2	S3	S4	S5	S6	S7	S8	S9	F_B	N_B	f
#1	1.45	0.6	0.1	0.05	0.42	0.75	500	2.2	6	36	75	92.85
Unit	[in]	[in]	[in]	[in]	[in]	[in]	-	[in]	[Volts]	N	-	%

Figure 87 shows a schematic for the final values of the design variables. In the Figure an artistic general view of the linear motor is presented (not to scale). Only three coils are plotted to clearly show the final results.

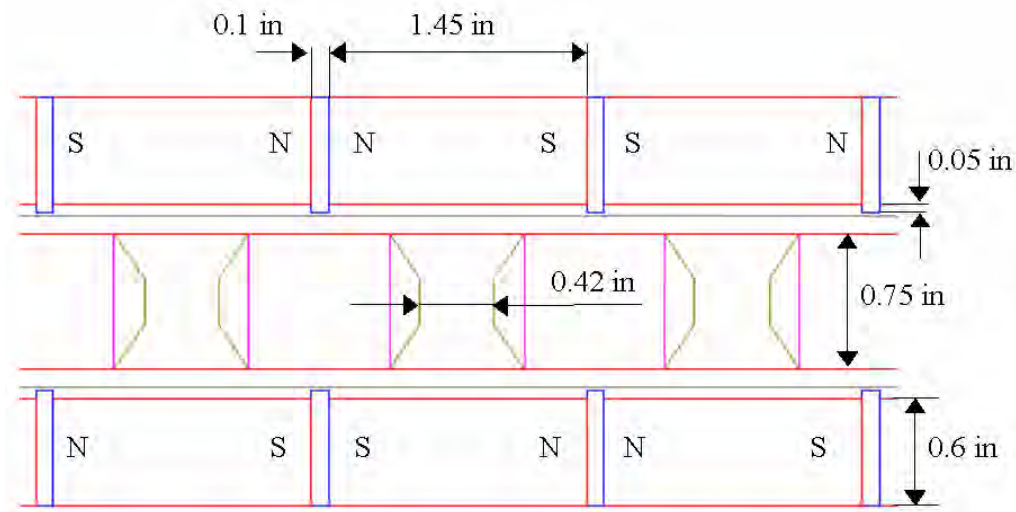


Figure 87: Final values for design variables

Finally it will be concluded that the Berdut linear motor can be used for this type of application with a good performance in the efficiency. In this thesis, the regenerative model was not studied. In many cases the efficiency of the motor is the same as that of the generator. This is an important issue because the technology was studied in ascent mode (as a motor), but in the descent mode it needs to work as a generator and the energy

should be stored. The study of the generator mode was not performed because the goal and scope of the thesis was the modeling and validation of the model for a linear motor based on the Berndt Technology. The elevator was chosen only as an application case study to show how the technology can be used and optimized. Note that, if some constraints were changed, another motor would be obtained. For example: if one wanted to optimize the motor for a Maglev train, the velocity would be changed and the resulting optimum design would therefore change.

CHAPTER VII: Conclusions and Future Work

7.1. Conclusions

The numerical model was developed with the objective of examining the behavior of the Berndt linear motor. Also, an experimental setup was made in order to validate the numerical model. The force profile as a function of position was determined and the effect of input current profile effect was analyzed as well as the efficiency and thrust force curves determined using a finite element model. These were the first analytical results on the behavior of the Berndt linear motor. The conclusions obtained from this work are that the optimum current profile does not require a dead time between switching in the polarity of the coil when the coils are passing in front of the “T” poles. Also, the proposed form of “T” pole was not the best design for the linear motor. It was found that a magnetic concentrator without the flange is the best solution. Another important parameter analyzed was the type of connection between each coil (or equivalently the current profile training for each coil). Two types of connections were selected (simultaneous and shift). The shift connection produced the best performances.

An optimization of the motor was carried out to maximize its efficiency. The optimization was constrained to relatively low speed applications such as those imposed for an elevator mechanism. The theoretical efficiency, obtained through the optimization by finite element analysis, was of the order of 92.85%. Also, through the steps presented in Chapter 6, optimum Berndt linear motor configuration for other applications can be obtained by varying the optimization statement (objective and constraints). The main objective was not to design an elevator but to develop a model that describes the behavior

of the Berdut linear motor and a procedure for reproducing designs under other constraints. The optimization of the elevator had the purpose of demonstrating the feasibility of this technology for different areas.

7.2. Future Work

The following items are included as improvements or additions to this research:

- 1) Perform additional experimental analysis of this technology, in order to validate the numerical simulation in other points of operation. The experimental results presented were based on existing prototypes. A prototype of the optimum configuration may be built and tested to validate the numerical optimum.
- 2) Perform an experimental and theoretical analysis of this technology used as generator.
- 3) Perform a theoretical analysis of this technology, for other materials and configurations such as those required for a Maglev train and for an aircraft carrier catapult. They can use the Berdut linear motor but they have different design constraints.
- 4) Perform an experimental analysis of the complete model motor-elevator in order to shown the working principle and the capabilities of this technology, including issues such as the generator, the energy storage devices, the control strategies and the economic issues.

- 5) Develop a model, validated and make an optimization of the orbital motor configuration of the Berdut technology for other applications such as manufacturing machines, robotics, vehicle starter/generator power tools, home appliances, etc.
- 6) Optimize the electronic required to control the linear motor.

The above areas motivate continuing research and development of the motor and technology to determine the feasibility of its use in different potentials applications.

APPENDIX A: Optimization Points

Table 8: Results obtained for the design variables

ITER	Variable	Value	P_{loss} [w]	I [A]	F_B [N]	N_B	L_{motor} [m]	$f_{(\vec{s})}$ [%]
FIRST RUN	S1	0.85	9.6	110	3.2	843.75	21.43125	25
		1.5	25	110	35	77.14286	3.233057	58.33333
		2	2.5	110	3	900	49.149	54.54545
	S2	0.4	25	110	35	77.14286	3.135086	58.33333
		0.6	22	110	48	56.25	2.286	68.57143
		1	48	110	70	38.57143	1.567543	59.32203
	S3	0.15	22	110	48	56.25	2.286	68.57143
		0.25	30	110	52	51.92308	2.242038	63.41463
		0.4	50	110	45	60	2.8194	47.36842
	S4	0	19	110	45	60	2.3622	70.3125
		0.1	19	110	43	62.7907	2.47207	69.35484
		0.2	24	110	41	65.85366	2.592659	63.07692
	S7	105	16	110	45	60	2.3622	73.77049
		210	69	110	75	36	1.41732	61.98347
		315	153	110	105	25.71429	1.012371	57.85124
	S6	0.42	16	110	45	60	2.3622	73.77049
		0.62	19	110	45	60	2.3622	70.3125
		0.82	23	110	45	60	2.3622	66.17647
	S5	0.75	16	110	45	60	2.3622	73.77049
		1	18	110	42	64.28571	2.530929	70
SECOND RUN	S1	1.6	16	110	45	60	2.5908	73.77049
		2	20	110	15	180	9.6012	42.85714
		2.3	15	110	5	540	32.9184	25
	S8	0.6	16	110	45	60	2.3622	73.77049
		1	27	110	70	38.57143	1.518557	72.16495
		1.4	39	110	100	27	1.06299	71.94245
		2	78	110	135	20	0.7874	63.38028
	S9	110	16	110	45	60	2.3622	73.77049
		72	7	72	30	90	3.5433	81.08108
		36	1.8	36	15	180	7.0866	89.28571
		24	0.8	24	10	270	10.6299	92.59259
	S7	105	1.8	36	15	180	7.0866	89.28571
		210	7	36	30	90	3.5433	81.08108
		315	15	36	40	67.5	2.657475	72.72727
THIRD RUN	S7	105	0.8	24	10	270	10.6299	92.59259
		210	3.1	24	20	135	5.31495	86.58009

FOURTH RUN	S8	315	7	24	30	90	3.5433	81.08108
		0.6	7	24	30	90	3.5433	81.08108
		1.4	16	24	70	38.57143	1.518557	81.39535
	S9	24	16	24	70	38.57143	1.518557	81.39535
		12	4.2	12	35	77.14286	3.037114	89.28571
		6	1.1	6	18	150	5.9055	94.24084
	S7	1.4	1.1	6	18	150	5.9055	94.24084
		2	1.535	6	25	108	4.25196	94.21519
		2.2	1.73	6	28	96.42857	3.796393	94.18096
	S8	315	1.73	6	28	96.42857	3.796393	94.18096
		400	2.77	6	36	75	2.95275	92.8553
		500	4.2	6	45	60	2.3622	91.46341
	S9	6	2.77	6	36	75	2.95275	92.8553
		4	1.9	4	30	90	3.5433	94.04389

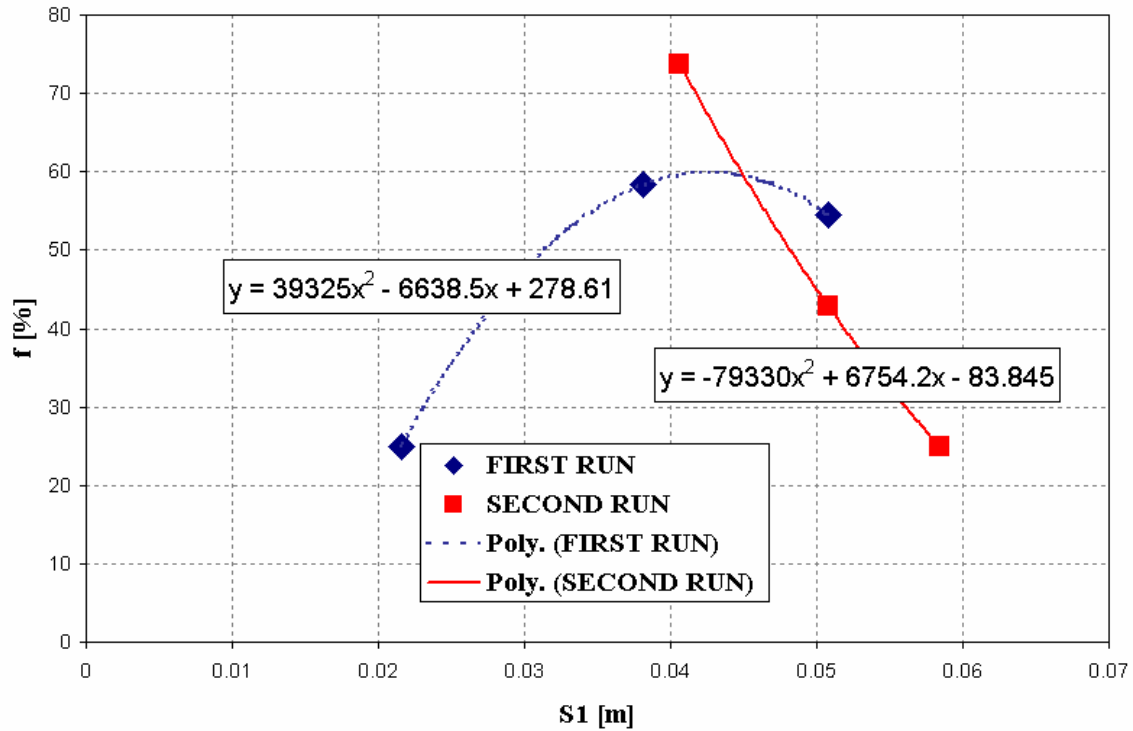


Figure 88: Efficiency as a function of permanent magnet length.

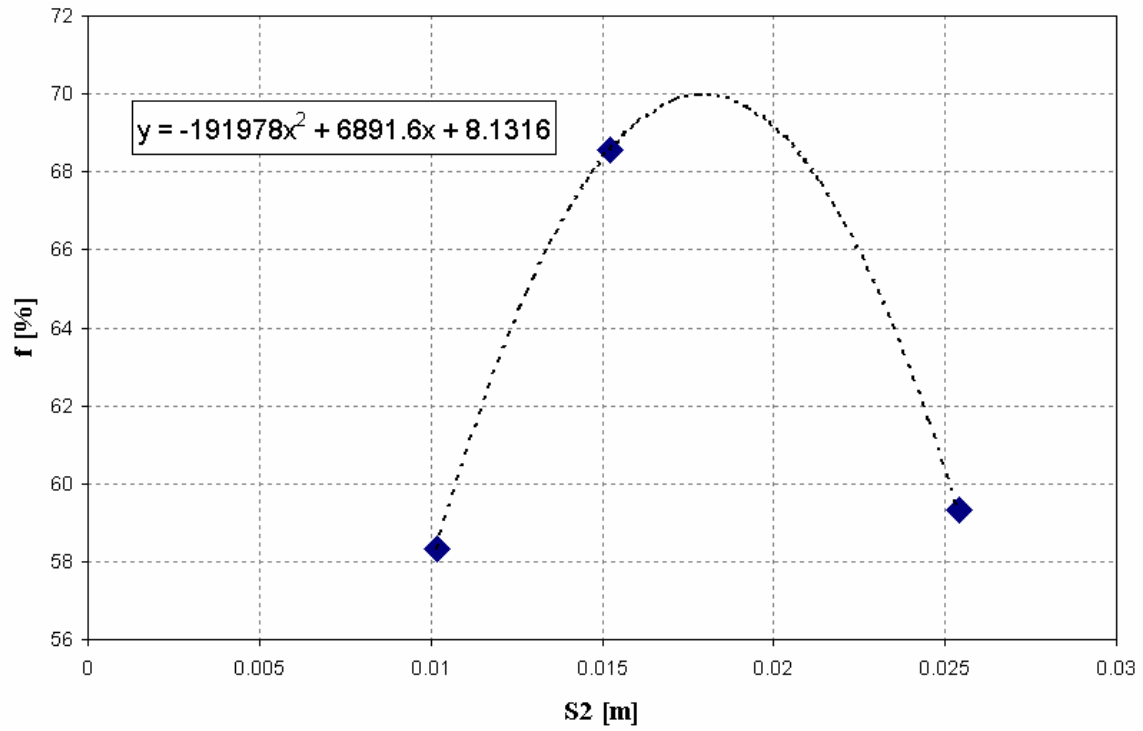


Figure 89: Efficiency as a function of permanent magnet width.

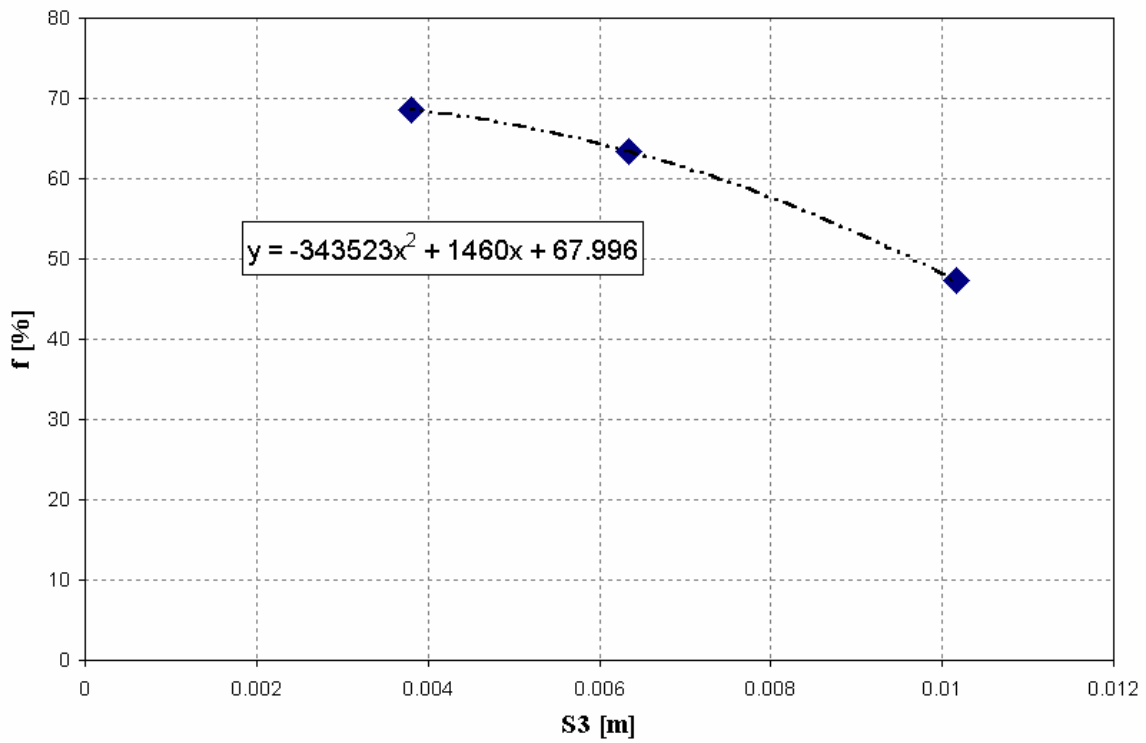


Figure 90: Efficiency as a function of "T" pole length.

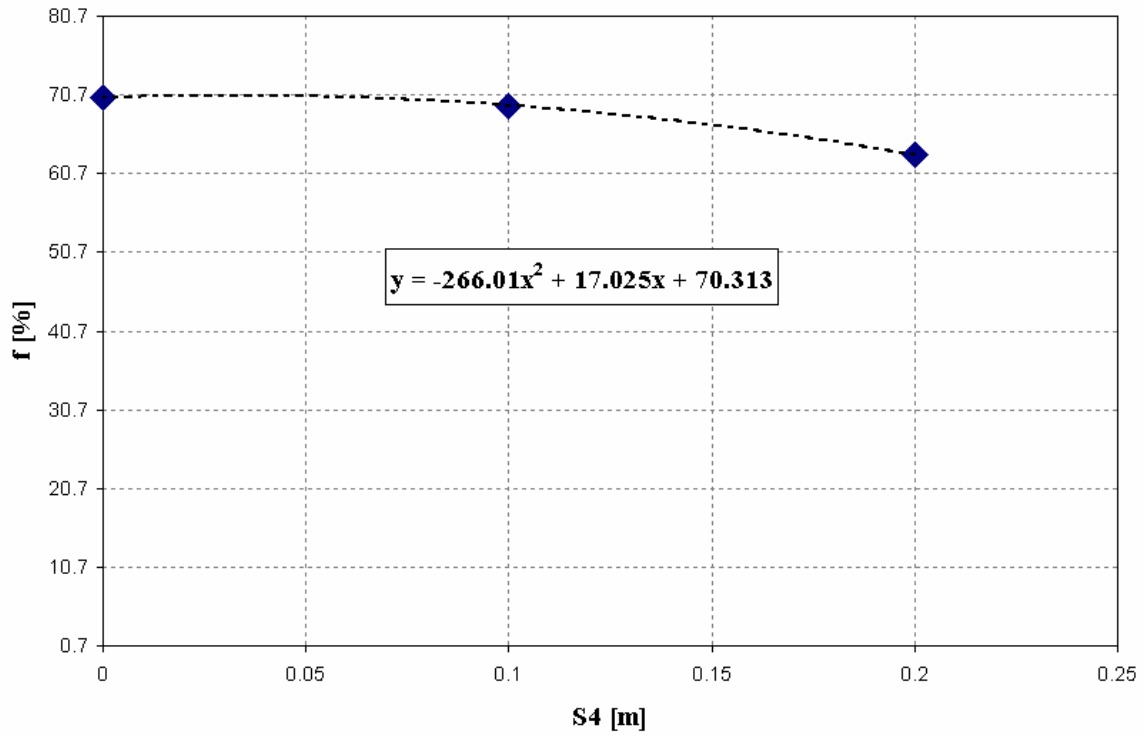


Figure 91: Efficiency as a function of “T” pole width.

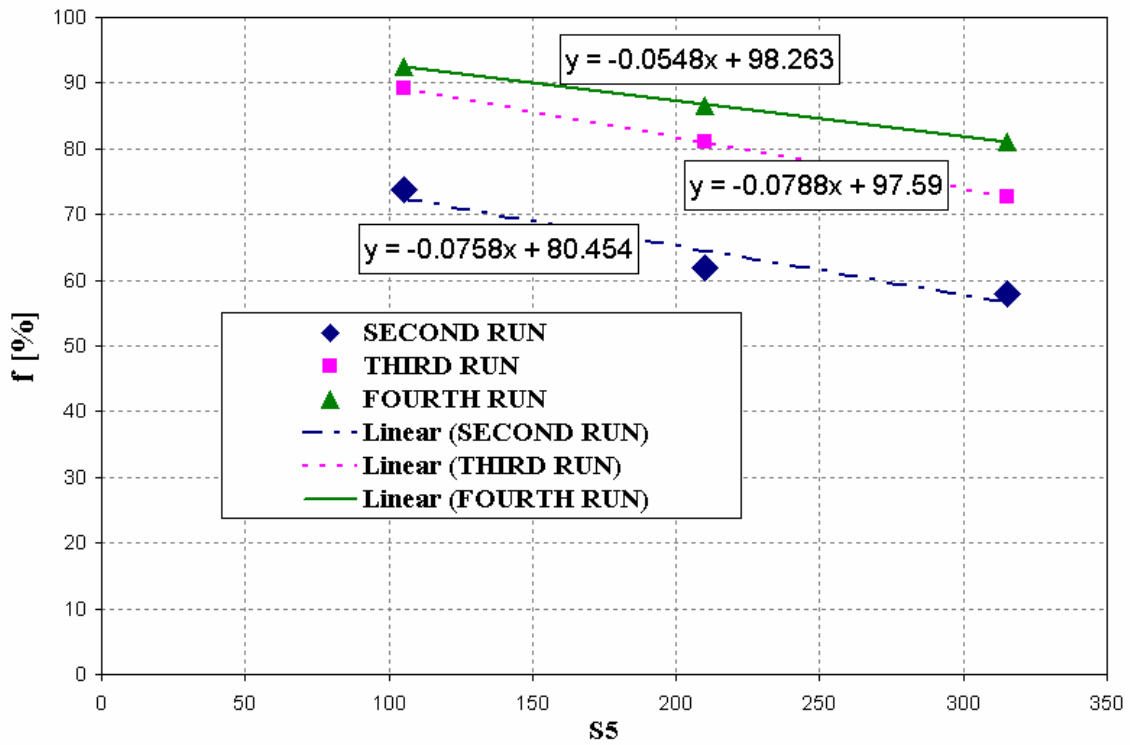


Figure 92: Efficiency as a function of number of turns.

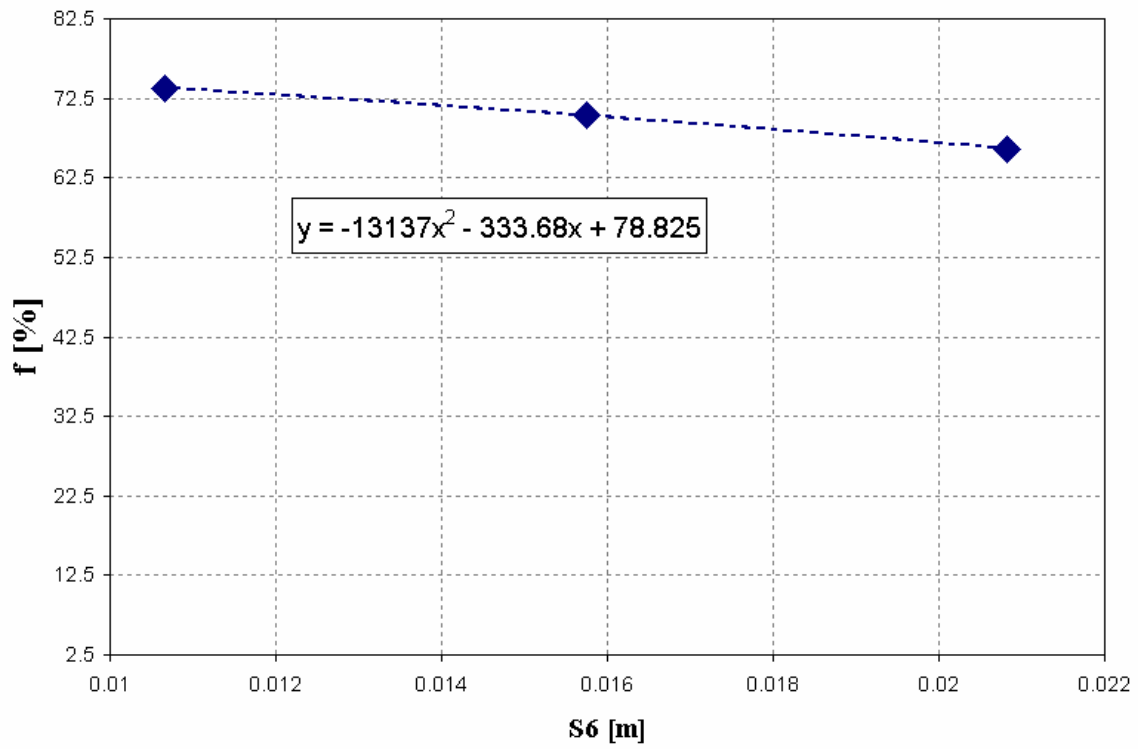


Figure 93: Efficiency as a function of coil length.

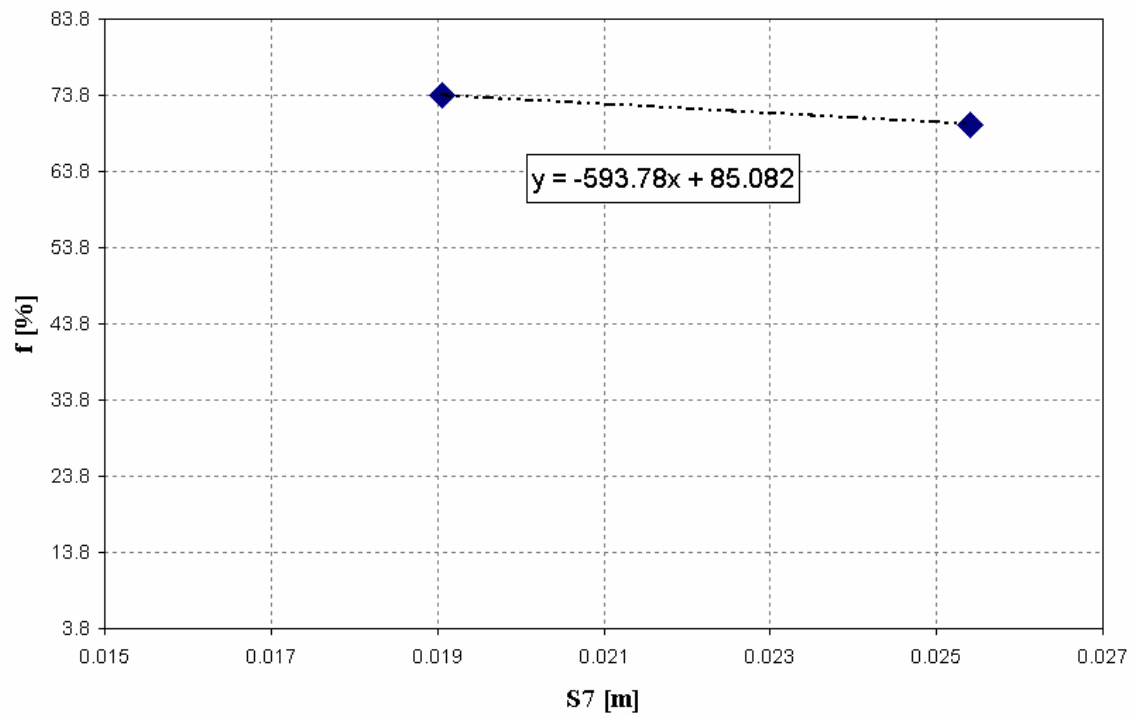


Figure 94: Efficiency as a function of coil width.

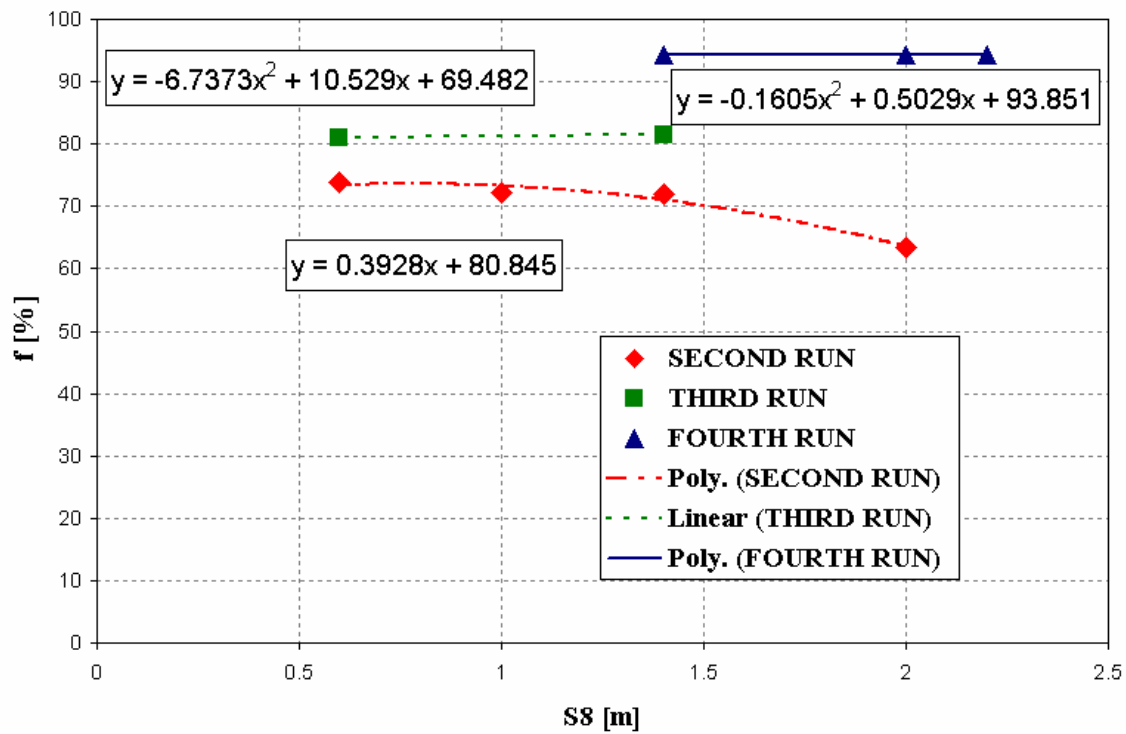


Figure 95: Efficiency as a function of the current

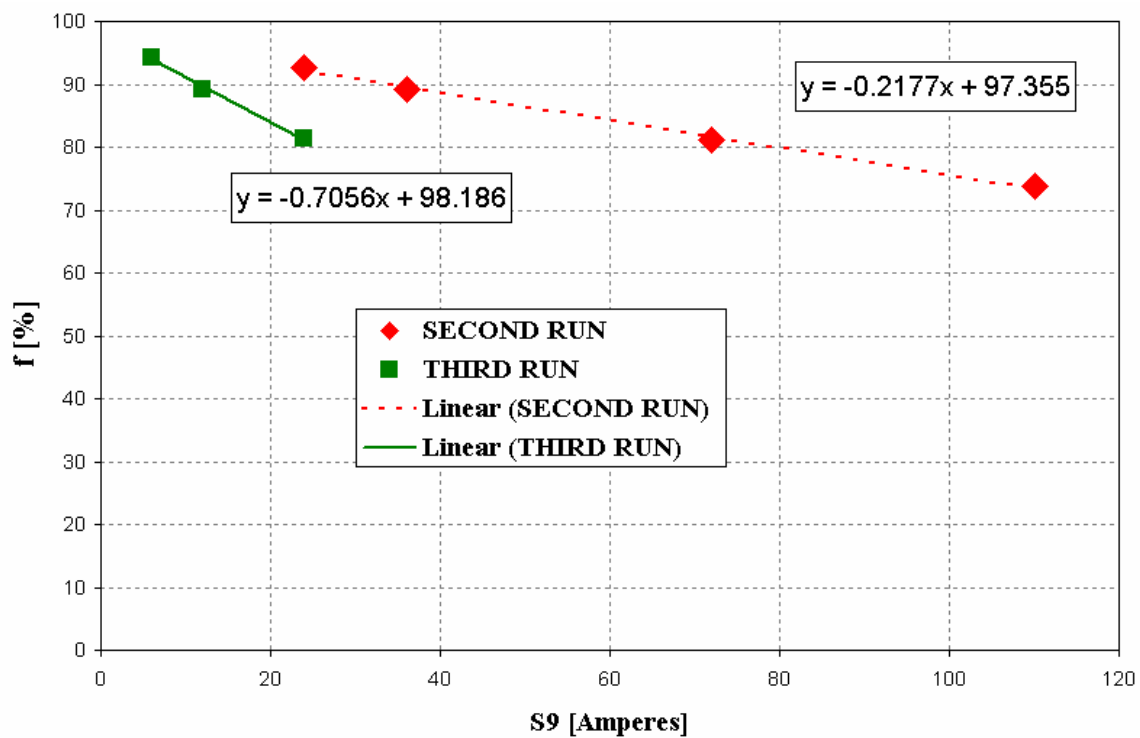


Figure 96: Efficiency as a function of model depth

References

-
- [1] E. Berdut, "Levitation and linear propulsion system using ceramic permanent magnets and interleaved malleable steel", U.S. Patent No 5.431.109, Jul. 1995.
- [2] E. Berdut, "Levitation And Propulsion System Using Permanent Magnets And Interleaved Iron Or Steel", U.S. Patent No 5,452,633, Oct. 1994.
- [3] E. Berdut, "Permanent magnet type automotive vehicle suspension", U.S. Patent No 5,584,367, Dec. 1996.
- [4] E. Berdut, "Orbital and modular motors using permanent magnets and interleaved iron or steel magnetically permeable members", U.S. Patent No 5,615,618, Apr. 1997.
- [5] R. G. Rhodes and B. E. Mulhall, "Magnetic Levitation for rail transport", Clarendon Press, Oxford, 1981.
- [6] L. A. Torres Morales, "Characterization and equivalent spring constant for a magnetic levitated train system using Berdut poles", UPRM, 2001.
- [7] J. Robles, "Dynamic Response and Damping Characteristics of a Berdut Skate for a Magnetically Levitated Train ", Master Thesis, UPRM, Dec. 2003.
- [8] O. Flores, "Analysis and Similation of EM Fields of Permanent Magnets DC Linear Motor used to Propulse a Magnetically Levitated Train", Master Thesis, UPRM, June 2004.
- [9] D. Serrano, A. Irizarrry and F. Just-Agosto, "Magnetically levitated Transport, Proof of Concept Development", COINAR, San Juan, PR, 2003.
- [10] L. A. Torres Morales and D. Serrano, "Finite Element Simulation of Magnetically levitated Train Using Berdut Poles", COINAR, San Juan, PR, 2003.

-
- [11] J. Robles and D. Serrano, "Damping Characteristics of a Magnetic Levitation Train", COINAR, San Juan, PR, 2003.
- [12] E. Médici and D. Serrano, "Finite Element Eimulations of Berdut linear motor", XIV Congress on Numerical Methods and their Applications, Bariloche, Argentina, November 2004.
- [13] E. Médici and D. Serrano, "Finite Element Simulations And Characterization Of Berdut Linear Motor", COINAR, Congress of Engineering and Survey, San Juan, Puerto Rico, March 2004.
- [14] <http://www.calmaglev.org/default.php?page=4>
- [15] http://www.rtri.or.jp/rd/maglev/html/english/maglev_frame_E.html
- [16] <http://travel.howstuffworks.com/maglev-train1.htm>
- [17] <http://www.physics.nwu.edu/classes/2001Fall/Phyx135-2/06/inductrack.html>
- [18] J. F. Gieras and M. Wing, "Permanent Magnet Motor Technology", Marcel Dekker Inc., New York, 2002.
- [19] <http://www.magnemotion.com/products/maglev/pdf/M3Summary052704.pdf>
- [20] MagneMotion, "The M3 Urban Transportation System", Part of FTA Project MA-26-7077, Jan. 2003.
- [21] Yaskawa Electric America, "Linear Servo Drive Linear Series", Japan, March 2001.
- [22] Nikon Tech., "Linear motor device, stage device and exposure apparatus", U.S. Patent No 6.590.355, Jun. 2000.
- [23] Nikon Tech., "Electric Linear motor", U.S. Patent No 6.570.273, Jan. 2001.
- [24] W. Kim and B. C. Murphy, "Design And Construction Of A Novel Tubular Linear Motor With Controller For Robotics Applications" Engineering Congress & Exposition

Proceedings of IMECE'03, 2003 ASME International Mechanical Engineering Congress
Nov., 2003.

[25] R. Erkelens, "The Helical Elevator", Elevator World, Inc., 1998.

[26] ThyssenKrupp Elevator Company, "TWIN –The revolutionary system in elevator design. Two cars. One shaft. One quantum leap". Technical information bulleting, 2004.

[27] T. Dünser, R. Deplazes, and M. Meier, "A New Elevator System and Its Implementation", 2003.

[28] http://www.roboticparking.com/home_broadband.php

[29] M. Schuwartz, "Principles of Electrodynamics", DOVER, New York, 1987.

[30] J. Reitz and F. Mildford, "Foundations of Electromagnetic Theory", Addison-Wesley Pub. Comp., Massachusetts, 1967.

[31] http://www.oulu.fi/atkk/tkpalv/unix/ansys-6.1/content/thy_emg2.html

[32] M. A. Plonus, "Electromagnetismo Aplicado", Ed. REVERTE S.A., Barcelona, Spain, 1992.

[33] Maxwell® 2D, "A 2D Electrostatic Problem", nov. 2002.

[34] Maxwell® 2D, "A 2D Magnetostatic Problem", nov. 2002.

[35] Maxwell® 2D, "A 2D Transient Linear Motion Problem", nov. 2000.

[36] "A Universal Motor Problem", Ansoft RMxpert Application Note.

[37] http://www.otis.com/products/dimensions/0,1356,CLI84_PRD7082_PRT229_PST427_RES1,00.html.

[38] G. N. Vanderplaats, Numerical Optimization Techniques for Engineering Design, with Applications, McGraw-Hill, 1984.